444
8-21-80

ANL/CEN/FE-79-15

Wu-1664

ANL/CEN/FE-79-15

MASTER

INVESTIGATION OF LIMESTONE SULFATION ENHANCEMENT AGENTS AND THEIR CORROSION RATES IN FBCs

Annual Report

October 1978—September 1979

by

Irving Johnson, K. M. Myles, J. F. Lenc, J. A. Shearer,
G. W. Smith, O. K. Chopra, F. G. Teats, F. F. Nunes,
C. B. Turner, W. I. Wilson, and A. A. Jonke

ARGONNE NATIONAL LABORATORY

ARGONNE NATIONAL LABORATORY, ARGONNE, ILLINOIS

Prepared for the U. S. DEPARTMENT OF ENERGY
under Contract W-31-109-Eng-38

DISCLAIMER

The facilities of Argonne National Laboratory are owned by the United States Government. Under the terms of a contract (W-31-109-Eng-38) among the U. S. Department of Energy, Argonne Universities Association and The University of Chicago, the University employs the staff and operates the Laboratory in accordance with policies and programs formulated, approved and reviewed by the Association.

MEMBERS OF ARGONNE UNIVERSITIES ASSOCIATION

The University of Arizona
Carnegie-Mellon University
Case Western Reserve University
The University of Chicago
University of Cincinnati
Illinois Institute of Technology
University of Illinois
Indiana University
The University of Iowa
Iowa State University
The University of Kansas
Kansas State University
Loyola University of Chicago
Marquette University
The University of Michigan
Michigan State University
University of Minnesota
University of Missouri
Northwestern University
University of Notre Dame
The Ohio State University
Ohio University
The Pennsylvania State University
Purdue University
Saint Louis University
Southern Illinois University
The University of Texas at Austin
Washington University
Wayne State University
The University of Wisconsin-Madison

Printed in the United States of America
Available from
National Technical Information Service
U. S. Department of Commerce
5285 Port Royal Road
Springfield, VA 22161

NTIS price codes
Printed copy: A06
Microfiche copy: A01

Distribution Category:
Coal Conversion and Utilization—
Direct Combustion of Coal
(UC-90e)

ANL/CEN/FE-79-15

ARGONNE NATIONAL LABORATORY
9700 South Cass Avenue
Argonne, Illinois 60439

INVESTIGATION OF LIMESTONE SULFATION ENHANCEMENT AGENTS AND THEIR CORROSION RATES IN FBCs

Annual Report
October 1978—September 1979

by

Irving Johnson, K. M. Myles, J. F. Lenc, J. A. Shearer,
G. W. Smith, O. K. Chopra, F. G. Teats, F. F. Nunes,
C. B. Turner, W. I. Wilson, and A. A. Jonke

Chemical Engineering Division

Prepared for the
U.S. Department of Energy
under Contract No. W-31-109-Eng-38
and the
U.S. Environmental Protection Agency
under Agreement IAG-D5-E681

Work on these subjects was previously reported in two series of reports:

Support Studies in Fluidized-Bed Combustion

ANL/CEN/FE-78-10	July 1977—September 1978
ANL/CEN/FE-79-3	October—December 1978
ANL/CEN/FE-79-5	January—March 1979
ANL/CEN/FE-79-8	April—June 1979

Regeneration of Sulfated Limestone from FBCs

ANL/CEN/FE-78-13	July 1977—September 1978
ANL/CEN/FE-79-2	October—December 1978
ANL/CEN/FE-79-6	January—March 1979

BIBLIOGRAPHIC DATA SHEET	1. Report No. ANL/CEN/FE-79-15	2.	3. Recipient's Accession No.
4. Title and Subtitle Investigation of Limestone Sulfation Enhancement Agents and Their Corrosion Rates in FBCs, Annual Report, October 1978—September 1979			5. Report Date 1979 6.
7. Author(s) Irving Johnson, K. Myles, J. Lenc, J. Shearer, G. Smith, O. Chopra, F. Teats, F. Nunes, C. Turner, W. Wilson and A. Jonke			8. Performing Organization Rept. No.
9. Performing Organization Name and Address Argonne National Laboratory 9700 South Cass Avenue Argonne, Illinois 60439			10. Project/Task/Work Unit No. 11. Contract/Grant No. W31-109-ENG-38 (DOE) IAG-D5-E681 (EPA)
12. Sponsoring Organization Name and Address U.S. Department of Energy and the U.S. Environmental Protection Agency			13. Type of Report & Period Covered October 1978—Sept. 1979 14.
15. Supplementary Notes			

16. Abstracts

This work supports the development studies for atmospheric and pressurized fluidized-bed coal combustion. Laboratory studies and runs in an atmospheric process-development-scale combustor are aimed at providing information on the effects of water addition and chemical additives such as $CaCl_2$, NaCl, and Na_2CO_3 on (1) the degree of sulfation of limestone sorbent at various operating conditions and (2) the corrosion of candidate materials for fluidized-bed coal combustion facilities.

17. Key Words and Document Analysis. 17a. Descriptors

Additives
Air Pollution
Calcium Chloride
Calcium Oxides
Calcium Sulfates
Coal
Combustion
Corrosion Products
Dolomite
Flue Gas
Fluidized-Bed Combustion
Fossil Fuels
Intergranular Corrosion
Limestone
Porosity
Scaling
Sodium Carbonate
Sodium Chlorides
Sulfur Oxides

17b. Identifiers/Open-Ended Terms

Sorbent Enhancement
Sorbent Regeneration
Sorbent Sulfation
Stone Morphology

17c. COSATI Field/Group

18. Availability Statement	19. Security Class (This Report) UNCLASSIFIED	21. No. of Pages
	20. Security Class (This Page UNCLASSIFIED	22. Price

FORM NTIS-35 (REV. 10-73) ENDORSED BY ANSI AND UNESCO. THIS FORM MAY BE REPRODUCED USCOMM-DC 8265-P74

TABLE OF CONTENTS

LIST OF FIGURES

LIST OF FIGURES (contd)

LIST OF FIGURES (contd)

LIST OF FIGURES (contd)

LIST OF TABLES

LIST OF TABLES (contd)

INVESTIGATION OF LIMESTONE SULFATION ENHANCEMENT AGENTS AND THEIR CORROSION RATES IN FBCs

Annual Report
October 1978—September 1979

by

Irving Johnson, K. M. Myles, J. F. Lenc, J. A. Shearer, G. W. Smith, O. K. Chopra, F. G. Teats, F. F. Nunes, C. B. Turner, W. I. Wilson, and A. A. Jonke

ABSTRACT

This work supports the development studies for atmospheric and pressurized fluidized-bed coal combustion. Laboratory studies and runs in an atmospheric process-development-scale combustor are aimed at providing information on the effects of water addition and chemical additives such as $CaCl_2$, NaCl, and Na_2CO_3 on (1) the degree of sulfation of limestone sorbent at various operating conditions and (2) the corrosion of candidate materials for fluidized-bed coal combustion facilities.

SUMMARY

Enhancement of Limestone Sulfation by Chemical Additives

Laboratory Studies. Among the effects of chemical additives on the sulfation of limestones are major changes in the physical structure of the stones. Scanning electron microscopy (SEM) has been successfully used in conjunction with mercury porosimeter data to describe in detail the changes that occur (after salt addition) during calcination and sulfation.

The effects of NaCl and $CaCl_2$ on limestone structure are presented in a series of SEM photographs which show the increase in pore size associated with increased salt addition, as well as evidence of the presence of small amounts of liquid phase during the interaction. The increased permeability of the system is indicated by the formation of $CaSO_4$ throughout the particles, as shown by sulfur scans of SEM photographs.

Data on the effects of NaCl and $CaCl_2$ on dolomite sulfation and particle structure show effects similar to those with limestones, but of less magnitude due to the inherent high reactivity of most untreated dolomites. There is an initial increase in sulfur capture with small amounts of salt additive, which is followed by a decrease as salt levels increase, and finally a long slow increase in sulfur-capturing ability at very high salt concentrations. Structural effects similar to those in limestones, such as increased pore size, are seen in dolomites.

The use of Na_2CO_3 additive was suggested as a possibility with the hope of decreased corrosiveness due to the absence of chloride ions and the low volatility of the salt. Data show marked improvement in sulfation of

limestones due to structural changes induced by the presence of Na_2CO_3 (similar to the changes effected by NaCl and $CaCl_2$). Due to its melting characteristics and low volatility, Na_2CO_3 appears to be more effective than NaCl or $CaCl_2$. The salt remains in contact with the limestone for a greater period of time, which results in dramatic increases in pore diameter as measured on a mercury porosimeter. SEM photographs illustrate the effect of impurity content on the structure changes and how they influence stone reactivity with sulfur species.

Thermogravimetric analysis of limestone sulfation reactions in the presence of NaCl and $CaCl_2$ at various temperatures indicates that these salts are effective as sulfation enhancers at all temperatures between 750°C and 1050°C, with greater sulfation enhancement occurring above 900°C for NaCl and above 950°C for $CaCl_2$. At high temperatures, the untreated stones have low reactivity due to sintering and loss of surface area.

Characterization of limestones is being carried out with data presented here on pore volume and surface area. The results show that stone reactivity does not correlate with total surface area nor with total pore volume. However, if only pores ≥ 0.3 μm are considered, there are correlations of surface area and pore volume with sulfur reactivity of limestones at 850°C. The addition of low concentrations of salt to limestones increases surface area; these data, plotted with data for untreated limestone, show a maximum conversion of approximately 50% of the CaO. Higher salt levels decrease the surface area, with subsequent loss of reactivity. From these plots of pore volume and surface area, a stone's reactivity compared with that of other limestones may be roughly determined.

Petrographic Examination of Limestones. Petrographic analyses of several calcareous stones have been made to understand the basic structural reasons for the wide variations in SO_2 reactivity of different limestones. Results of the examinations of eight stones reveal no obvious structural differences correlated with their SO_2 reactivities.

PDU Studies. Laboratory-scale experiments have demonstrated that the degree of sulfation of the partially sulfated lime solids within a fluidized-bed combustor can be increased by the addition of sulfation-enhancement agents (chemical additives) to virgin limestones or by water treatment of partially sulfated limestones. Chemical additives such as $CaCl_2$, NaCl, and Na_2CO_3 added in small quantities increase both the rate and the extent of sulfation for many virgin limestones. Water treatment of partially sulfated limestones also increases the degree of sulfation.

In a commercial FBC, increasing the SO_2 retention would decrease the lime solids requirement for the combustion process and, in turn, reduce both the process cost and the environmental impact of solids waste disposal. The recently constructed PDU-scale automated atmospheric-pressure fluidized-bed coal combustion facility (AFBC) is being used for short-term runs (≤ 24 h) to evaluate (1) various concentrations of different sulfation-enhancement agents and (2) water treatment of partially sulfated limestones.

The effects on SO_2 retention of adding low concentrations (1.0 mol % or less) of $CaCl_2$ or NaCl to Grove limestone were evaluated in a series of 31 short-term runs (SAL and NAC series runs). Percent sulfur retention and percent calcium utilization are reported as a function of the Ca/S mole ratio for these runs.

In these runs, the degree of sulfation enhancement due to the addition of $CaCl_2$ or NaCl was generally lower than in laboratory-scale experiments previously reported. The differences in the two sets of data are thought to be due to the different manner of conducting the two series of experiments. The laboratory-scale experiments had been carried out with a simulated flue gas and no coal combustion. Consequently, no coal ash constituents were present in the reactor. In contrast, combustion experiments were performed in the PDU-scale AFBC.

In an attempt to clarify the disparity between the data for the PDU-scale experiments and the laboratory-scale experiments, four additional short-term (8 h) runs were conducted in the AFBC. Higher concentrations of sulfation-enhancement agents in the Grove limestone sorbent were used in the first three runs. The sorbent contained ∿2.3 mol % NaCl in the first run (NAC-10), ∿2.1 mol % $CaCl_2$ in the second run (SAL-20), and ∿1.6 mol % Na_2CO_3 in the third run (NCO-1). In the fourth run (NCO-2), ∿0.6 mol % of Na_2CO_3 was added to the sorbent since no data had been obtained previously on how sulfation enhancement was affected by this particular chemical additive at a relatively low concentration. The Ca/S mole ratios required to maintain 700 ppm SO_2 in the dry off-gas (equivalent to 85% sulfur retention) during the four runs were 2.7, 2.6, 2.2, and 2.9, respectively. These results suggest (1) that the concentration of a chemical additive required to enhance sulfation of the limestone sorbent in actual coal combustion experiments is greater than in laboratory experiments conducted with a simulated flue gas and (2) that Na_2CO_3 is a better sulfation-enhancement agent on a mole basis than either $CaCl_2$ or NaCl at both relatively high (∿2.0 mol %) and relatively low (∿0.5 mol %) concentrations.

To gain insight on the chemical composition of the fluidized-bed material as a function of time, samples of the bed material were taken at a height of ∿254 mm above the coal injection point at intervals during sulfation (starting bed, virgin Grove limestone) in the first of the four short-term runs mentioned above. After the samples were withdrawn from the bed, they were sealed in glass jars (containing an inert nitrogen atmosphere to prevent reaction with oxygen and/or water in the air). Analyses of S^{2-}, SO_4^{2-}, and CO_3^{2-} concentrations in the bed samples were performed. Very little sulfide (<100 ppm) was found. Based on SO_4^{2-} analyses, $CaSO_4$ content in one run increased to ∿45 wt % during the first 7.5 h and then leveled off. The $CaCO_3$ content dropped from 31.8 wt % after the first 1 h to 1.1 wt % after 9 h of sulfation.

Another series of four runs (SG-1 to SG-4) was conducted in the new AFBC to compare its performance with that of an older atmospheric-pressure fluidized-bed combustor under similar operating conditions. A major difference in the experiments done in the new AFBC and those done in the old AFBC was in the sulfur content of the coals. The Sewickley coal used in the

recent runs contained 5.46 wt % S, compared with 3.7 wt % S for the Illinois coal used in the previously reported runs. Percent sulfur retentions as a function of Ca/S mole ratio for these four recent runs are reported. Sulfur retentions were in general agreement with those of previous atmospheric-pressure fluidized-bed combustion experiments. At a Ca/S mole ratio of 3, sulfur retention was about 80% in the recent series of runs, compared with about 87% in the previous series. Carbon, sulfur, and calcium material balances for 4.5 h steady state periods of each of the four runs are presented. Sulfur balances ranged from 78 to 101% and calcium balances from 96 to 114%. Combustion efficiencies varied from 86 to 88%.

A series of short-term runs was begun to determine Ca/S mole ratios as a function of combustion temperature, for various untreated sorbents (*i.e.*, containing no sulfation-enhancement agents), required for 85% sulfur retention. Two limestone sorbents, one calcitic and the other dolomitic, have been evaluated. For the calcitic limestone (Grove), the Ca/S mole ratios needed for 85% sulfur retention were 6.0, 3.4, and 3.7 at 800, 850, and 900°C, respectively. For the dolomitic limestone (Pfizer), the corresponding values for the Ca/S mole ratio were 1.2, 1.7, and 1.7 at 800, 850, and 900°C, respectively.

An additional short-term test (HYS-1) was performed in which the sorbent consisted of partially sulfated Grove limestone that had been water-sprayed. The purpose of water-spraying was to determine whether the sulfur retention capability of the partially sulfated material would be increased by $Ca(OH)_2$ formed by the reaction with water of the CaO in the material. The $Ca(OH)_2$ decomposes at the combustion temperature, providing additional reaction sites for sulfation. In this short-term test, calcium utilization of the partially sulfated sorbent before water treatment was ∿23% and was ∿40% upon reuse of the water-treated partially sulfated sorbent, an increase of ∿74%.

Corrosion Studies. There is concern that volatilization of sulfation-enhancement agents (alkali metal compounds) in a commercial fluidized-bed coal combustion system might cause unacceptable corrosion of the metal structural materials. To measure the corrosion rates of candidate metals of construction in the presence of sulfation-enhancement agents in a PDU-scale unit and identify factors that could decrease the lifetime and reliability of system components, long-term (>100 h) corrosion test runs are being conducted in the AFBC. Objectives of experimental programs are (a) to evaluate the effect of sulfation-enhancement agents on the corrosion behavior of candidate materials for an atmospheric-pressure fluidized-bed combustion system, (b) to determine the types of deposits formed on metal surfaces, (c) to study the nature of the corrosion reactions resulting from these deposits, and (d) to correlate the corrosion results with process conditions.

100-h Corrosion Tests. Four 100-h corrosion test runs (CT-1, -2, -3, and -4) were completed in the recently constructed PDU-scale atmospheric-pressure fluidized-bed coal combustion facility (AFBC). In each run, seven corrosion probes, each holding seven metal specimens, were installed at various locations in the bed and the freeboard section of the combustor. Three of the probes in each run were the air-cooled type, and the remaining four probes were the uncooled coupon type. The types of metal specimens (24 different alloys), their locations in the combustor, and the mean temperatures for each of the seven corrosion probes used in each run are reported.

The sorbent used in the four runs was Grove limestone. No sulfation-enhancement agent was added in Run CT-1, ∿0.3 mol % $CaCl_2$ was added in Run CT-2, ∿0.5 mol % NaCl in Run CT-3, and ∿1.9 mol % Na_2CO_3 in Run CT-4. The Ca/S mole ratio in each run was adjusted to maintain ∿700 ppm SO_2 in the dry off-gas (equivalent to ∿85% sulfur retention). The resultant Ca/S mole ratios were 3.4, 3.5, 3.6, and 2.0 for Runs CT-1, -2, -3, and -4, respectively. Neither the low-concentration addition of $CaCl_2$ in Run CT-2 nor of NaCl in Run CT-3 enhanced the sulfation of the Grove limestone sorbent. These results, relative to sulfation enhancement, disagree with those of previously reported laboratory-scale experiments in which a simulated flue gas was used (*i.e.*, with no actual coal combustion). However, the high-concentration addition of Na_2CO_3 in Run CT-4 did enhance sulfation of the Grove limestone sorbent. The Ca/S mole ratio of 2.0 in the latter run is ∿41% less than the Ca/S ratio of 3.4 in Run CT-1 conducted with untreated Grove limestone sorbent.

Carbon, sulfur, and calcium material balances are reported for the four 100-h corrosion test runs (CT-1, -2, -3, and -4), as well as combustion efficiencies. Carbon balances ranged from 89 to 102%, sulfur balances from 88 to 111%, and calcium balances from 98 to 109%. Calculated combustion efficiencies were 88% in the first and third runs, 87% in the second run, and 91% in the fourth run.,

Evaluation of Corrosion Behavior. Metallographic examination of the specimens from 100-h screening corrosion tests (CT-1 to CT-4) has been completed. The results indicate that at ∿850°C, the addition of 0.3 mol % $CaCl_2$ to the sorbent feed had no effect on the corrosion behavior of the various candidate materials tested, whereas 0.5 mol % NaCl or 1.9 mol % Na_2CO_3 increased the corrosion rates of the nickel-base alloys. When specimens were exposed in the fluidized bed or the freeboard section of the combustor at temperatures between 525 and 730°C, the addition of a sulfation-enhancement agent, *viz.*, 0.3 mol % $CaCl_2$, 0.5 mol % NaCl or 1.9 mol % Na_2CO_3, had no significant effect on the corrosion rates of the materials tested. Except in the high-chromium alloys (>15%), the specimens developed only 2- to 3-μm-thick surface scale and 2- to 5-μm internal corrosive penetration; for the high-chromium alloys, the total scale penetration thickness was significantly greater, independent of the presence of salt.

TASK A. ENHANCEMENT OF LIMESTONE SULFATION BY CHEMICAL ADDITIVES

1. Laboratory Studies

(J. A. Shearer, C. B. Turner, and K. M. Myles)

Among the effects of chemical additives on the sulfation of limestones are major changes in the physical structure of the stones. Scanning electron microscopy has been successfully used in conjunction with mercury porosimeter data to describe in detail the changes that occur (after salt addition) during calcination and sulfation of limestones.

a. Effect of NaCl Additive on Particle Structure of Limestone

The use of NaCl as a sulfation enhancer has received most of the experimental attention.[1] A mechanism has been proposed involving the formation of trace amounts of liquid phase that lowers the activation energy of decomposition and recrystallization, thus accelerating the ionic rearrangement and development of porosity in the lime produced. Whether a liquid or vapor phase forms is uncertain. The SEM photographs in Fig. 1 provide a partial answer. Figure 1 shows two views of a calcite spar particle treated with a minute amount of NaCl. The salt crystallized as discrete crystals during treatment. Upon heating at 850°C for 40 min, the particles formed a liquid which interacted in a gradually enlarging sphere around the point of contact with the calcite crystal. The presence of a vapor phase would have produced a more uniform attack over the entire sample. Radiating circles of lessening structural changes strongly suggest a local liquid phase interaction around the salt particle.

In the case of NaCl addition, substantial solution of CaO does not occur upon the addition of large amounts of salt to a structure that is still space-restrictive to $CaSO_4$ formation beyond about 50% conversion.

Figure 2 is a series of photographs showing the effect of sodium chloride addition on a previously sulfated sample of ANL-9501 stone (Grove limestone). Figures 2-I and 2-Ia show a sample of untreated ANL-9501 stone completely sulfated at 850°C with 0.3% SO_2; a dense layer of $CaSO_4$ formed at the particle surface, as indicated by the sulfur scan in Fig. 2-Ia. Figure 2-II shows this same sample after treatment with a small amount of powdered NaCl and reheating. The structure definitely altered, and pores are much larger. Figure 2-IIa shows the deep penetration of sulfur into the stone. The enhanced mobility of the system contributed by the low-melting salt caused the $CaSO_4$ to migrate to the particle interior and to undergo massive recrystallization, as shown in the more highly magnified view (Fig. 2-III). This phenomenon explains the effects of NaCl in renewing the sulfur-removal capabilities of spent bed material, as reported by Pope, Evans, and Robbins.[2] In the treated material, the dense diffusion-limiting layer of $CaSO_4$ is no longer intact and, with major growth in pore size, there is a more favorable pore distribution for further sulfur capture.

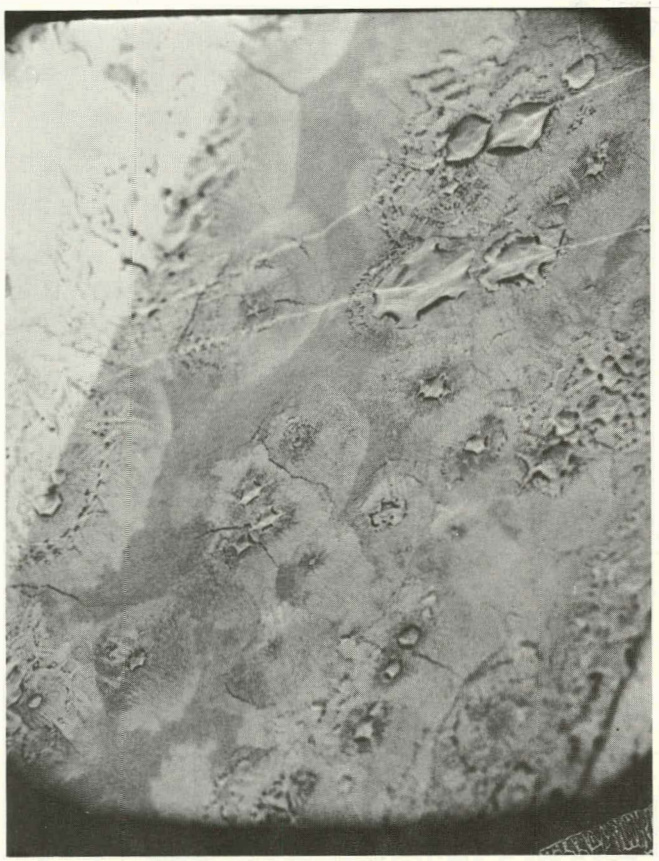

(260X)

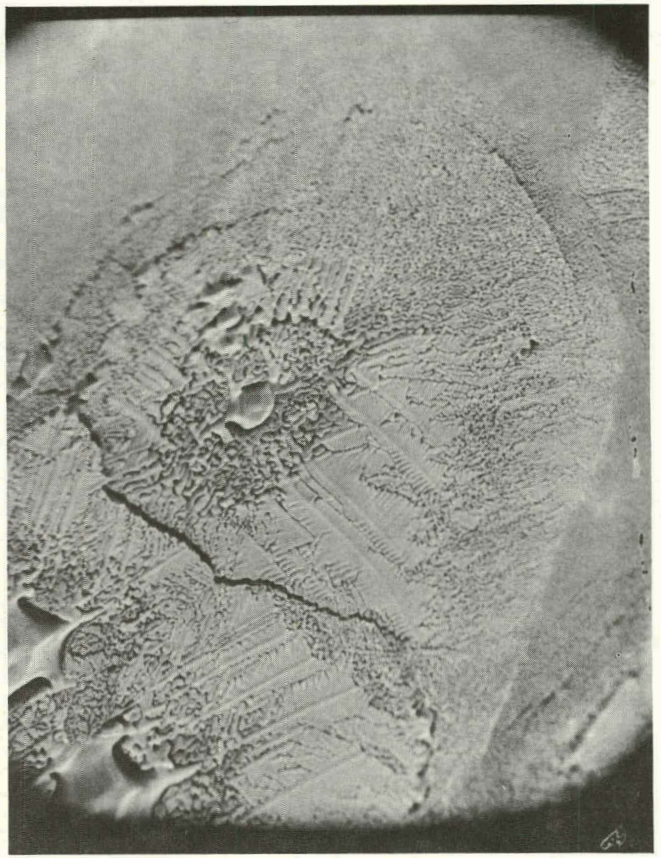

(1300X)

Fig. 1. Surface of Calcite Spar Particle (two views), Calcined with 0.2 wt % NaCl in 20% CO_2, 5% O_2, and the Balance N_2 at 850°C for 40 min. ANL Neg. No. 308-78-418

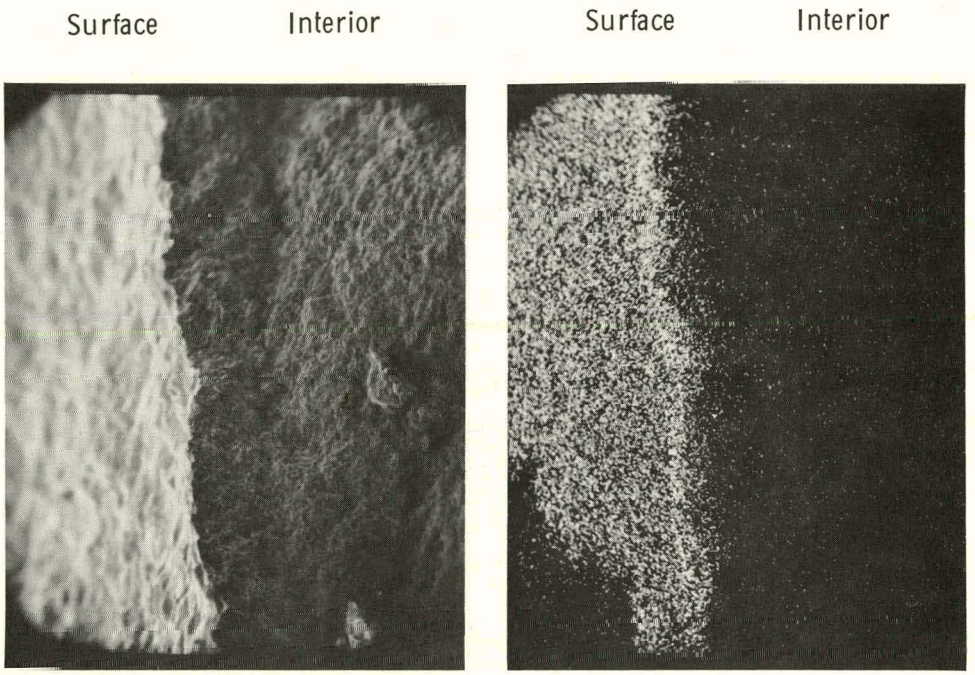

I 9501 Calcined 1 h
Sulfated 2 h
Reheated 2 h
385X

Ia Sulfur Scan
of I
385X

Fig. 7. Effects of Heating with NaCl on a Sample of ANL-9501 Stone (Cross Sections) Previously Sulfated at 850°C for 6 h in 0.3% SO_2, 5% O_2, 20% CO_2, and the Balance N_2. ANL Neg. No. 308-78-758

(Contd)

II

Surface Interior

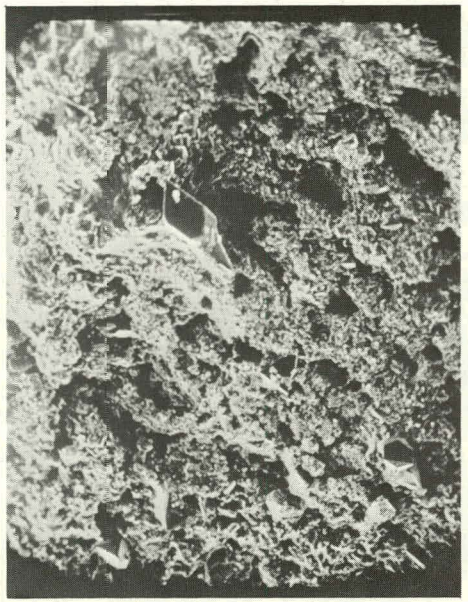

9501 Calcined 1 h
Sulfated 2 h
Reheated with NaCl 2 h
385X

IIa

Surface Interior

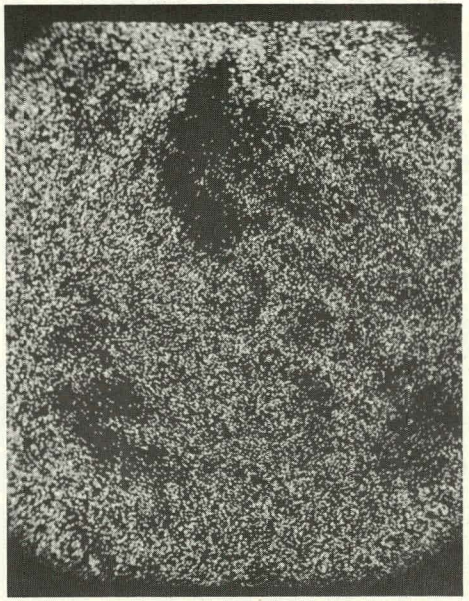

Sulfur Scan
of II
385X

III

Surface Interior

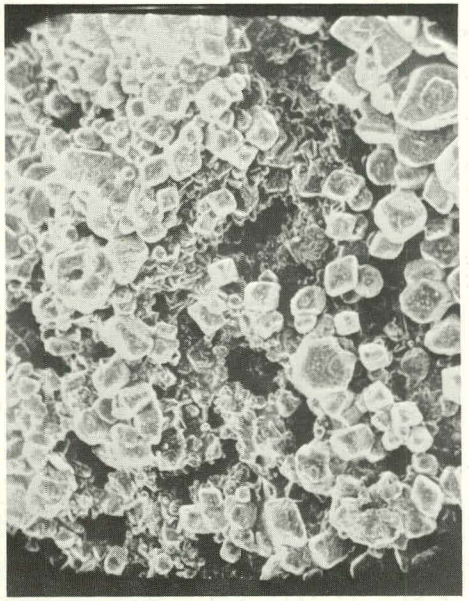

9501 Calcined 1 h
Sulfated 2 h
Reheated with NaCl 2 h
770X

Fig. 2. (Contd)

b. Effect of $CaCl_2$ Additive on Particle Structure of Limestone

As part of this study, scanning electron microphotographs (SEM) were taken for visual confirmation of structural changes indicated by previous porosimetry measurements. Figure 3 shows calcite spar which has been calcined after a very small addition of $CaCl_2$. The intent here was to isolate individual particles of the salt and to note the effects on the limestone of the intense recrystallization occurring during calcination when $CaCl_2$ is present. The salt's effectiveness decreases from the point of contact and appears to follow structural lines of the original rhombic calcite particle. The effect on pore structure is evident--even at a distance from the point of immediate contact. Initial melting of the $CaCl_2$ strongly affected the stone at the point of contact. As a result, a single large crystal of CaO formed having visible growth rings, as in Fig. 3b.

Figure 4 is a series of microphotographs of ANL 9701 stone calcined with various amounts of $CaCl_2$. The same structural changes as in calcite (Fig. 3) are observed, modified by the impurities and the less crystalline nature of this limestone. At the highest concentration of salt (1.0 mol % $CaCl_2$), crystal growth begins to be evident, as well as initial fusion of particles. This fusion is a result of sufficient $CaCl_2$ liquid being present to dissolve substantial amounts of CaO, with subsequent loss of structural integrity. At this level of salt addition, conversion to $CaSO_4$ does not depend on the space created by initial decarbonation but can continue indefinitely since dissolution of CaO and loss of structural integrity make the CaO readily available for sulfation.

Figure 5 illustrates the effect of adding various amounts of $CaCl_2$ and calcining ANL-9501 (Grove) limestone, a commonly used limestone. Also illustrated are two samples calcined without additive for different lengths of time. Firing for a long duration has the effect of increasing the porosity, as indicated by Fig. 5b, which shows uniform pores over the entire particle. These pores are larger than those produced by one hour firing as in Fig. 5a.

The addition of small amounts of $CaCl_2$ has a much greater effect than does the addition of small amounts of NaCl. Extensive pore growth and crystallite clumping occurred similarly to the effects of NaCl addition in large amounts, as shown in photographs presented earlier. As the concentration of $CaCl_2$ increased, the extent of crystal growth increased and pore size gradually increased. At levels of salt addition greater than 1 mol % $CaCl_2$, the lime particles began to fuse. At this point, large amounts of liquid phase formed that were capable of dissolving substantial amounts of CaO, as shown by the phase diagram for this system.[3] Figure 6 illustrates this characteristic flow structure in ANL-9501 limestone. Figures 6b and 6c show the junction of two separate limestone particles at two magnifications. The point of contact is between the darker image and the lighter one. The particles have fused, yet retain some coarse porosity. At the sulfation temperature, this is a very fluid system containing dissolved CaO and hence has great potential to react with SO_2/O_2 mixtures. The extent of reaction is limited only by the presence of sufficient liquid phase to dissolve residual unreacted CaO.

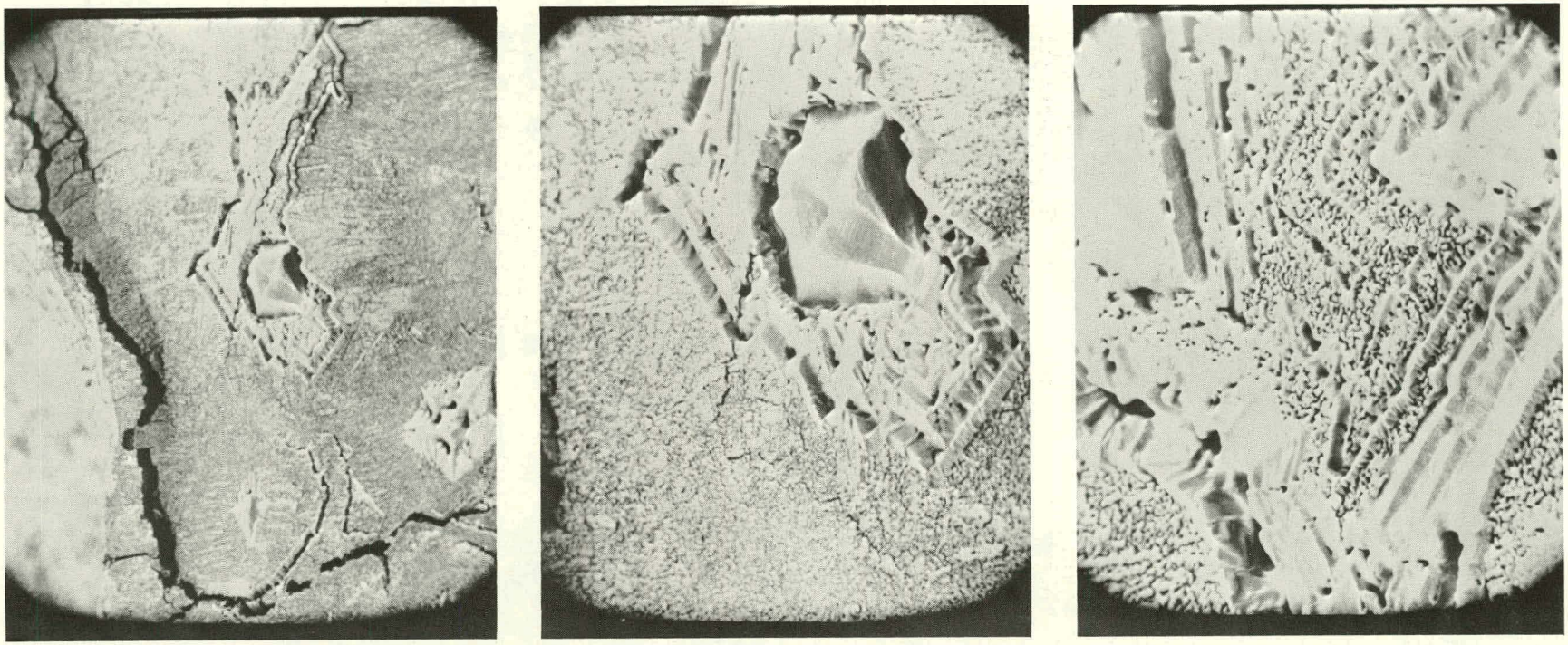

a
181X

b
451X

c
902X

Fig. 3. Cross Sections of Calcite Spar Calcined with 0.05 mol % $CaCl_2$ at 850°C in 5% O_2, 20% CO_2, and the Balance N_2. ANL Neg. No. 308-78-639

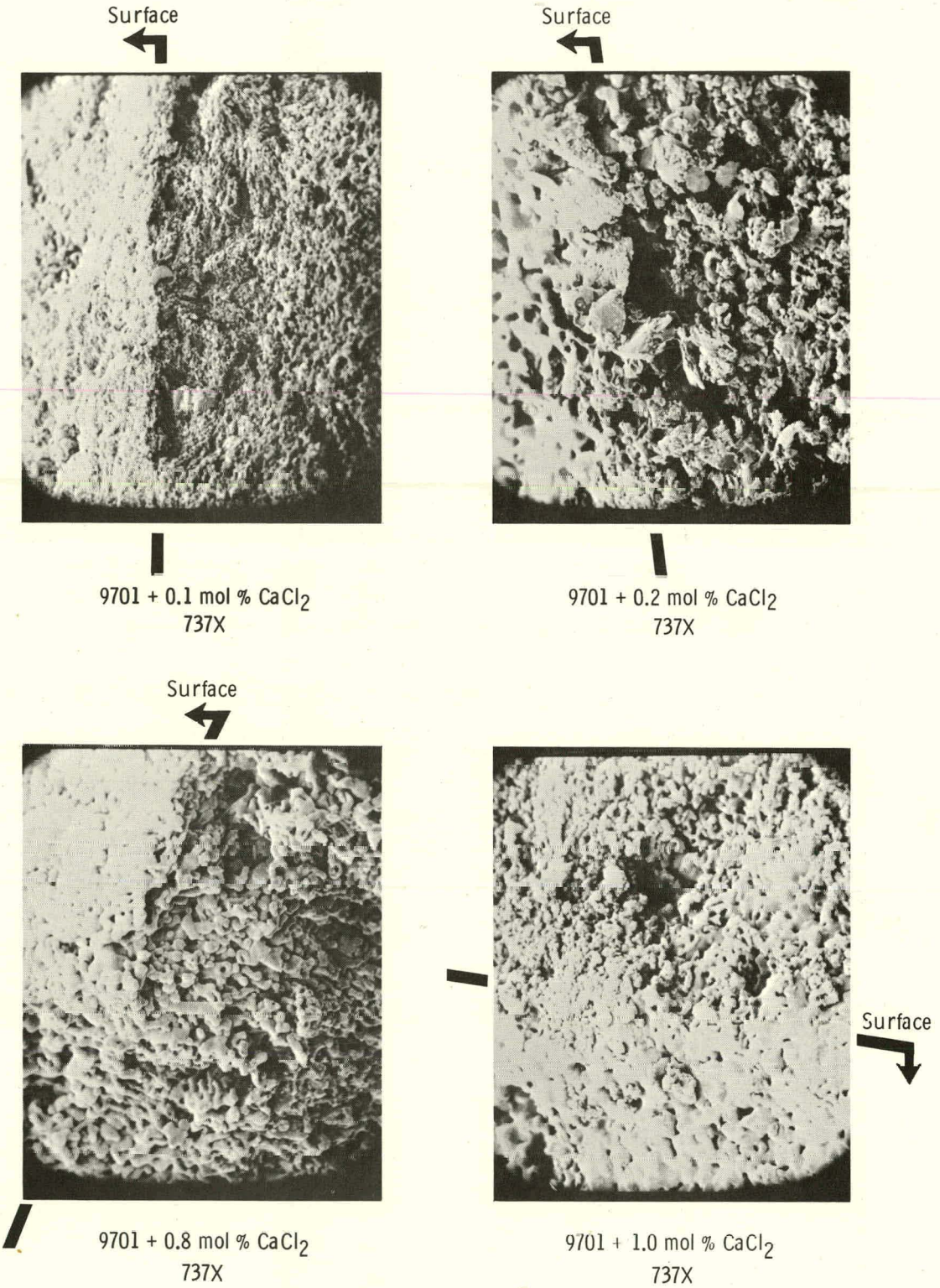

Fig. 4. Effect of $CaCl_2$ on ANL-9701 Stone (Cross Sections) Calcined at 850°C for 1 h in 5% O_2, 20% CO_2, and the Balance N_2. ANL Neg. No. 308-78-640

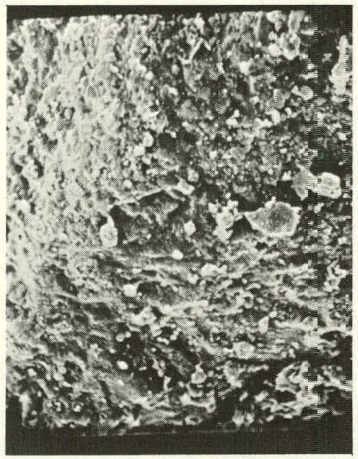

(a) 9501 Calcined 2 h
700X

(b) 9501 Calcined 6 h
700X

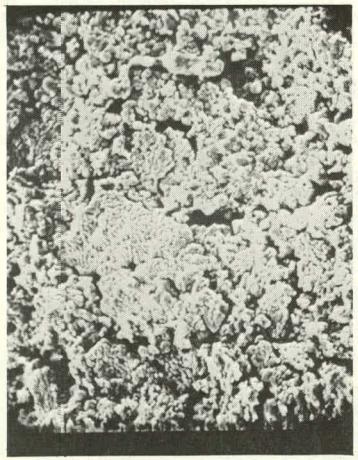

(c) 9501 + 0.1 mol % $CaCl_2$
Calcined 1 h
700X

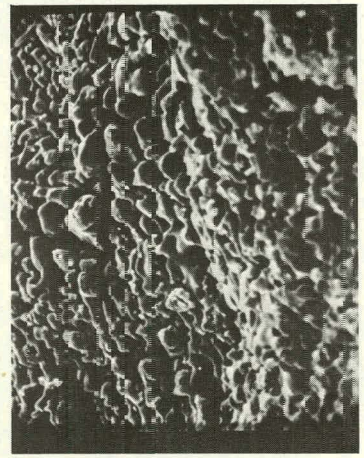

(d) 9501 + 0.5 mol % $CaCl_2$
Calcined 1 h
650X

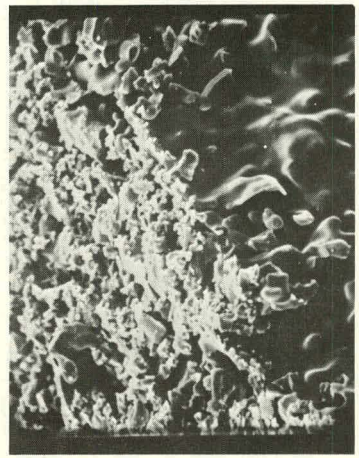

(e) 9501 + 1.0 mol % $CaCl_2$
Calcined 1 h
675X

Fig. 5. Cross Sections of Limestone ANL-9501 Particles After Various Treatments and Calcination at 850°C in 5% O_2, 20% CO_2, and the Balance N_2. ANL Neg. No. 308-78-420

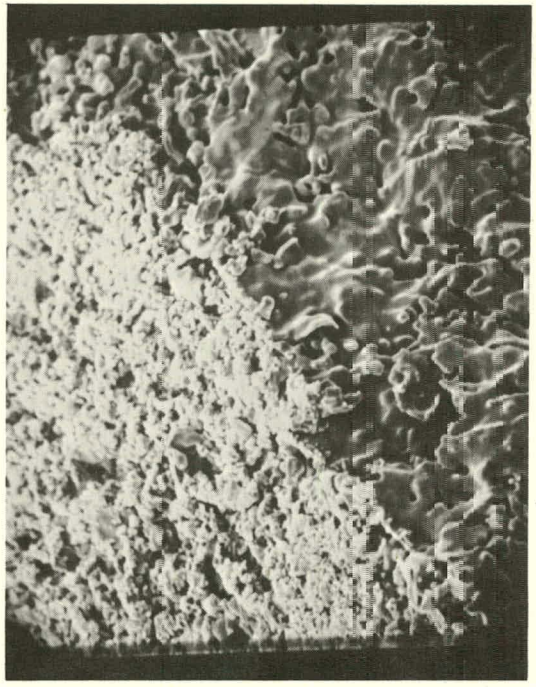

(a) 9501 + 1.0 Mol % $CaCl_2$
520X

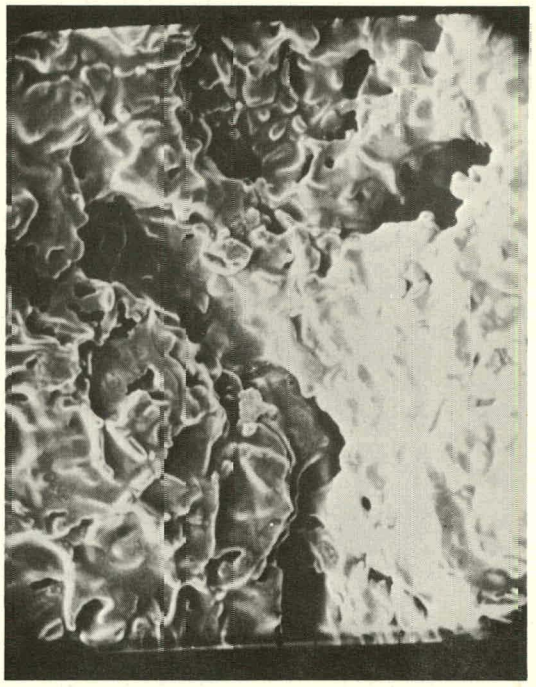

(b) 9501 + 2.0% $CaCl_2$
Junction of Two Particles
520X

(c) 9501 + 2.0% $CaCl_2$
Junction of Two Particles
1920X

Fig. 6. Limestone ANL-9501 with $CaCl_2$. Calcined 1 h at 850°C in 5% O_2, 20% CO_2, and the Balance N_2. ANL Neg. No. 308-78-419

Sulfation experiments show that indeed, there is one maximum of sulfation (at 50% conversion) at low salt concentrations; conversion then starts to decrease when these low $CaCl_2$ additions are exceeded. At $CaCl_2$ concentrations above 1.0 mol %, however, the extent of sulfation begins to increase rapidly; with continued $CaCl_2$ addition, sulfation approaches 100%. Practical application of this information is limited since the high salt concentrations produce sticky particles that may cause problems in maintaining fluidization in a fluid-bed combustor. However, $CaCl_2$ added to limestone powder that was injected into fixed-bed combustors has enhanced the sulfation, removing sulfur from exhaust gases at very high temperatures (>1000°C).[1]

c. Effect of Calcium Chloride Additive on Sulfation of and Particle Structure of Dolomites

The experimental work with enhancement agents has been primarily concerned with limestones, but dolomites also are under consideration as sulfur-capturing species. Addition of inorganic salts to dolomites that are very unreactive to increase their reactivity may be of interest.

Most dolomites react readily with SO_2. Apparently, at the conditions existing in a fluidized-bed coal combustor, the porosity of the stones is enhanced by decomposition of $MgCO_3$ to form MgO (which is unreactive with SO_2).

Horizontal tube furnaces supplied with a simulated flue gas are being used to establish sulfation capacities for a series of precalcined dolomites treated with $CaCl_2$. Measurements with a mercury porosimeter on similarly prepared calcines are also currently under way. Table 1 lists percent conversions for several stones treated with 0, 0.1, 0.5, 1.0, 3.0, and 5.0 mol % $CaCl_2$ (treated by adding an aqueous slurry and then evaporating). The percent conversions were arrived at from final weight-change measurements and are subject to correction when analyses for sulfate are completed. The data show that salt addition tends to enhance sulfation--both at low concentrations (0.1 to 0.5 mol %) and at higher concentrations ($\geq$3.0 mol %). The lower conversion for the intermediate addition of salt has been ascribed to the initial increase in porosity (by increased ionic mobility) being offset by a concomitant decrease in surface area. The second gradual increase in conversion is due to dissolution of CaO in the large amount of liquid salt present, a situation in which the reactivity of the lime is not limited by structural restrictions.

Figures 7-9 show scanning electron microphotographs of cross sections of three dolomites that had been treated with several concentrations of $CaCl_2$. They illustrate that with very high concentrations of salt (as in Fig. 9 for dolomite ANL-5601 with 5 mol % $CaCl_2$), average pore size increases dramatically and fused structures develop. Even a trace of $CaCl_2$ (0.1 mol %) causes noticeable pore enlargement, increasing the sulfation capacity of the stones. Dolomite ANL-5601, an especially unreactive stone in its microporous original state, responds to salt treatment with dramatic pore enlargement and consequent enhanced sulfation. This type of highly crystalline stone, which forms a calcine having very small pores, is the sort of dolomite most benefitted by salt addition, which affects the pore size of the calcined stone.

Table 1. Conversion of CaO to $CaSO_4$ for Dolomites Treated with Calcium Chloride

Stone Designation	Percent Conversion, CaO to $CaSO_4$[a]				
	Untreated Stone	0.1 mol % $CaCl_2$ Added	0.5 mol % $CaCl_2$ Added	1.0 mol % $CaCl_2$ Added	3.0 mol % $CaCl_2$ Added	5.0 mol % $CaCl_2$ Added
ANL-4801	79.7	>100.00	99.4	80.8	72.3	89.7
ANL-4902	92.0	>100.00	94.0	70.9	69.7	77.1
ANL-4903	77.9	83.9	82.2	76.9	77.8	97.8
ANL-5101[b]	88.6	99.3	96.8	88.6	85.8	90.7
ANL-5102	76.7	79.8	71.7	67.3	81.7	93.6
ANL-5201	76.0	80.7	76.6	58.7	55.1	88.7
ANL-5207	46.3	48.8	35.7	49.6	55.9	64.5
ANL-5501	31.0	33.9	38.7	37.1	43.9	54.5
ANL-5601	18.1	23.8	54.6	46.8	56.1	57.0

[a]All stones calcined for 1 h at 850°C in 5% O_2, 20% CO_2, and the balance N_2, and sulfated in 0.3% SO_2, 5% O_2, 20% CO_2, and the balance N_2 for 6 h at 850°C.

[b]Tymochtee dolomite.

Very reactive stones do not show as great a percent increase in reactivity as a result of salt addition, although the enhancement of reaction rate achievable by salt addition may be important in a commercial-scale combustor system. For dolomites, enhancement of reactivity by very high $CaCl_2$ additions can lead to almost complete sulfation of the CaO component.

d. Summary of Percent Conversions to Sulfate for Treated and Untreated Dolomites

Table 2 lists analyses and percent conversions of CaO to $CaSO_4$ for untreated dolomites included in this study. $CaCO_3$ content ranges from 48.7% to 67.3%, with the major secondary component, $MgCO_3$, ranging from 27.7% to 45.7%. Sulfation at 850°C in 0.3% SO_2, 5% O_2, 20% CO_2, and the balance N_2, has been measured for all stones; it ranges from 18.1% to 92.0% conversion.

Figure 10 shows the conversion of CaO to $CaSO_4$ for the dolomites at various added NaCl concentrations. The geometric mean at each salt concentration is included as a curve covering the entire range of salt addition. The data show marked similarity to earlier reported work on NaCl effects on limestones[4] in that a maximum sulfation occurs at low concentrations of salt, after which sulfation decreases at higher levels of salt addition as surface area declines, and then reactivity again increases when sufficient liquid is present to begin to dissolve and disrupt the restraining lattice structure.

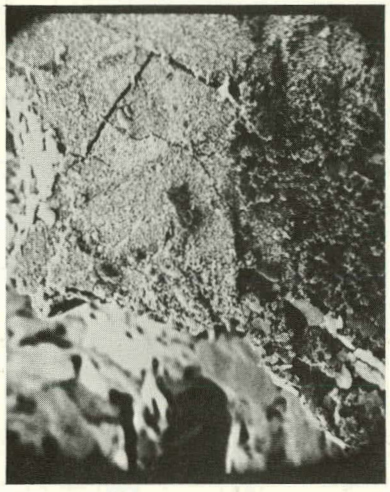

5101 Calcined 1h 850°C
638X

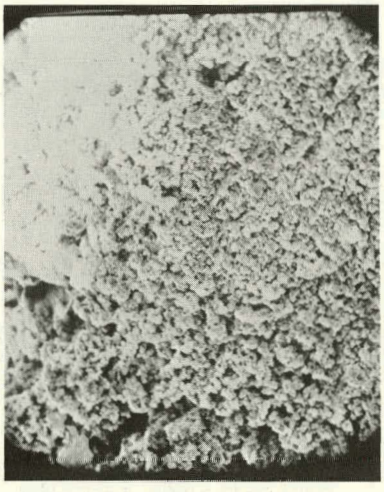

5101 + 0.1 mol % $CaCl_2$
Calcined 1h 850°C
638X

5101 + 2.0 mol % $CaCl_2$
Calcined 1h 850°C
638X

5101 + 5.0 mol % $CaCl_2$
Calcined 1h 850°C
638X

Fig. 7. Cross Sections of Untreated ANL-5101 Dolomite Particles and ANL-5101 Particles Treated with $CaCl_2$. Calcined at 850°C. ANL Neg. No. 308-78-684

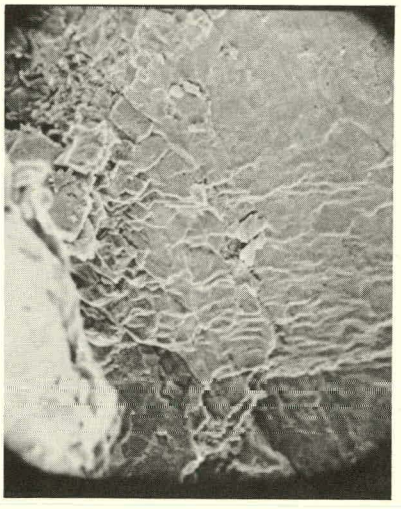

5401 Calcined
1h 850°C
1276X

5401 + 0.1 mol % $CaCl_2$
Calcined 1h 850°C
1276X

5401 + 0.5 mol % $CaCl_2$
Calcined 1h 850°C
1276X

5401 + 3 mol % $CaCl_2$
Calcined 1h 850°C
1276X

5401 + 5 mol % $CaCl_2$
Calcined 1h 850°C
1276X

Fig. 8. Cross Sections of Untreated ANL-5401 Dolomite Particles and ANL-5401 Particles Treated with $CaCl_2$. Calcined at 850°C. ANL Neg. No. 308-78-685

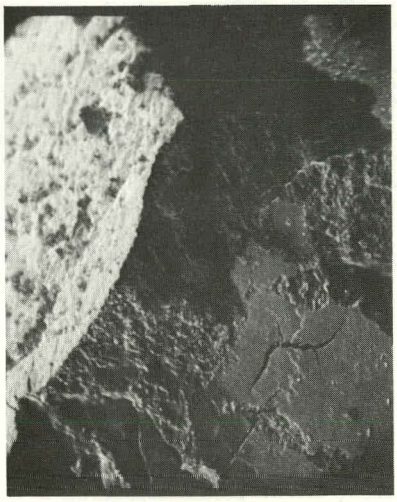

5601 Calcined
1h 850°C
638X

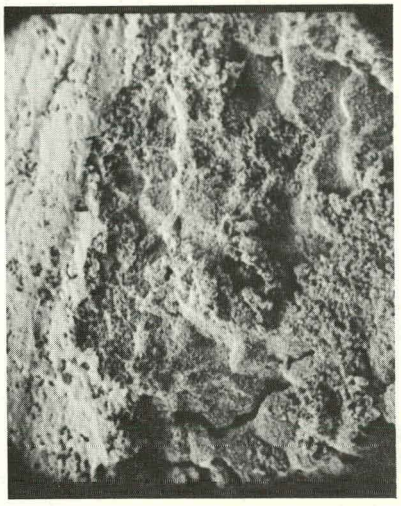

5601 + 0.1 mol % $CaCl_2$
Calcined 1h 850°C
638X

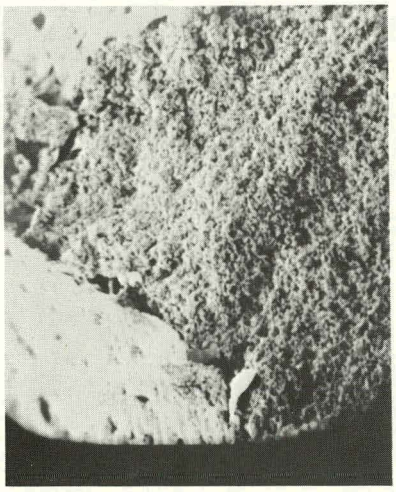

5601 + 0.5 mol % $CaCl_2$
Calcined 1h 850°C
638X

5601 + 1.0 mol % $CaCl_2$
Calcined 1h 850°C
638X

5601 + 5.0 mol % $CaCl_2$
Calcined 1h 850°C
638X

Fig. 9. Cross Sections of Untreated ANL-5601 Dolomite Particles and ANL-5601 Particles Treated with $CaCl_2$. Calcined at 850°C. ANL Neg. No. 308-78-683

Table 2. Compositions[a] and Conversions to Sulfate of Dolomite Samples

Stone Designation, ANL-	$CaCO_3$, wt %	$MgCO_3$, wt %	Fe_2O_3, wt %	Al_2O_3, wt %	SiO_2, wt %	Na_2O, wt %	K_2O, wt %	Σ wt %	Conversion[b] To Sulfate, %
4801	48.7	40.2	0.66	1.81	7.0	0.09	0.38	98.84	79.7
4902	49.7	43.8	0.43	0.87	5.71	0.03	0.30	100.84	92.0
4903	49.2	44.6	0.52	0.80	8.77	0.05	0.50	104.44	77.9
5101	51.8	43.3	0.41	1.46	3.61	0.07	0.22	100.87	88.6
5102	51.2	43.4	0.62	0.43	1.18	0.05	0.19	97.07	76.7
5201	52.2	43.0	0.26	0.68	1.22	0.07	0.13	97.56	76.0
5202	52.7	42.0	0.34	0.87	1.60	0.11	0.15	97.77	72.6
5203	52.6	36.4	0.58	1.13	8.77	0.04	0.18	99.70	78.4
5207	52.3	36.5	2.35	1.00	3.64	0.09	0.16	97.04	46.3
5301	53.4	45.4	0.07	0.08	0.69	0.05	0.03	99.72	79.3
5401	54.5	42.9	0.07	0.34	1.04	0.04	0.10	98.99	39.8
5402	60.0	27.7	5.30	3.06	6.29	0.24	0.43	103.02	89.9
5501	55.6	43.3	0.23	0.18	2.97	0.03	0.03	102.34	24.8
5601	56.9	45.7	0.09	0.01	0.18	0.02	0.01	102.91	18.1
6101	61.2	28.7	5.56	0.51	3.15	0.13	0.18	99.43	63.7
6301	63.2	32.6	0.39	0.28	2.54	0.04	0.05	99.10	57.6
6401	64.2	29.5	0.33	0.59	5.10	0.15	0.31	100.28	30.0
6701	67.3	31.5	0.37	0.22	1.25	0.04	0.05	100.73	65.6

[a] Analyses performed by Analytical Chemistry Laboratory, Argonne National Laboratory.

[b] In a tube furnace at 850°C, in 0.3% SO_2, 5% O_2, 20% CO_2, and the balance N_2.

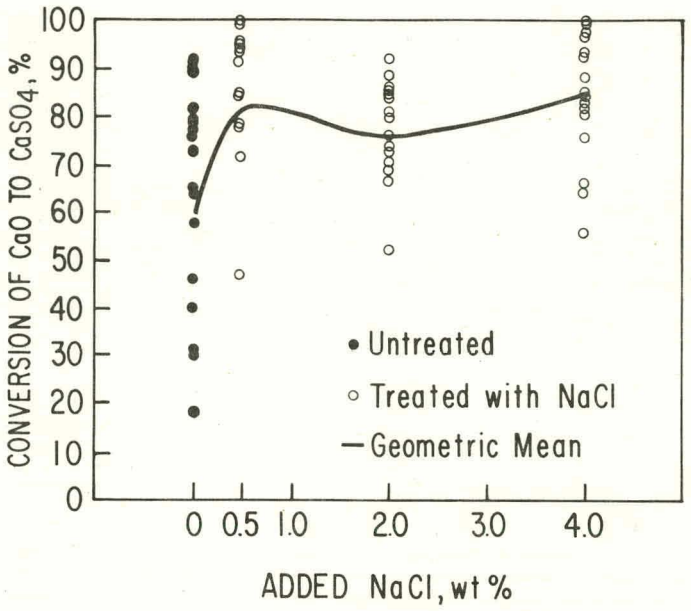

Fig. 10. Conversion to Sulfate for Dolomites Precalcined with NaCl and Sulfated 6 h at 850°C in 0.3% SO_2, 5% O_2, 20% CO_2, and the Balance N_2

This allows the formation of additional $CaSO_4$, previously prevented by volumetric limitations. The enormous variability in the reactivity of the untreated dolomites is carried over to the salt-treated samples with a lesser spread. The shape of the curve of geometric means is also the shape of the curve for each stone, though the curves for the latter differ in magnitude of increase or decrease. The reactivity of the most unreactive dolomites is most dramatically increased by salt addition. Naturally reactive stones have an inherent pore structure that readily accepts the large $CaSO_4$ molecules. For this same reason, the overall reactivity of dolomites (in relation to their $CaCO_3$ content) is much higher than for limestones.

Figure 11 shows a similar set of data points for $CaCl_2$-treated dolomites. The trends in reactivity are the same as for NaCl at increasing salt concentrations. When compared on the basis of weight percent salt added, $CaCl_2$ has less effect than NaCl. However, at low salt concentrations, $CaCl_2$ has a greater effect on a mol % basis than NaCl. Again, the scatter associated with natural stones carries over to the salt-treated stones, but becomes less important as the amount of salt added increases and residual structural and compositional differences are removed.

Porosimetry curves have been completed for all precalcined stones and for the various salt-treated dolomites. These data will be included in a forthcoming guide to limestone characteristics and reactivities.

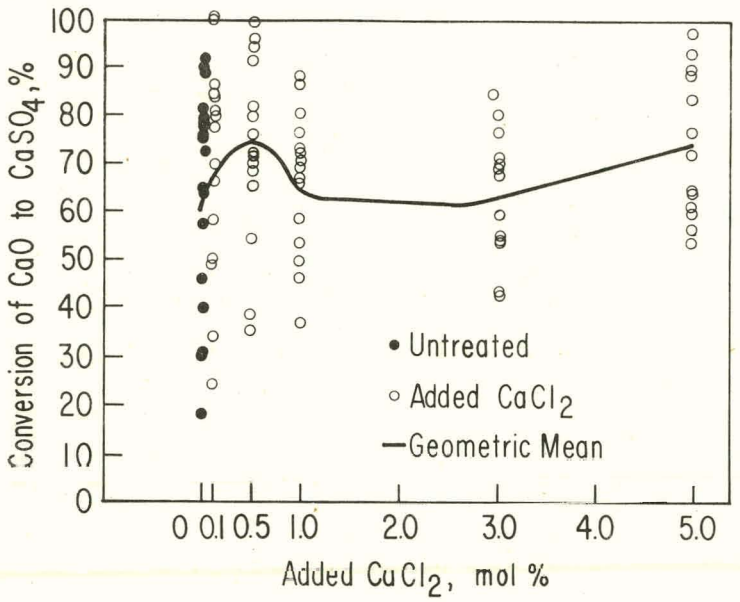

Fig. 11. Conversion to Sulfate for Dolomites Precalcined with $CaCl_2$ and Sulfated 6 h at 850°C in 0.3% SO_2, 5% O_2, 20% CO_2, and the Balance N_2

e. Effect of Na_2CO_3 Additive on Sulfation of Limestones

In addition to sodium chloride and calcium chloride, other salts were investigated as additives for possible positive effects on the sulfation of limestone. It had been found in materials corrosion studies that the major attack by NaCl and $CaCl_2$ was through the chloride ion (ANL/CEN/FE-78-10). Sodium carbonate showed promising effects in some early screening experiments, and it is hoped that this salt would cause considerably less corrosion of materials in a fluidized-bed coal combustor than would the chlorides.

Figure 12 is a bar graph summarizing the data for three limestones treated with various amounts of Na_2CO_3. Also included are data for ANL-8001 stone treated with Na_2CO_3 and then simultaneously calcined and sulfated; in contrast, the rest of the sulfation data is for precalcined material, as is most of the data presented for other salts. The data show marked positive effects due to small additions of Na_2CO_3 on all three stones. The effects occurred most readily in ANL-8001 stone, which has the highest impurity content and the smallest initial grain size. However, under simultaneous calcination/sulfation conditions, the same stone requires a much larger amount of salt to obtain the same conversion.

Scanning electron microphotographs have been made of laboratory-prepared calcines treated with Na_2CO_3. Figure 13 shows the effect of trace amounts (0.2 wt %) of Na_2CO_3 evaporated on the surface of a calcite spar crystal and calcined at 850°C in 5% O_2, 20% CO_2, and the balance N_2. The linear features illustrate preferential deposition and interaction along a

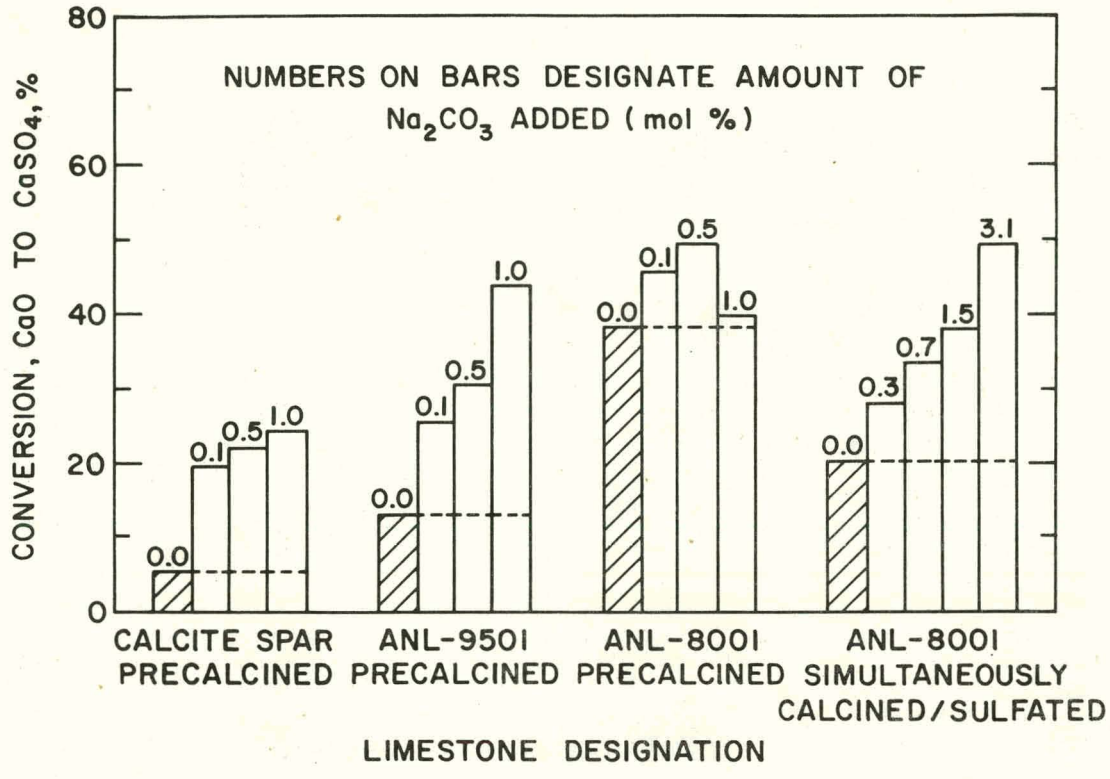

Fig. 12. Effect of Na_2CO_3 on Sulfation of Limestone at 850°C in 0.3% SO_2, 5% O_2, 20% CO_2, and the Balance N_2

cleavage plane of the crystal. The three-dimensionality of the photograph clearly shows the penetration of the fused salt into the crystal, causing increased ionic diffusion with resulting pore structure changes. The photographs are similar to those obtained in earlier reported work with NaCl and $CaCl_2$. Since Na_2CO_3 is less volatile than NaCl or $CaCl_2$, there was a longer contact time with the stone as a liquid phase.

Figure 14 illustrates the effect of Na_2CO_3 on limestone ANL-9501 during calcination at 850°C. An increasingly open nature of the pore structure as the Na_2CO_3 concentration increased is apparent. The surface of the particle (which is on the left and lower side of each photograph) shows enhanced crystallization due to the increased contact time with the salt at the beginning of calcination.

Structural changes as a result of $CaCO_3$ addition differ for different limestones, as shown in Fig. 15. These four limestones have different impurity contents, as shown by the first two digits of their number designations (which indicate nominal wt % $CaCO_3$ content before firing). Impurities interfere with the growth of pores and with the recrystallization of the CaO. This is illustrated by comparison of the continuous rounded nature of grains in the matrix of calcite spar with the discontinuous angular grain arrangement of the less pure ANL-8001 limestone, in which impurities migrated to the surface of the recrystallizing CaO.

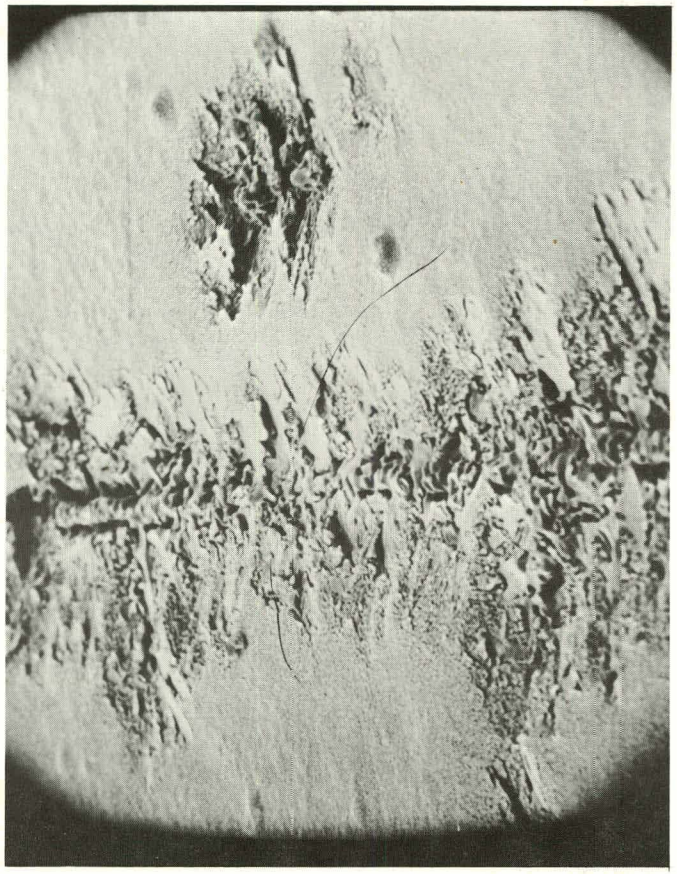

550X

2600X

Fig. 13. Calcite Plus 0.2 wt % Na_2CO_3 after Calcination 1 h at 850°C in 5.0% O_2, 20% CO_2, and the Balance N_2. ANL Neg. No. 308-79-55

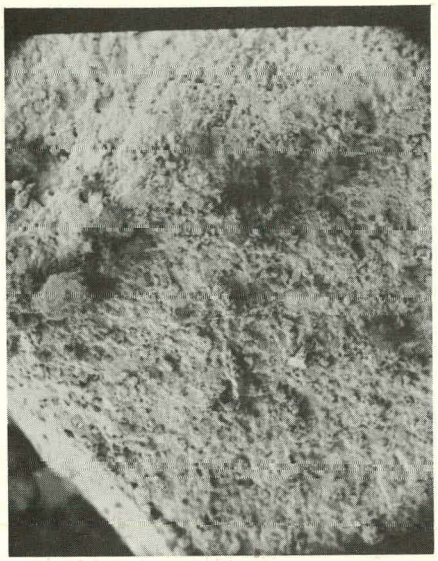

ANL-9501
369X

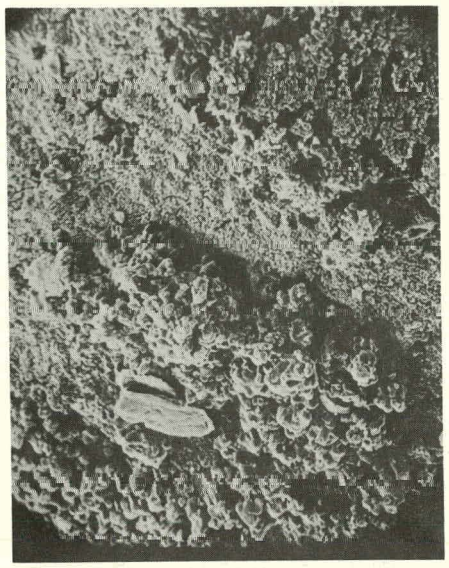

ANL-9501 + 0.5 mol %
Na_2CO_3
369X

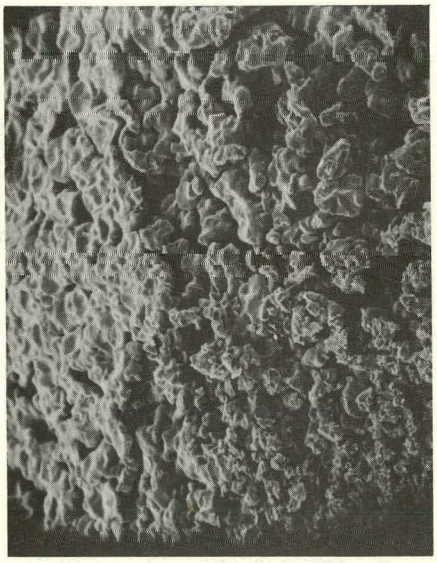

ANL-9501 + 1.0 mol %
Na_2CO_3
369X

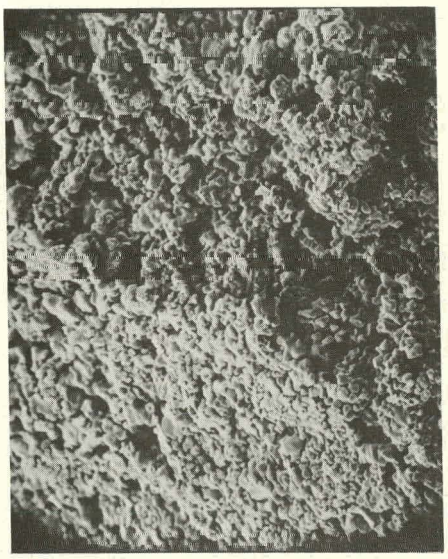

ANL-9501 + 2.0 mol %
Na_2CO_3
369X

Fig. 14. Cross Sections of ANL-9501 (1359, Grove) Limestone Particles Containing Na_2CO_3 Additive. Calcined 1 h at 850°C in 5% O_2, 20% CO_2, and the Balance N_2. ANL Neg. No. 308-79-72

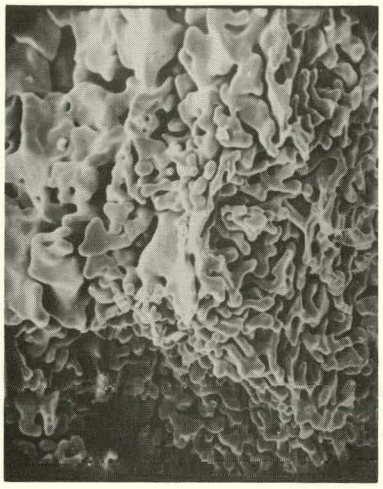

Calcite Spar
638X

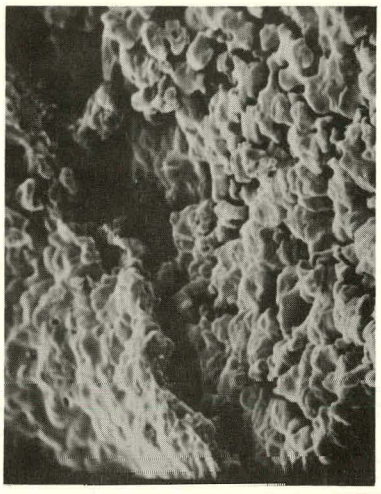

ANL-9501
(1359, Grove)
638X

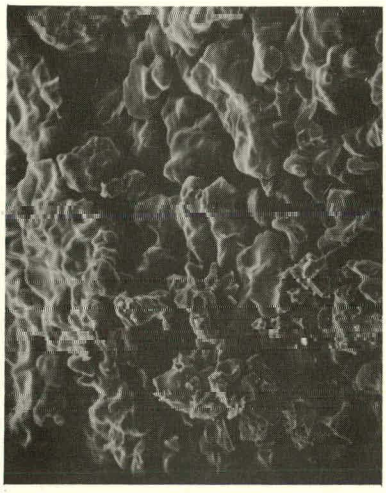

ANL-9701
(Germany Valley)
638X

ANL-8001
(Greer)
638X

Fig. 15. Cross Sections of Limestone Particles, Each Treated with 2.0% Na_2CO_3 and Fired at 850°C 1 h in 5% O_2, 20% CO_2, and the Balance N_2. ANL Neg. No. 308-79-68

In conjunction with the sulfation experiments using Na_2CO_3 as a sulfation enhancement agent, porosity distribution measurements were done using a mercury porosimeter. The sulfation results reported earlier in Fig. 12 showed that in contrast to NaCl and $CaCl_2$ addition, sodium carbonate addition did not result in maximum reactivity at low salt concentrations but that instead the reactivity of each type of stone increased gradually as the concentration of the salt increased. Only Greer limestone (ANL-8001, containing ∿20% impurities) showed a slight decline at 1 mol % salt addition.

Porosity distributions for three limestones have been completed and are shown in Figs. 16, 17, and 18. The limestones are calcite spar (a highly crystalline $CaCO_3$), ANL-9701 (Germany Valley, a high purity limestone), and ANL-9501 (Grove, a stone with about 5% impurities). Comparison of the three series of curves shows a very large shift in pore diameter with even a small addition (*e.g.*, 0.1 mol %) of Na_2CO_3. Calcite spar shows very little effect after 0.5 mol % Na_2CO_3 addition, whereas the less pure limestones are affected by greater Na_2CO_3 additions. From the results reported earlier for small amounts of NaCl or $CaCl_2$, the peak of sulfur reactivity is at an optimum average pore diameter 0.3 μm. With Na_2CO_3, however, even 0.1 mol % is enough to increase the average pore diameter beyond 0.3 μm and hence beyond an optimum pore structure. However, the low volatility of the salt and the presence of a liquid melt allows sulfation to occur *via* this liquid phase; as salt concentration increases, the amount of liquid increases with a subsequent rise in reactivity. A series of porosity measurements will be made on a very impure limestone so as to have a complete set of representative limestones and their responses to Na_2CO_3 addition.

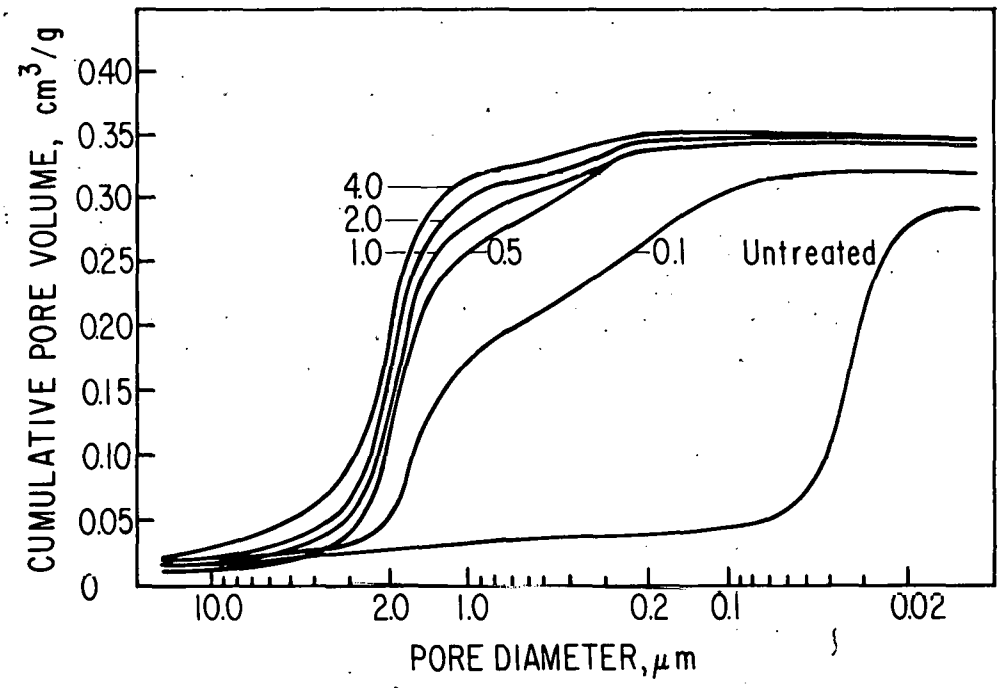

Fig. 16. Porosimetry Curves for Calcite Spar Treated with Indicated mol % Na_2CO_3 and Calcined at 850°C in 5% O_2, 20% CO_2, and the Balance N_2.

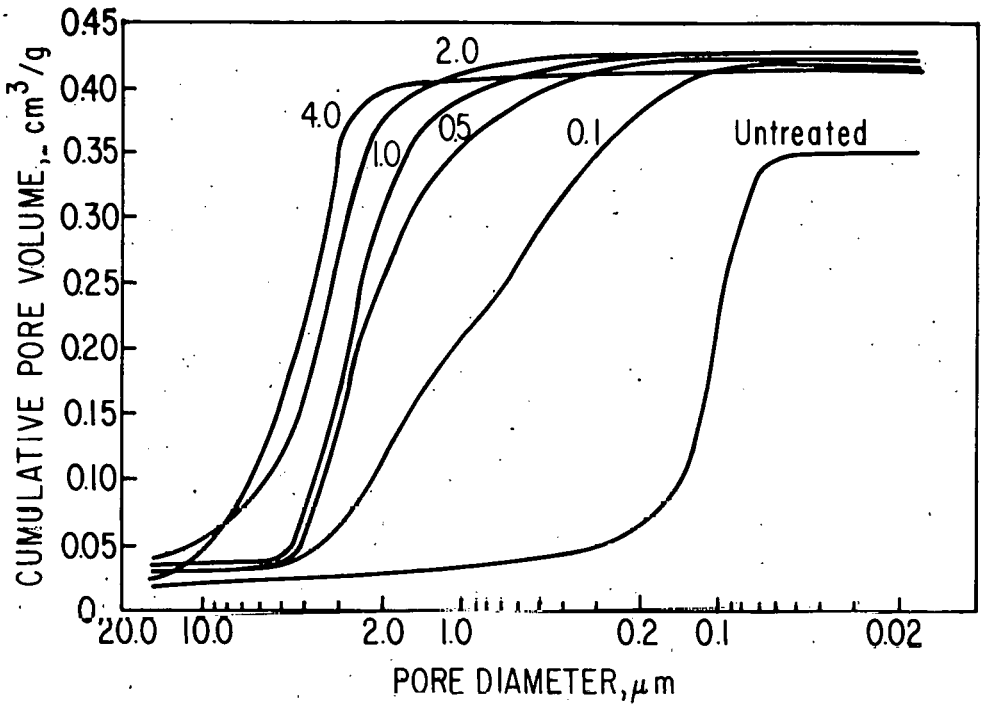

Fig. 17. Porosimetry Curves for ANL-9701 (Germany Valley) Treated with the Indicated mol % Na_2CO_3 and Calcined at 850°C in 5% O_2, 20% CO_2, and the Balance N_2.

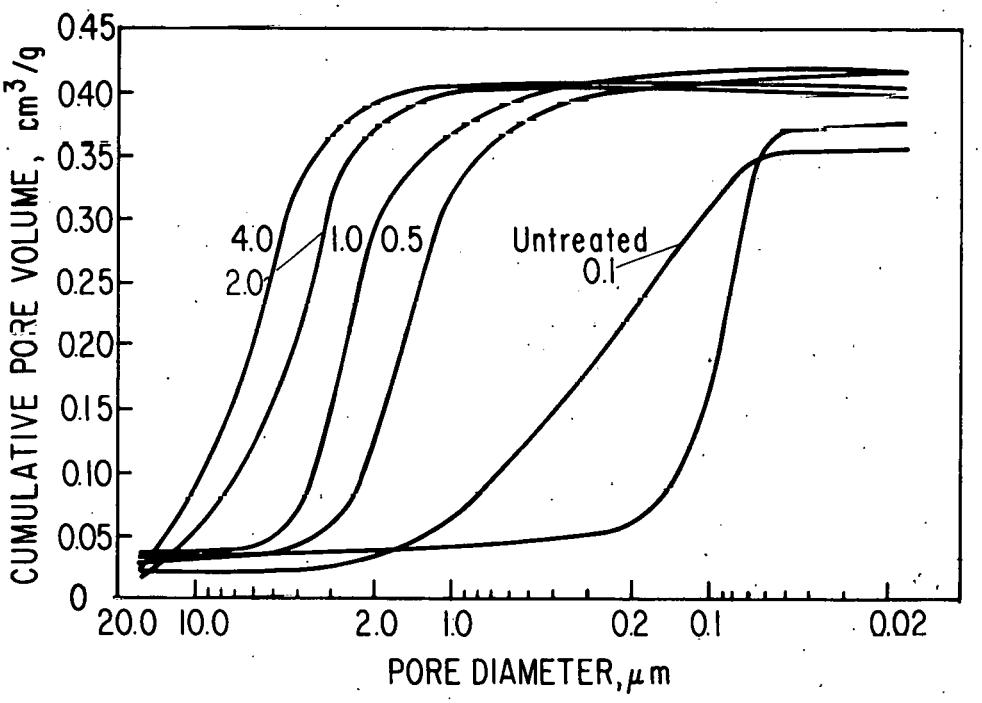

Fig. 18. Porosimetry Curves for ANL-9501 (Grove) Treated with the Indicated mol % Na_2CO_3 and Calcined at 850°C in 5% O_2, 20% CO_2, and the Balance N_2.

f. Effect of Temperature on Sulfation Enhancement and Sulfation Rate

In conjunction with the salt additive work in horizontal tube furnaces, a series of TGA runs were made to investigate the effects of temperature on sulfation enhancement and rate of sulfation of limestone ANL-9501 (Grove). Figures 19 and 20 are bar graph plots of the sulfation data for NaCl-treated ANL-9501 and $CaCl_2$-treated ANL-9501 stones, respectively. Also shown in each case are conversions for untreated limestone at each temperature. These were all precalcined at the temperature of sulfation. For both salts, there is a pronounced decrease in sulfation in the 850-900°C range and very high sulfations at lower temperatures. At high temperatures (>900°C or >950°C, the increase in sulfation of salt-treated samples in comparison to the increased sulfation of untreated stones is much greater than at lower temperatures due to the increased dissolution of CaO.

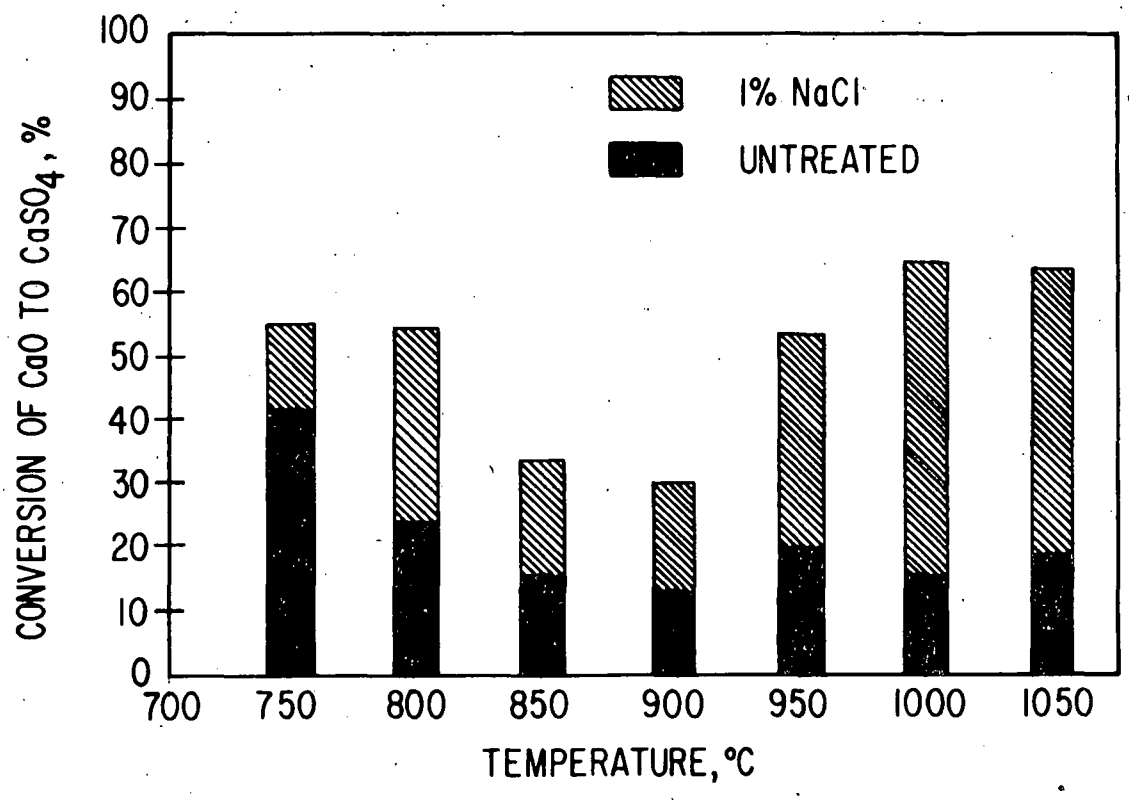

Fig. 19. Sulfation of ANL-9501 Limestone as a Function of Temperature. Precalcined stones treated with 1 mol % NaCl (5 h)

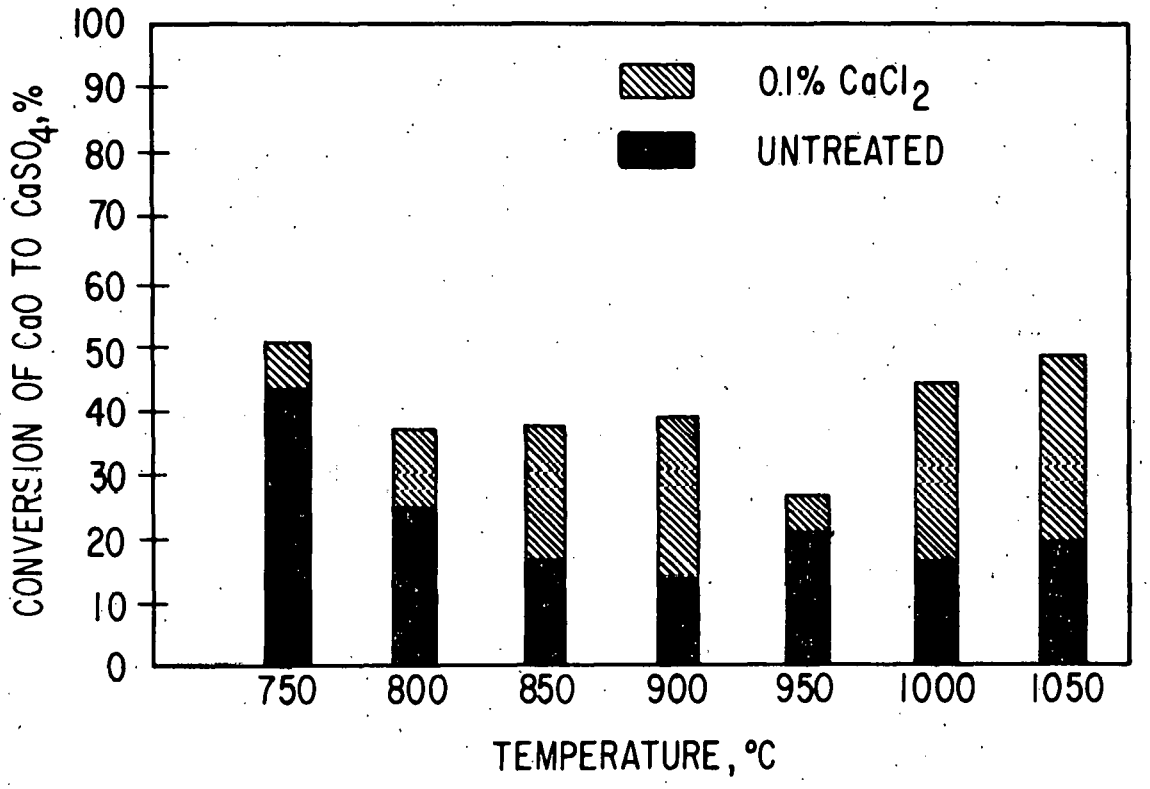

Fig. 20. Sulfation of ANL-9501 Limestone as a Function of Temperature. Precalcined stones treated with 0.1 mol % $CaCl_2$ (5 h)

A series of TGA measurements is under way to obtain conversion values under simultaneous calcination/sulfation conditions at various temperatures with and without salt addition. The data shown for precalcined stones exhibit a definite minimum reactivity in all cases near 800-950°C and a high reactivity at 750°C for both treated and untreated samples. At higher temperatures (≥1000°C), the salt effect is enhanced--presumably by the enhanced mobility of the phases when liquid salt is present. The untreated stone, however, continues to have a low reactivity at higher temperatures due to the loss of surface area from solid-solid sintering.

The reaction curves for the previous bar graphs are shown for untreated, NaCl-treated, and $CaCl_2$-treated samples, in Figs. 21, 22, and 23, respectively. In all three cases, there is a very high rate of reaction initially with a rapid leveling-off at the lowest temperatures. At the next higher temperatures, the rate of initial reaction decreases (because the surface area decreases), but reaction continues longer (because the pore size increases). At still higher temperatures when a salt is present (either NaCl or $CaCl_2$), the reaction rate again increases and significant reaction continues for a longer time due to the presence of large amounts of liquid. For untreated stone, however, the reactivity, initially high, rapidly falls off until there is no further reaction, suggesting that only the immediately available surface is reacting. A more detailed discussion of these data will be made when they can be compared with results obtained with simultaneous calcination and sulfation.

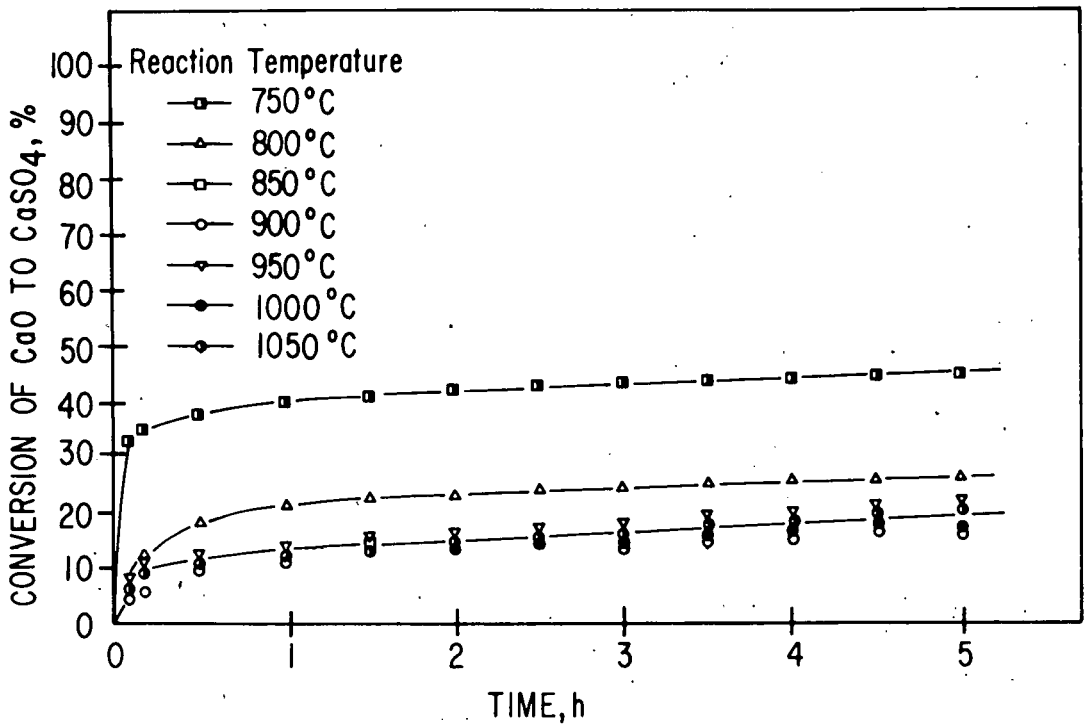

Fig. 21. Sulfation of ANL-9501 Limestone as a Function of Temperature in Precalcined Stones. Sulfation with 0.3% SO_2, 5% O_2, 20% CO_2, and the balance N_2

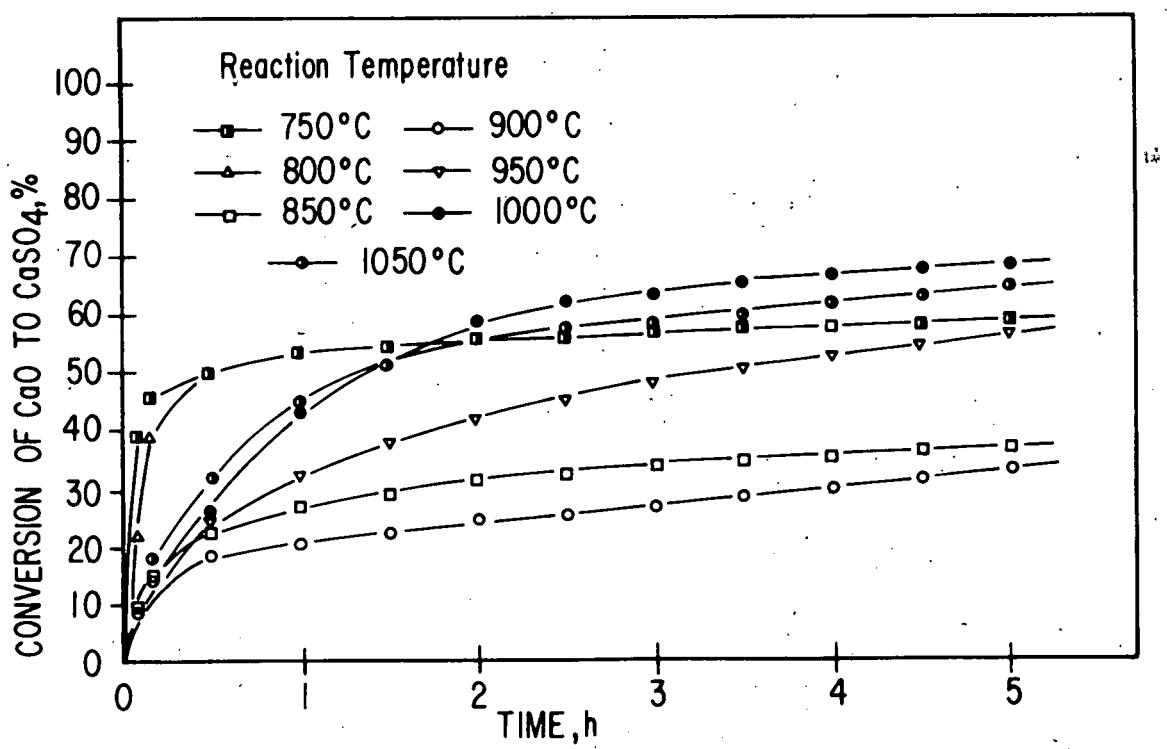

Fig. 22. Sulfation of ANL-9501 Limestone as a Function of Temperature in Precalcined Stones Treated with 1 mol % NaCl. Sulfation with 0.3% SO_2, 5% O_2, 20% CO_2, and the balance N_2

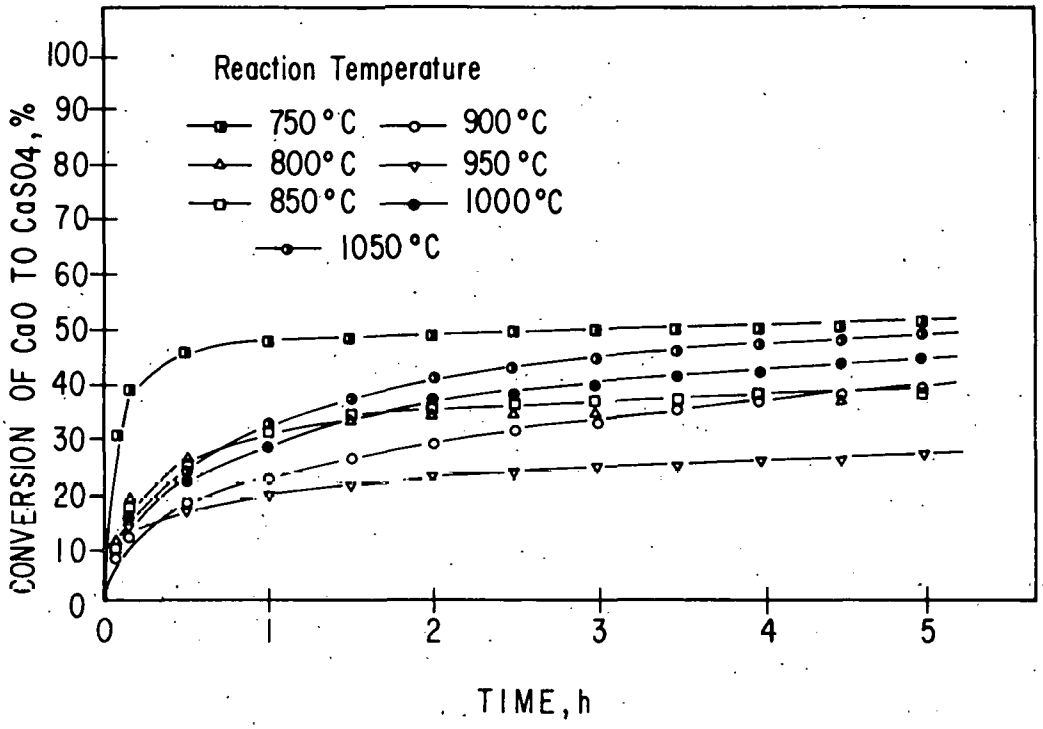

Fig. 23. Sulfation of ANL-9501 Limestone as a Function of Temperature in Precalcined Stones Treated with 0.1 mol % $CaCl_2$. Sulfation with 0.3% SO_2, 5% O_2, 20% CO_2, and the balance N_2

Work to characterize coal combustor overflow samples and steady-state samples is continuing. This work will be extended to include laboratory simulation of combustor variables (such as water content and ash content) not considered previously.

The occurrence of transient reducing conditions in the laboratory combustor as a possible source of sulfation enhancement will also be investigated. In an effort to more clearly define conditions in a fluidized-bed coal combustor, duplication of combustor variables in a small quartz fluidized bed will be attempted.

Extensive work in this laboratory on characterizing the effects of inorganic salts on limestone sulfation has shown that for all limestones investigated, maximum sulfation is achieved when the average pore diameter of the calcined material is near 0.3 μm.[1,4] Previous work on limestone sulfation demonstrated that pores larger than 0.3 μm appear to be most important in reactions with SO_2/O_2 mixtures.[5] In our work, surface areas, as well as porosities, have been measured for the untreated limestones investigated. Table 3 lists total surface areas, of pores $\geq$0.3 μm for limestones calcined 1 h in 5% O_2, 20% CO_2, and the balance N_2. The stones are listed in the order of their increasing $CaCO_3$ content (indicated by the first two digits of their number designations).

Table 3. Pore Volumes and Surface Areas for 18-20 Mesh Limestones[a] Calcined 1 h in 20% CO_2, 5% O_2, and the Balance N_2 at 850°C

Stone	Total Surface Area, cm^2/g	Surface Area for Pores ≥0.3 μm, cm^2/g	Total Pore Volume, cm^3/g	Pore Volume for Pores ≥0.3 μm, cm^3/g
ANL-6702	87,742	12,510	0.423	0.219
ANL-7401	89,795	6,764	0.423	0.130
ANL-8001	58,114	8,868	0.325	0.118
ANL-8101	129,121	3,612	0.453	0.175
ANL-8301	163,603	2,108	0.403	0.058
ANL-8701	68,297	14,537	0.396	0.161
ANL-8901	109,217	6,253	0.357	0.109
ANL-8902	92,397	3,236	0.310	0.055
ANL-8903	91,923	6,478	0.369	0.107
ANL-9201	134,793	1,315	0.325	0.080
ANL-9401	87,146	29,066	0.508	0.280
ANL-9402	124,779	1,370	0.277	0.050
ANL-9501	188,442	877	0.375	0.051
ANL-9502	73,057	12,770	0.382	0.156
ANL-9503	113,907	9,227	0.512	0.243
ANL-9504	112,596	2,981	0.351	0.055
ANL-9505	80,099	4,660	0.338	0.130
ANL-9601	197,599	2,099	0.454	0.160
ANL-9602	116,824	4,251	0.345	0.092
ANL-9603	90,043	3,297	0.295	0.070
ANL-9701	120,202	2,090	0.351	0.051
ANL-9702	175,777	2,285	0.353	0.090
ANL-9703	108,540	9,736	0.519	0.281
ANL-9704	82,474	8,378	0.388	0.120
ANL-9801	113,486	4,393	0.430	0.144
ANL-9802	93,698	6,727	0.488	0.260
ANL-9901	110,056	6,187	0.392	0.116
ANL-9902	100,952	9,655	0.473	0.214
Calcite	285,350	619	0.281	0.038

[a]Stone compositions are given in Reference 4.

No correlation of either area or pore volume with $CaCO_3$ content is apparent. The porosity of the calcined stones reflects the original porosity of the natural limestones, as well as the effects of impurities on the resultant porosity of the calcined material.

As mentioned earlier, literature data on the reactivity of calcium carbonate-containing rocks with SO_2 indicated that porosity and reactivity are related. Data collected during this investigation on sulfation reactivity of limestones exposed to a simulated flue gas at 850°C are plotted against total pore surface area (Fig. 24) rather than porosity or pore volume. There is no correlation of reactivity with total porosity. However, there is an

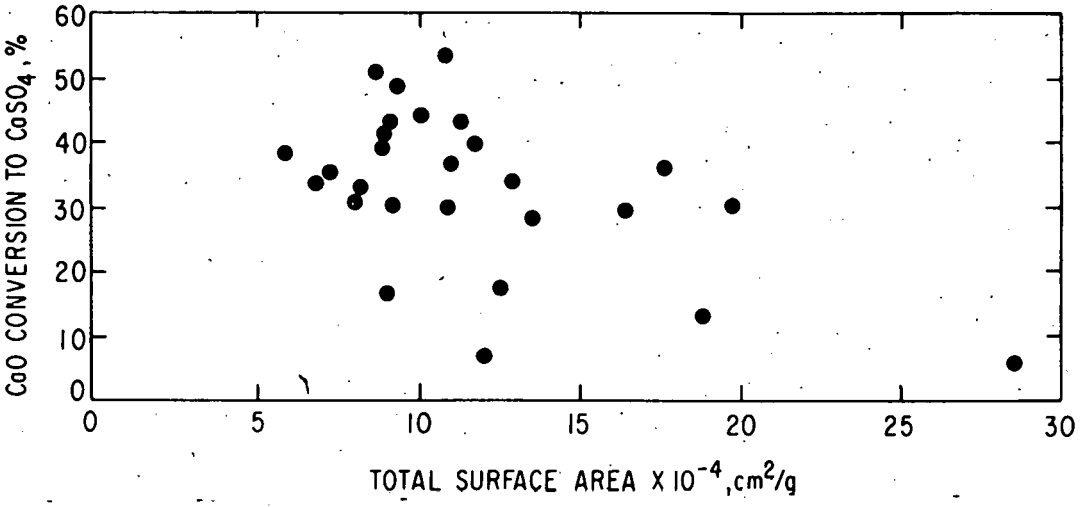

Fig. 24. Sulfation *vs.* Total Surface Area for 18-20 Mesh Untreated Limestone Sulfated at 850°C for 6 h in 0.3% SO_2, 5% O_2, 20% CO_2, and the Balance N_2.

obvious relationship (Fig. 25) of the percent conversion to sulfate and the surface area of pores ≥0.3 μm in diameter (as measured with a mercury porosimeter). The data indicate that as the surface area of pores larger than 0.3 μm diameter increases, sulfation of the lime increases, leveling off at 50-60% conversion (the apparent maximum range of sulfation for pure limestones).

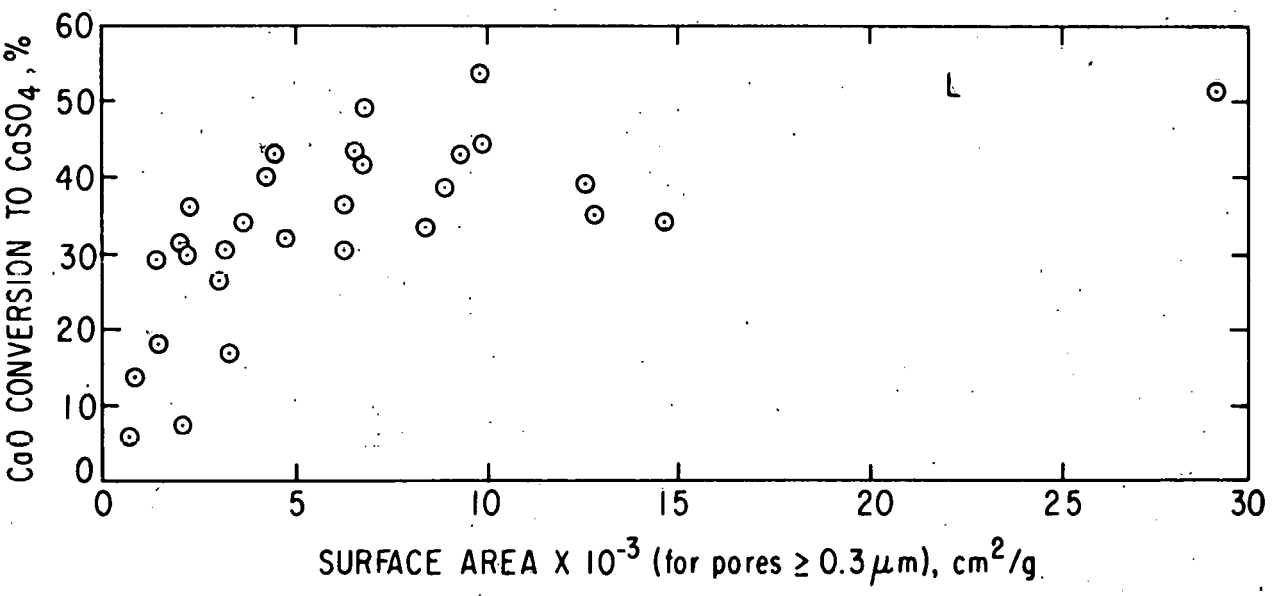

Fig. 25. Percent Sulfation *vs.* Surface Area of Pores ≥0.3 μm in Untreated 18-20 Mesh Limestones Sulfated at 850°C for 6 h in 0.3% SO_2, 5% O_2, 20% CO_2, and the Balance N_2

When these limestones are treated with either NaCl or $CaCl_2$, their surface areas change greatly. At low levels of salt addition, pore surface area increases, but with greater salt additions and subsequent enlargement of pores and loss of micropores, pore surface area decreases. Figure 26 shows conversion *vs.* surface area of pores ≥0.3 μm for (1) untreated stones (also given in Fig. 25) and (2) salt-treated stones having a wide variety of reactivities. Conversion for all treated stones approaches 50%, a conversion exhibited by only the most reactive of untreated limestones.

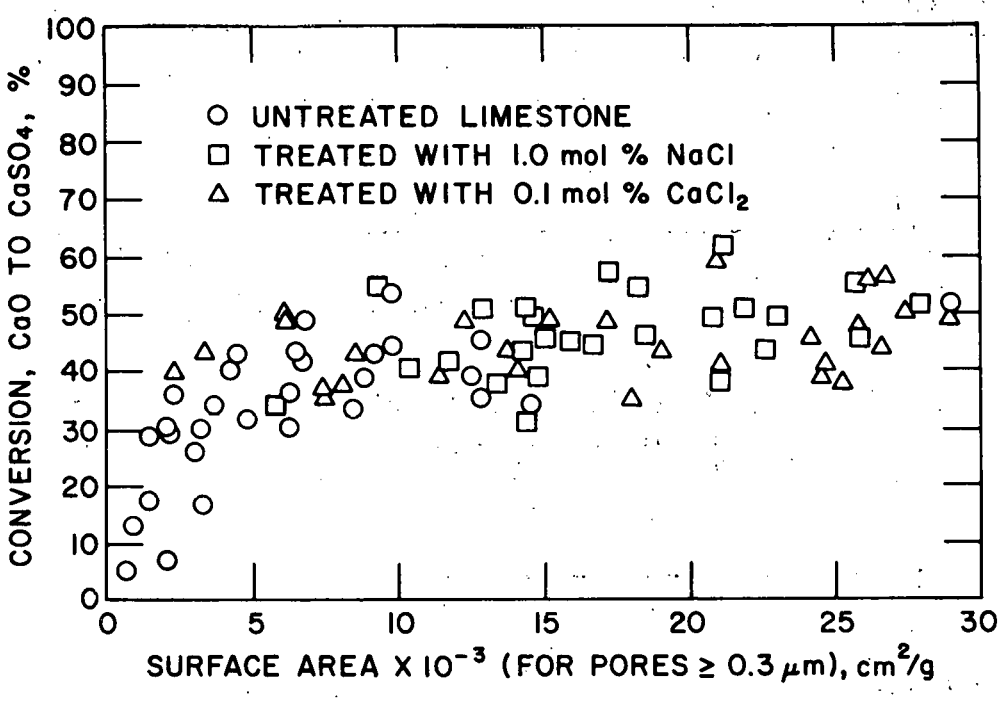

Fig. 26. Percent Sulfation *vs.* Surface Area of Pores ≥0.3 μm for Untreated 18-20 Mesh Limestone and Limestones Treated with NaCl and $CaCl_2$. Sulfation at 850°C for 6 h in 0.3% SO_2, 5% O_2, 20% CO_2, and the balance N_2.

Pore volumes (determined directly from mercury porosimetry measurements) are related to surface areas of limes. Whereas Fig. 27 shows a weak correlation between total pore volume and conversion to sulfate of the available CaO, the correlation with sulfation reactivity is greatly improved by considering only the volume of pores with diameters larger than 0.3 μm (Fig. 28). This correlation allows the reactivity of a given limestone with SO_2/O_2 to be roughly predicted relative to the reactivity of other limestones being considered. This has application to fluidized-bed coal combustion for which the choice of limestone is limited more by geographic location of limestone formations than by any other factor.

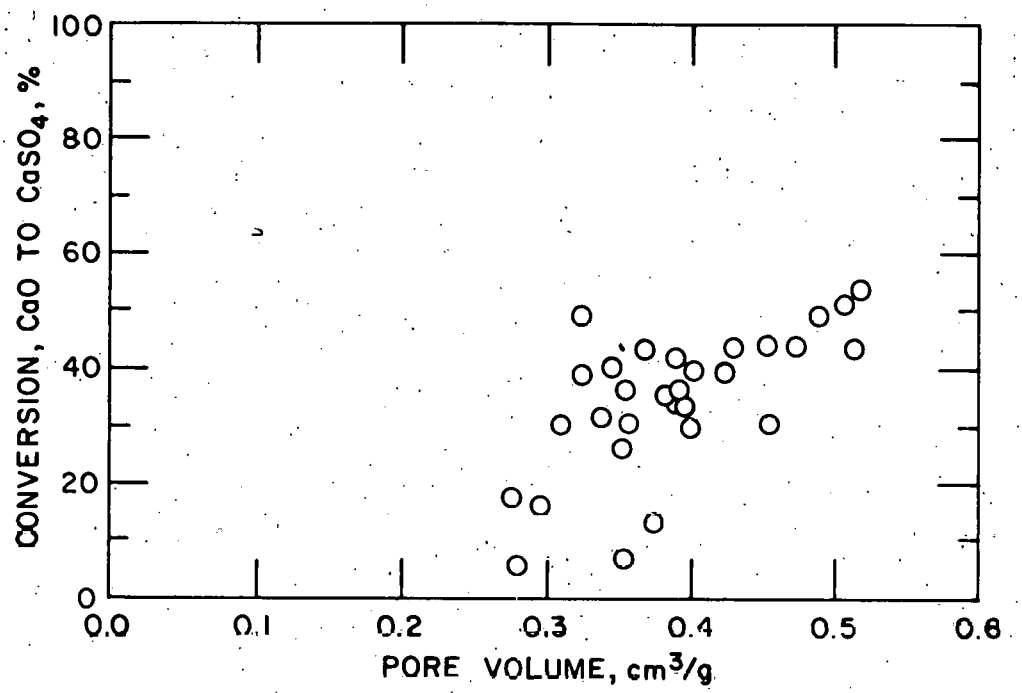

Fig. 27. Sulfation *vs.* Total Pore Volume in Untreated Limestones. Sulfation at 850°C for 6 h in 3% SO_2, 5% O_2, 20% CO_2, and the balance N_2.

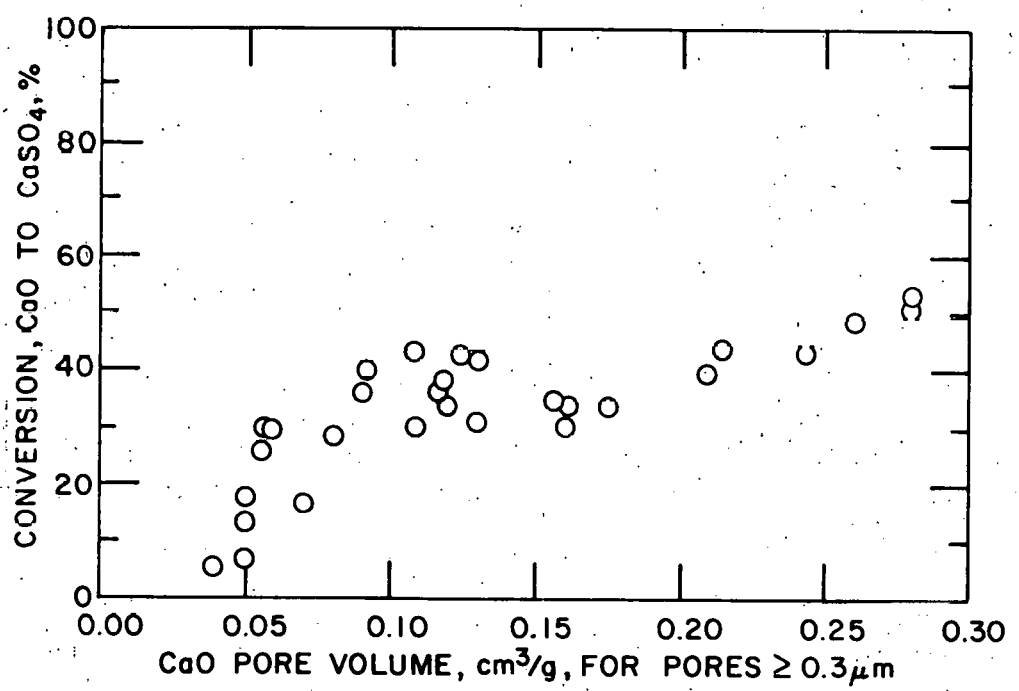

Fig. 28. Sulfation *vs.* Pore Volume for 18-20 Mesh Untreated Limestones Sulfated at 850°C for 6 h in 0.3% SO_2, 5% O_2, 20% CO_2, and the balance N_2.

2. Petrographic Examination of Limestones
(W. I. Wilson and J. A. Shearer)

Petrographic analyses of several calcareous rocks were made and compared with their SO_2 reactivities to determine the basic structural reasons for wide variations in calcium utilization for carbonate racks which have essentially the same chemical composition. The calcareous rocks studied have $CaCO_3$ contents ranging from 95 to 100 wt % (Table 4). One limestone has a total calcium utilization of approximately 20%. Four have total calcium utilizations ranging from approximately 31 to 38%, and three have total calcium utilizations ranging from approximately 52 to 66%.

Following vacuum impregnation with epoxy resin of particles from each of the eight rocks, polished sections were made. These sections were examined in reflected polarized light. Average grain sizes were estimated. (These estimates may be in error by a factor of two to three.) To obtain an estimate, the predominant size of the grains present in the sample was determined with the microscope, and these values were assigned to one of three size categories: (1) fine, 4 to 63 μm across; (2) medium, 63 to 250 μm across, and (3) coarse, 250 μm across. More quantitative grain size measurement will be made by point-counting several hundred grains in thin sections of each sample (to be prepared later).

a. ANL-9802*

Because the finer grains in this stone tend to pluck out during polishing, it is difficult to estimate the average grain size from the polished section of this limestone. Crushed particles viewed in transmitted light show that the average size is 3 to 6 μm. Normally, the vacuum impregnation treatment promotes greater retention of grains unless the permeability to epoxy is very low. The high reactivity of this limestone is probably linked with its high porosity, yet is limited somewhat by its apparently low gaseous permeability.

b. ANL-9801 Limestone

This coarse-grained calcitic limestone is gray and contains a few dark gray seams which are probably carbonaceous stylolites. This limestone appears to be an equigranular rock (grains are all approximately the same size). The low reactivity of this stone is probably linked with its coarse granularity and its low porosity.

c. ANL-9703 Limestone

This stone appears to be a fine-grained porous carbonated limestone. The texture is somewhat loose, making it more highly reactive. The high reactivity of this stone is probably linked with its high porosity and fine grains.

---

*Examined by L. H. Fuchs, Chemistry Division, ANL.

Table 4. Compositions of Limestones

Limestone	$CaCO_3$, wt %	$MgCO_3$, wt %	Fe_2O_3, wt %	Al_2O_3, wt %	SiO_2, wt %	Na_2O, wt %	K_2O, wt %	TGA Total Ca Utilization, %
ANL-9802	98.2	0.47	0.18	0.10	0.29	0.04	0.01	61.8
ANL-9801	98.3	0.6	0.15	0.16	0.20	0.04	0.20	35.3
ANL-9703	97.6	0.58	0.19	0.50	1.08	0.03	0.17	66.2
ANL-9702	97.5	0.68	0.05	0.05	0.21	0.01	0.01	31.0
ANL-9701 (Germany Valley)	97.8	0.6	0.10	1.8	0.2	0.25	--	18.7
ANL-9603	96.4	1.56	0.10	0.30	0.70	0.05	0.11	32.1
ANL-9602	96.2	0.43	0.12	0.21	1.19	0.03	0.01	51.7
ANL-9501 (Grove)	95.3	1.3	0.09	0.25	0.77	0.03	--	37.5

d. ANL-9702 Limestone

This sample, more than any of the others, shows a distinct twinning characteristic (groups of two or more crystals in which the individuals grow together symmetrically so that they share a common plane). The grains vary greatly in size from medium to coarse. The coarse grains show the twinning characteristic of the limestone.

It is not certain what caused twin crystals in this limestone. However, the nature of this texture, as well as the low stone porosity, may be significant in causing the low reactivity of the stone.

e. ANL-9701* (Germany Valley) Limestone

This limestone is fine grained and dense, but contains some coarser vein-deposited calcite. Grain sizes are predominantly near 5 μm. The fine-grained texture of this limestone is not conducive to high reactivity. The densely packed crystallites probably indicate a low porosity.

f. ANL-9603 Limestone

The grain sizes of this limestone vary from fine to coarse. The coarse grains show a twinning characteristic similar to that of the ANL-9702 limestone sample. The total calcium utilization is also essentially the same as that of ANL-9702. Therefore, the nature of this stone's texture, as well as its porosity, may be significant in determining the low reactivity of the stone.

g. ANL-9602 Limestone

The grains of this sample appear to have uniform sizes for the most part. They appear to be loosely packed crystallites, indicating high porosity and high permeability.

h. ANL-9501 (Grove) Limestone

This fine-grained limestone is uniformly gray and equigranular. The grains appear to be tightly interlocked. A few veinlets of calcite occur in some particles. The low reactivity of this stone probably results from its grains being tightly interlocked.

i. Conclusion

It remains uncertain whether the petrographic properties of the limestones account for their differences in reactivities. The data do not clearly indicate that petrographic texture influences SO_2 reactivity. Further work, in which crystal defects such as intracrystalline or intragranular voids, fluid inclusions, and twin lamellae will be studied, may enable us to predict sulfur reactivity more accurately from petrographic data.

*Examined by L. H. Fuchs, Chemistry Division, ANL.

3. PDU Studies

(J. F. Lenc, G. W. Smith, R. W. Mowry, F. G. Teats, and K. M. Myles)

Laboratory-scale experiments have demonstrated that the degree of sulfation of the partially sulfated lime solids within a fluidized-bed combustor is increased either by the addition of chemical additives (sulfation-enhancement agents) to virgin limestones or by water treatment of partially sulfated limestones (see ANL/CEN/FE-78-10, -79-3, and -79-5). Chemical additives such as NaCl, $CaCl_2$, and Na_2CO_3 added in small quantities increase both the rate and the extent of sulfation for many virgin limestones. Water treatment of partially sulfated limestones also increases the degree of sulfation.

In a commercial FBC, increased SO_2 retention would result in a decrease in the lime solids requirement for the combustion process. Such a decrease would reduce both the process cost and the environmental impact of solid waste disposal.

To verify the results of the laboratory-scale experiments on a larger scale and under actual coal combustion conditions (the laboratory-scale experiments were conducted with a simulated flue gas), an experimental program is being carried out in the recently constructed automated PDU-scale atmospheric-pressure fluidized-bed coal combustion facility (AFBC). This facility, including its process-control system for automated operation, was described in ANL/CEN/FE-78-13. The experimental program consists of a series of short-term (≤24 h) runs to evaluate (1) various concentrations of limestone sulfation-enhancement agents and (2) water treatment of partially sulfated limestones.

a. Sulfation Enhancement by $CaCl_2$ and NaCl Additives

In the first series of runs, the effects on SO_2 retention by Grove limestone (ANL-9501 stone) sorbent due to the addition of 1.0 mol % or less of $CaCl_2$ or NaCl were evaluated. Sewickley coal (either -6 +100 mesh or -12 +100 mesh) was combusted at a bed temperature of 850°C, a pressure of 101.3 kPa (1 atm), a fluidizing-gas velocity of 1 m/s, and a fluidized-bed height of 813 mm, with 3% O_2 in the dry off-gas. The above variables were maintained at the values stated in all of the runs; only the composition of the sorbent and the Ca/S mole ratio were altered. In all runs, Grove limestone (-10 +30 mesh), with or without $CaCl_2$ or NaCl addition, was the sorbent used.

Particle size distribution and chemical characteristics of the Sewickley coal (-12 +100 mesh) used for all runs except SAL-1 through SAL-10, and the Grove limestone sorbent used in these runs and subsequent runs are presented in Tables 5 and 6, respectively.

A total of 31 runs were conducted in this series at Ca/S mole ratios ranging from 1.0 to 4.4. The percent sulfur retention and the percent calcium utilization for each of the 31 runs as a function of the $CaCl_2$ or NaCl concentrations in the sorbent and the Ca/S mole ratios are listed in Table 7.

Table 5. Particle-Size Distribution and Chemical Characteristics of Sewickley Coal (-12 +100 mesh)

Sieve Analysis	
U.S. Sieve No.	% on Sieve
+12	0.0
-12 +20	22.5
-20 +30	25.1
-30 +60	42.0
-60 +80	4.2
-80 +100	1.8
-100	4.4

Mass mean particle dia: ~560 μm

	Proximate Analysis, wt %	
	As Received	Dry Basis
Moisture	1.11	-
Ash	19.06	19.27
Volatile Matter	36.56	36.97
Fixed Carbon	43.27	43.76
	100.00	100.00
Sulfur, wt %	5.46	5.52
Heating value, Btu/lb	11969	12103

	Ultimate Analysis, wt %	
	As Received	Dry Basis
Moisture	1.11	-
Carbon	64.88	65.61
Hydrogen	4.41	4.46
Nitrogen	1.04	1.05
Chlorine	0.04	0.04
Sulfur	5.46	5.52
Ash	19.06	19.27
Oxygen (by difference)	4.00	4.05
	100.00	100.00

Table 6. Particle-Size Distribution and Chemical Characteristics of Grove Limestone (ANL-9501 stone)

Sieve Analysis	
U.S. Sieve No.	% on Sieve
+18	0.79
-18 +20	10.23
-20 +25	25.27
-25 +30	31.46
-30 +40	29.89
-40 +60	2.36
-60	0.00

Mass mean particle dia: ∿640 μm

Component	Chemical Analysis, wt %
Ca	38.12
Mg	0.37
CO_2	42.61
H_2O	1.56
Derived Composition, wt %	
$CaCO_3$	95.3
$MgCO_3$	1.3

Three concentrations (∿0.1, ∿0.3, and ∿0.5 mol %) of $CaCl_2$ additive and two concentrations (∿0.5 and ∿1.0 mol %) of NaCl additive were evaluated. Two methods were used to prepare the $CaCl_2$ or NaCl-containing Grove limestone. In the first method, which was used for preparing nominal 0.1 and 0.5 mol % $CaCl_2$ and nominal 0.5 and 1.0 mol % NaCl material, a batch of Grove limestone particles was spread in a shallow stainless steel tray. The particles were then sprayed with a water solution containing the weight of $CaCl_2$ or NaCl that would give the desired concentration after evaporation of the water by air drying. In the second method, which was used for preparing nominal 0.3 mol % $CaCl_2$ material, a batch of Grove limestone particles was soaked in a heated water solution containing $CaCl_2$ in excess of that required to obtain the desired concentration. After soaking, excess $CaCl_2$ solution was drained from the limestone particles through a screen. The particles were then oven-dried at 232°C to evaporate residual water.

Table 7. Eight-hour Runs to Evaluate the Effects of $CaCl_2$ or NaCl Addition on Sulfur Retention of Grove Limestone (ANL-9501)

Run Designation	Ca/S Mole Ratio	SO_2 in Off-Gas, ppm[a]	Sulfur Retention,[b] %	Calcium Utilization,[c] %
Grove limestone (ANL-9501) with no $CaCl_2$ or NaCl addition				
SAL-1A2	1.3	2200	37.1	28.5 (76.9)
SAL-9[d]	1.4	2100	40.0	28.6 (71.4)
SAL-11C1	2.1	1300	72.9	34.7 (47.6)
SAL-13	2.4	750	84.4	35.2 (41.7)
SAL-1B	2.6	1300	62.9	24.2 (38.5)
SAL-12	2.8	750	84.4	30.1 (35.7)
SAL-8[d]	3.0	450	87.1	29.0 (33.3)
SAL-11C2	3.4	700	85.4	25.1 (29.4)
SAL-10[d]	3.6	500	85.7	23.8 (27.8)
Grove limestone (ANL-9501) plus ∿0.1 mol % $CaCl_2$[e]				
SAL-2B2	1.0	2300	34.3	34.3 (100)
SAL-2B1	1.6	1700	51.4	32.1 (62.5)
SAL-2A	2.6	1000	71.4	27.5 (38.5)
SAL-15	2.8	950	80.2	28.6 (35.7)
SAL-14	2.9	900	81.2	28.0 (34.5)
SAL-7[d]	3.0	450	87.1	29.0 (33.3)
SAL-6[d]	4.2	450	87.1	20.7 (23.8)
Grove limestone (ANL-9501) plus ∿0.3 mol % $CaCl_2$[f]				
SAL-16A	1.2	2500	47.9	39.9 (83.3)
SAL-19	2.4	800	83.3	34.7 (41.7)
SAL-18	3.3	900	81.2	24.6 (30.3)
Grove limestone (ANL-9501) plus ∿0.5 mol % $CaCl_2$[e]				
SAL-3B	1.4	1800	48.6	34.7 (71.4)
SAL-3A	1.9	1250	64.3	33.8 (52.6)
SAL-4	3.0	700	80.0	26.7 (33.3)
SAL-5	4.4	300	91.4	20.8 (22.7)

(contd)

Table 7. (contd)

Run Designation	Ca/S Mole Ratio	SO_2 in Off-Gas, ppm[a]	Sulfur Retention,[b] %	Calcium Utilization,[c] %
Grove limestone (ANL-9501) plus ~0.5 mol % NaCl[e]				
NAC-1	1.3	1800	62.5	48.1 (76.9)
NAC-3	2.2	1550	67.7	30.8 (45.4)
NAC-4	3.0	1100	77.1	25.7 (33.3)
NAC-2A	3.2	1400	70.8	22.1 (31.2)
Grove limestone (ANL-9501) plus ~1.0 mol % NaCl[e]				
NAC-8	1.3	2000	58.3	44.8 (76.9)
NAC-5	1.4	2400	50.0	35.7 (71.4)
NAC-6	2.0	1300	72.9	36.4 (50.0)
NAC-7	3.5	900	81.2	23.2 (28.6)

[a] Dry basis.

[b] Based on the assumptions of 3500 ppm SO_2 in dry off-gas if there had been zero sulfur retention for runs designated SAL-1 through SAL-10, inclusive, and 4800 ppm SO_2 in dry off-gas if there had been zero sulfur retention for the other runs. Sewickley coal (4.33% S, 70.75% C, heating value of 13018 Btu/lb, -6 +100 mesh) was used in runs SAL-1 through SAL-10, inclusive. Sewickley coal (5.46% S, 64.88% C, heating value of 11969 Btu/lb, -12 +100 mesh) was used in the remaining runs.

[c] Percentage of available calcium in the sorbent converted to $CaSO_4$. Numbers in parentheses indicate maximum percent calcium utilizations based on the Ca/S mole ratios (equivalent to the reciprocals of the Ca/S mole ratios, times 100).

[d] Run was conducted following a run made with a higher $CaCl_2$ concentration in the sorbent.

[e] $CaCl_2$ or NaCl was added to the sorbent by a spraying method (see the text).

[f] $CaCl_2$ was added to the sorbent by a soaking method (see the text).

Examination of the data presented in Table 7 indicates that in this series of runs, sulfation enhancement due to the addition of the $CaCl_2$ or NaCl was generally less than that obtained in previously reported laboratory-scale experiments (ANL/CEN/FE-78-10). For example, with 0.5 mol % NaCl addition, calcium utilization was 22-48% in these runs and 52% in a laboratory-scale run; with 1 mol % NaCl addition, calcium utilization was 23-45% in these runs and 45% in a laboratory-scale run. It is suspected that the differences in the two sets of data are due to different manners of conducting the two series of experiments. The laboratory-scale experiments were

carried out with a simulated flue gas and no actual coal combustion occurred. As a consequence, no constituents of the coal ash were present in the reactor. In contrast, combustion runs were conducted in the AFBC.

b. Sulfation Enhancement in PDU-Scale Experiments

Next discussed (and also discussed in Task B) are four 360-ks (100-h) corrosion test runs conducted in the PDU-scale AFBC. The Grove limestone sorbent contained no sulfation-enhancement agent in the first run (CT-1), ∿0.3 mol % $CaCl_2$ in the second run (CT-2), ∿0.5 mol % NaCl in the third run (CT-3), and ∿1.9 mol % Na_2CO_3 in the fourth run (CT-4). Except for the Ca/S mole ratio, operating conditions for these four runs were the same as those reported above for the short-term runs.

The Ca/S mole ratio required to maintain ∿700 ppm SO_2 in the dry off-gas (equivalent to ∿85% sulfur retention) was ∿3.5 in the first three 360-ks runs, indicating that there was virtually no sulfation enhancement of the Grove limestone sorbent due to addition of low concentrations (<1 mol %) of $CaCl_2$ and NaCl in Runs CT-2 and CT-3, respectively. These results disagree with sulfation enhancements previously reported for laboratory-scale experiments. The higher treatment level in run CT-4 (1.9 mol % Na_2CO_3), however, did enhance sulfation, lowering the Ca/S mole ratio from 3.4 to 2.0.

In an attempt to clarify the disparity between the data from the laboratory-scale experiments and PDU-scale experiments (CT-1, CT-2, and CT-3), four additional short-term (8 h) runs were conducted in the AFBC after CT-3 and before CT-4. Higher concentrations of sulfation-enhancement agents were added to the sorbent in the first three of these four runs. The Grove limestone sorbent contained ∿2.3 mol % NaCl in the first run (NAC-10), ∿2.1 mol % $CaCl_2$ in the second run (SAL-20), and ∿1.6 mol % Na_2CO_3 in the third run (NCO-1). In the fourth run (NCO-2), ∿0.6 mol % Na_2CO_3 was added to the sorbent since no data had been obtained previously on the effects on sulfation enhancement of a relatively low concentration of this particular chemical additive. Experimental conditions for these four short-term runs were the same as those for the four 360-ks corrosion test runs.

Table 8 lists the Ca/S mole ratios required to maintain ∿700 ppm SO_2 in the dry off-gas during nominal 8-h steady state periods in the four short-term runs. To allow comparison, the Ca/S mole ratios for the four 360-ks corrosion test runs (discussed in a following section) are included in this table. The data in Table 8 suggest that (1) the concentration of a chemical additive required to enhance sulfation of the sorbent in actual coal combustion experiments is greater than in laboratory experiments conducted with a simulated flue gas and (2) on a mole basis, Na_2CO_3 is a better sulfation-enhancement agent than either $CaCl_2$ or NaCl at both relatively high (∿2.0 mol %) and relatively low (∿0.5 mol %) concentrations. (On a weight basis, $CaCl_2$ is 5% heavier than an equal number of moles of Na_2CO_3 and NaCl is 55% lighter than an equal number of moles of Na_2CO_3.)

Each of the four short-term runs (SAL-20, NAC-10, NCO-1, and NCO-2) was conducted in two steps. The first step consisted of sulfating a starting bed of untreated Grove limestone by combusting Sewickley coal without sorbent addition. Sulfation of the bed was terminated when the SO_2 concentration in

Table 8. Ca/S Mole Ratio Required to Maintain ∿700 ppm SO_2 in the Dry Off-Gas

Experimental Conditions

Temperature: 850°C
Pressure: 101.3 kPa (1 atm)
Fluidizing-gas velocity: 1 m/s
Fluidized-bed height: 813 mm
Excess Air: 3% O_2 in dry off-gas
Coal: Sewickley (-12 +100 mesh), 5.46% S
Sorbent: Grove limestone (ANL-9501) (-10 +30 mesh), 95.3% $CaCO_3$

Run Designation	Sulfation Enhancement Agent[a]	Ca/S Mole Ratio
CT-1[b]	None	3.4
CT-2[b]	∿0.3 mol % $CaCl_2$	3.5
SAL-20[c]	∿2.1 mol % $CaCl_2$	2.6
CT-3[b]	∿0.5 mol % NaCl	3.6
NAC-10[c]	∿2.3 mol % NaCl	2.7
CT-4[b]	∿1.9 mol % Na_2CO_3	2.0
NCO-1[c]	∿1.6 mol % Na_2CO_3	2.2
NCO-2[c]	∿0.6 mol % Na_2CO_3	2.9

[a]Added to Grove limestone sorbent.

[b]Nominal 100-h run.

[c]Nominal 8-h steady state run.

the dry off-gas increased to 2000-3000 ppm. In the second step, steady state conditions were established by adding sufficient Grove limestone sorbent containing a sulfation-enhancement agent to the fluidized bed to maintain the SO_2 concentration in the dry off-gas at 700 ppm.

In an effort to gain some insight about the chemical composition of the bed as a function of time during the first sulfation step, in Run NAC-10, samples of the bed material were taken at 0.5-h intervals at a height ∿254 mm above the coal injection point. Following withdrawal from the bed, each sample was sealed in a glass jar containing an inert nitrogen atmosphere to prevent reaction with oxygen and/or water in the air. Grinding and weighing of the samples for analyses was performed in a helium-atmosphere glove box. The samples were analyzed for Ca^{2+}, S^{2-}, SO_4^{2-}, and CO_3^{2-}. Changes in the pore structure of the bed samples were also analyzed by mercury porosimeter measurements.

Analytical results indicate that very little sulfide was present in the bed during the first sulfation step of Run NAC-10. The first sample, obtained 0.5 h after the start of sulfation, contained 100 ppm S^{2-} and the next-to-last sample, obtained 0.5 h before the end of the sulfation

period, contained <70 ppm S^{2-}. Based on SO_4^{2-} analyses of bed samples taken during the first sulfation step of Run NAC-10, the $CaSO_4$ contents of the bed samples were calculated and are plotted as a function of time in Fig. 29.

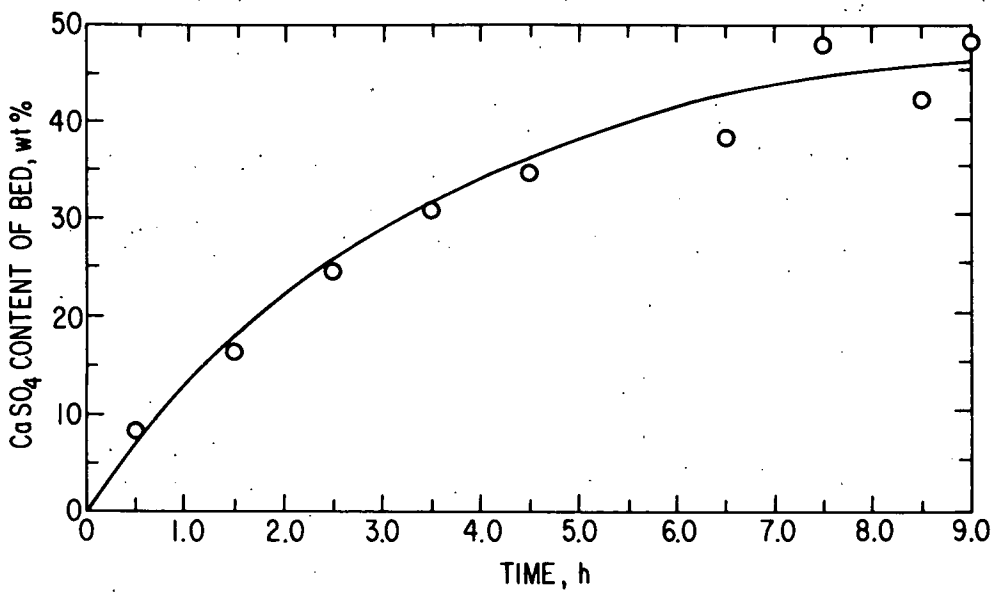

Fig. 29. $CaSO_4$ Content of Fluidized Bed *versus* Time Based on Sulfate Analyses of Bed Samples Obtained during First Sulfation Step of Run NAC-10

As shown in Fig. 29, the $CaSO_4$ content of the bed samples increased to ∿45 wt % during the first 7.5 h of the first sulfation step and leveled off at this value between the 7.5-h and the final 9.0-h samples. It should be pointed out that these data are based on grab samples taken at only one height in the bed. Consequently, it is not certain that the compositions of these bed samples are representative of the entire bed. However, it can be seen that the sulfation in the fluidized bed shows the same trends as in the laboratory-scale TGA.

Gas chromatography was used to determine the CO_2 concentration in two of the bed samples from the initial sulfation step of Run NAC-10. The two samples were obtained at 1 h and 9 h, near the beginning and at the end of the initial sulfation step. From the results of the CO_2 analyses, the $CaCO_3$ content was calculated to be 31.8 wt % in the 1.0-h bed sample and 1.1 wt % in the 9.0-h sample. This indicates that the initial uncalcined bed undergoes essentially complete calcination during the initial sulfation period of 9 h.

c. Comparison of Sulfur Retention in Old and New Fluidized-Bed Combustors

To compare the performance of the new AFBC with the performance of an older atmospheric-pressure fluidized-bed combustor, a series of four runs (SG-1 to SG-4) were conducted in the new unit with only the Ca/S mole ratio varied. In these runs, a single batch of well-mixed Sewickley coal (-12 +100 mesh) was combusted at a bed temperature of 850°C, a pressure of 101.3 kPa (1 atm), a fluidizing-gas velocity of 1 m/s, a fluidized-bed height of 813 mm, and 3% O_2 in the dry off-gas. The above variables were maintained at the values stated, with only the Ca/S mole ratio varied.

In the older combustor, Illinois coal was also combusted in a fluidized bed of Grove limestone. Thus, a major difference in the two sets of experiments was the different sulfur contents of the coals. The Sewickley coal used in the recent runs contained 5.46% S, compared with 3.7% S for the Illinois coal used in the experiments in the older atmospheric-pressure combustor.

In Runs SG-1 to SG-4, the sorbent was from the same batch of well-mixed Grove limestone (-10 +30 mesh) as in the earlier runs, with no $CaCl_2$, NaCl, or Na_2CO_3 added.

The percent sulfur retentions, the percent calcium utilizations, and the Ca/S mole ratios for these four runs are listed in Table 9.

Table 9. Sulfur Retentions and Calcium Utilizations for Run Series SG

Run Designation[a]	Ca/S Mole Ratio	SO_2 in Off-Gas, ppm[b]	Sulfur Retention,[c] %	Calcium Utilization,[d] %
SG-2	1.3	3310	31.0	23.8 (76.9)
SG-3	2.1	1730	64.0	30.5 (47.6)
SG-4	2.9	1030	78.5	27.1 (35.5)
SG-1	3.2	760	84.2	26.3 (31.2)

[a] SG designates runs with Sewickley coal (5.46% S) and Grove limestone (ANL-9501, 95.3% $CaCO_3$) sorbent. Run numbers indicate the chronological order of the runs.

[b] Dry basis.

[c] Based on the assumption of 4800 ppm SO_2 in the dry off-gas at zero sulfur retention. (Sewickley coal, 5.46% S, 64.88% C, heating value of 11969 Btu/lb, -12 +100 mesh).

[d] Percentage of available calcium in the sorbent converted to $CaSO_4$. Numbers in parentheses indicate maximum calcium utilizations based on Ca/S mole ratios (numbers in parentheses are equivalent to 100 times the reciprocals of the Ca/S mole ratios).

Figure 30 is a plot of the percent sulfur retention for the four runs as a function of the Ca/S mole ratio. The plot of sulfur retentions for this series is in general agreement with that for previous atmospheric-pressure fluidized-bed combustion experiments.[6] For a Ca/S mole ratio of 3, Fig. 30 shows a sulfur retention of about 80% for the recent run series, compared with about 87% for the earlier reported experiments.

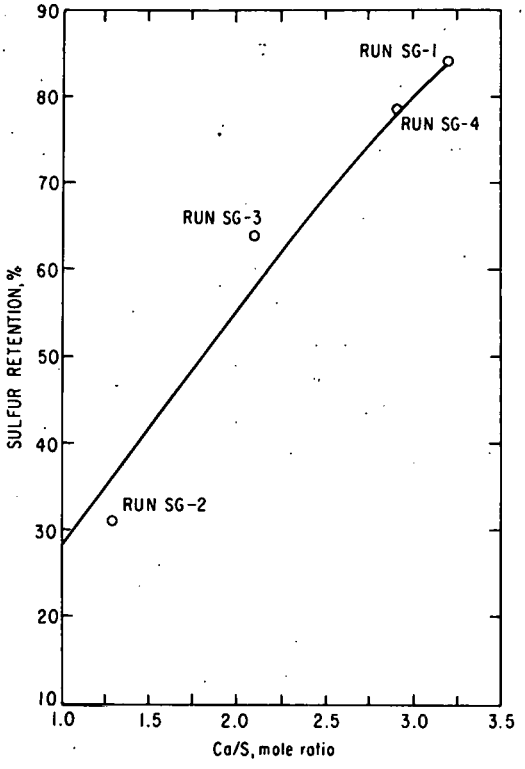

Fig. 30.

Sulfur Retention by Grove Limestone as a Function of Ca/S Mole Ratio. Temperature, 850°C; pressure, 101.3 kPa (1 atm); gas velocity, 1 m/s; coal, Sewickley (5.46% S), -12 +100 mesh; sorbent, Grove limestone, ANL-9501, (95.3% $CaCO_3$), -10 +30 mesh.

Carbon, sulfur, and calcium material balances, as well as combustion efficiencies during a 16.2-ks (4.5-h) steady state period for each of the four runs, are listed in Table 10. Carbon balances ranged from 118 to 128%, sulfur balances from 78 to 101%, and calcium balances from 96 to 114%. Combustion efficiencies ranged from 86 to 88%. These results are similar to the results obtained with the old atmospheric combustor.

d. Effect of Temperature on Sulfur Retention

A series of tests was begun to determine, as a function of combustion temperature, Ca/S mole ratios required for 85% sulfur retention for various untreated sorbents (*i.e.*, containing no sulfation-enhancement agents). Two sorbents have been evaluated to date. The first sorbent was Grove limestone (ANL-9501), -10 +30 mesh, containing 95.3% $CaCO_3$. Four short-term runs were conducted with this sorbent, Run SG-6A at 800°C, Run SG-5R1 at 850°C, and Runs SG-7 and SG-7A, both at 900°C. Figure 31 is a plot of the Ca/S mole ratios required for 85% sulfur retention as a function of temperature for these four runs. The second sorbent evaluated was Pfizer dolomite (ANL-5301), -12 +30 mesh, containing 53.4% $CaCO_3$. Three short-term runs were conducted

Table 10. Carbon, Sulfur, and Calcium Material Balances and Combustion Efficiencies for 4.5-h Steady-State Periods of SG Runs

Experimental Conditions

Temperature: 850°C
Pressure: 101.3 kPa (1 atm)
Gas Velocity: 1 m/s
Fluidized-Bed Height: 813 mm
Excess O_2: 3% (in dry off-gas)

Run Designation[a]	Ca/S Mole Ratio	Percent Accounted for			Combustion Efficiency,[b] %
		Carbon	Sulfur	Calcium	
SG-1	3.2	120	78	96	88
SG-2	1.3	118	101	114	88
SG-3	2.1	128	89	100	87
SG-4	2.9	127	93	99	86

[a] SG designates runs with Sewickley coal containing 5.46% S (-12 +100 mesh) and Grove limestone (ANL-9501) sorbent containing 95.3% $CaCO_3$ (-10 +30 mesh).

[b] Defined as the percentage of total combustible carbon fed that was completely burned to CO_2.

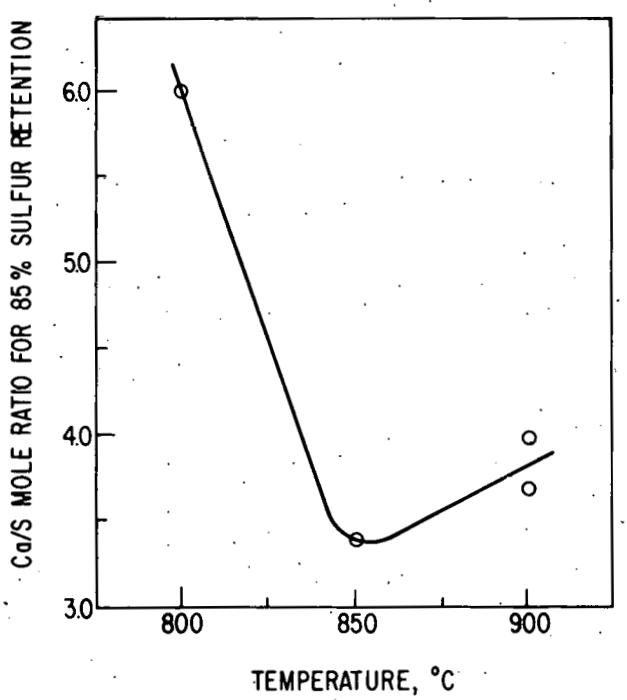

Fig. 31.

Ca/S Mole Ratio for 85% Sulfur Retention as a Function of Temperature (Sewickley coal, 5.46% S, and Grove limestone sorbent, ANL-9501, 95.3% $CaCO_3$).

with this sorbent, Run SP-3 at 800°C, Run SP-1 at 850°C, and Run SP-2 at 900°C. Figure 32 is a plot of the Ca/S mole ratios required for 85% sulfur retention as a function of temperature for these three runs.

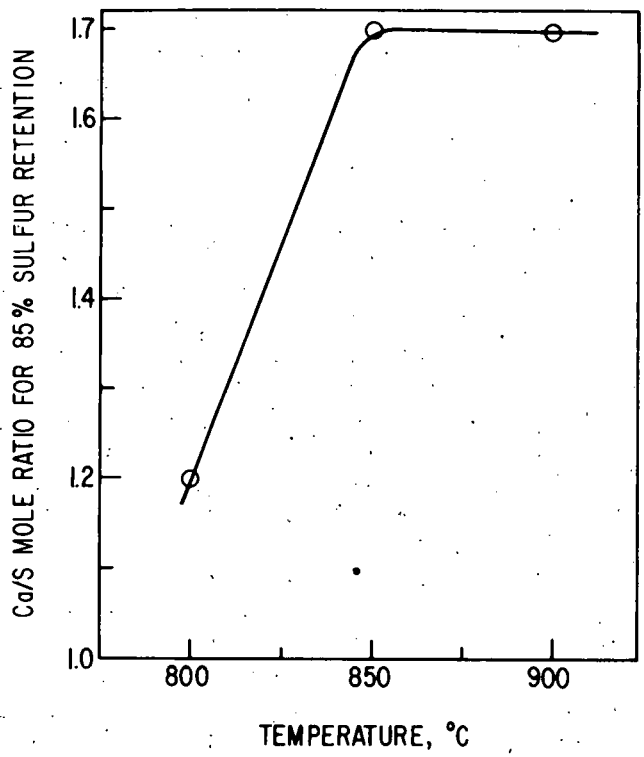

Fig. 32. Ca/S Mole Ratio for 85% Sulfur Retention as a Function of Temperature (Sewickley coal, 5.46% S, Pfizer dolomite sorbent, ANL-5301, 53.4% $CaCO_3$).

As seen in Fig. 31, the lowest Ca/S mole ratio giving 85% sulfur retention for Grove limestone was 3.4 at 850°C. Temperatures either lower or higher than 850°C required higher Ca/S mole ratios. For Pfizer dolomite sorbent, the pattern (shown in Fig. 32) is quite different. The lowest Ca/S mole ratio giving 85% sulfur retention was 1.2 at 800°C. This ratio was 1.7 at both 850°C and 900°C. Similar tests are planned to determine the effect of temperature on the Ca/S mole ratios required for 85% sulfur retention for other sorbents.

e. Sulfation-Enhancement by Water Treatment of Sorbent

Another short-term run (HYS-1) was conducted to determine whether the addition of water to untreated, partially sulfated Grove limestone sorbent would increase its sulfur retention capability. The source of the untreated, sulfated Grove limestone was (1) the bed overflow material from two short-duration runs (SG-5 and SG-5R1) and (2) the final bed from

Run SG-5R1 in which virgin Grove limestone was the sorbent. Sulfur retention during these two runs was 85%.

Water was added to this material by the spray method described near the beginning of this section (PDU Studies). Heating of a sample of the water-treated sulfated material to 850°C resulted in a weight loss of 14.5%. This weight loss was assumed to be the water content of the sulfated material due to decomposition of the $Ca(OH)_2$ that had formed during water treatment by the following reaction:

$$CaO + H_2O \rightarrow Ca(OH)_2$$

Run HYS-1 was conducted in two steps under the same experimental conditions as those listed in Table 8. To minimize startup difficulties, a starting bed of untreated Grove limestone was sulfated by combusting Sewickley coal at 850°C until the SO_2 level in the dry off-gas increased to ∿2500 ppm. Steady-state operation was then established by adding the water-treated partially sulfated Grove limestone as the sorbent at a feed rate required to achieve the 85% sulfur retention which was obtained in previous runs (CT-1 and SG-5R1) in which virgin Grove limestone was the sorbent. With the water-treated partially sulfated Grove limestone as the sorbent in Run HYS-1, the SO_2 level in the dry off-gas was 470 ppm (equivalent to 90% sulfur retention). Thus, the water treatment not only increased the degree of sulfation of the partially sulfated material but also increased the percent sulfur retention above that previously achieved in tests made with virgin Grove limestone. This increased sulfur retention capability is attributed to the structural rearrangement of the partially sulfated limestone that occurs when its CaO content is converted to $Ca(OH)_2$ upon water treatment. The $Ca(OH)_2$ subsequently decomposes at the temperatures used in fluidized-bed combustion, providing additional reaction sites for sulfation.

Percent calcium utilizations (percent calcium converted to $CaSO_4$) were calculated for the starting bed, for the water-treated partially sulfated sorbent inlet solids streams, and for the final bed and bed overflow outlet solids streams for the second step of Run HYS-1. Except for the starting bed material, these calculations were based on calcium and sulfur analyses of representative samples of the various solids streams. Since the bed material was not drained after the first step of Run HYS-1, calculation of the percent calcium utilization for the starting bed for the second step was based on estimated calcium and sulfur contents. The calculations indicate that calcium utilization increased from ∿23% in the inlet solids streams to ∿40% in the outlet solids streams, an increase of ∿74% which is attributed to water treatment of the partially sulfated sorbent.

TASK B. CORROSION STUDIES

(J. F. Lenc, G. W. Smith, R. W. Mowry, F. G. Teats, F. F. Nunes
S. D. Smith, A. R. Pumphrey, J. R. Falkenberg,
J. J. Stockbar, and K. M. Myles)

There is concern that volatilization of sulfation-enhancement agents (alkali metal compounds) might cause unacceptable corrosion of the metal components of a commercial fluidized-bed coal combustion system. To measure the corrosion rates of candidate metals of construction in the presence of sulfation-enhancement agents in a PDU-scale unit, a series of long-term (≥100-h) corrosion test runs are being conducted in the AFBC. Compositions and geometries of corrosion specimens, as well as locations of exposure, in these long-term runs were selected. Parameters to be measured during the corrosion tests were identified.

1. 100-h Corrosion Tests

Four 100-h corrosion test runs (CT-1, -2, -3, and -4, also discussed on p. 45) were successfully conducted in the recently constructed AFBC. In these four runs, Sewickley coal (-12 +100 mesh) containing 5.46% S was combusted at a bed temperature of 850°C, a pressure of 101.3 kPa (1 atm), a fluidizing-gas velocity of 1 m/s, a fluidized-bed height of 813 mm, and with 3% O_2 in the dry off-gas. The sorbent was Grove limestone (-10 +30 mesh, containing 95.3% $CaCO_3$) with or without $CaCl_2$, NaCl, or Na_2CO_3 addition. In the first run (CT-1), the Grove limestone sorbent contained no sulfation-enhancement agent. The sorbent contained ∿0.3 mol % $CaCl_2$ in the second run (CT-2), ∿0.5 mol % NaCl in the third run (CT-3), and ∿1.9 mol % Na_2CO_3 in the fourth run (CT-4). The Ca/S mole ratio in each of the four runs was adjusted to maintain ∿700 ppm SO_2 in the dry off-gas in order to meet the EPA emission standard of 1.4 g $SO_2/10^6$ cal (1.2 lb $SO_2/10^6$ Btu).

For each corrosion test, three air-cooled probes and four coupon holders, each holding seven corrosion specimens, were installed at various locations in the fluidized-bed and freeboard sections of the combustor. The compositions of the candidate materials evaluated in the corrosion studies are given in Table 11. Two types of corrosion specimens were fabricated from the various materials. Tubular ring specimens (22.2-mm diameter and 22.2-mm long) were used with the air-cooled corrosion probes and ∿8-mm-thick circular disk specimens were used with the uncooled corrosion coupon holders. Schematic diagrams of the air-cooled probe and the coupon holder are shown in Figs. 33 and 34, respectively.

The temperatures along the length of an air-cooled probe were recorded at three locations, *i.e.*, at the two end corrosion specimens and at the center specimen. The temperature gradient between the cooling-air inlet and the outlet for the air-cooled probes was approximately 100°C. The materials, specimen locations, and temperatures of the corrosion probes for the four runs are listed in Tables 12, 13, 14, and 15.

The temperature of the air-cooled probe located in the freeboard sections (Probe AC-3) was intended to be controlled at 649°C (1200°F) during the 100-h test runs. However, the highest actual temperature of this probe (observed in Run CT-3) was only 645°C (1193°F), and so no coolant air was required for this probe in the four runs.

Table 11. Compositions (in wt %) of Candidate Materials

	Fe	Ni	Cr	Co	Mo	Mn	Si	C	Other Elements
Cobalt-Base Alloy									
Haynes 188	1.6	22.9	21.5	Bal.	-	0.9	0.4	0.10	13.6 W, 0.06 La
Nickel-Base Alloy									
Inconel 601	14.1	Bal.	23.0	-	-	0.5	0.25	0.05	1.35 Al, 0.25 Cu
Inconel 617	-	Bal.	22.0	12.5	9.0	-	-	0.07	1.0 Al
Inconel 625	2.5	Bal.	21.5	-	9.0	0.25	0.25	0.05	3.6 Nb, 0.2 Al, 0.2 Ti
Inconel 671	-	Bal.	48.0	-	-	-	-	0.05	0.35 Ti
Inconel 718	18.5	Bal.	19.0	-	3.0	0.18	0.18	0.04	5.1 Nb, 0.9 Ti, 0.5 Al, 0.2 Cu
Alloy 713C (c)[a]	-	Bal.	13.5	-	4.2	-	-	0.10	2.0 Nb, 0.8 Ti, 6.1 Al, 0.1 Zr
IN 738 (c)	-	Bal.	16.0	8.1	1.6	-	-	0.10	2.6 W, 0.8 Nb, 3.4 Ti, 3.4 Al, 1.8 Ta, 0.04 Zr
Hastelloy-X	19.2	Bal.	21.7	2.1	8.8	0.7	0.5	0.08	0.7 W
RA 333	18.0	Bal.	25.0	3.0	3.0	1.5	1.25	0.05	3.0 W
Austenitic Steel									
Type 304 SS	Bal.	9.5	19.0	-	-	2.0[b]	0.5[b]	0.03[b]	
Type 309 SS	Bal.	13.5	23.0	-	-	2.0[b]	1.0[b]	0.20[b]	
Type 310 SS	Bal.	20.5	25.0	-	-	2.0[b]	1.5[b]	0.25[b]	
Type 316 SS	Bal.	12.0	17.0	-	2.5	2.0[b]	0.5[b]	0.10[b]	
Type 321 SS	Bal.	10.5	18.0	-	-	2.0[b]	-	0.08[b]	Ti
Type 347 SS	Bal.	11.0	18.0	-	-	2.0[b]	-	0.08[b]	Nb, Ta
Incoloy 800	Bal.	32.5	21.0	-	-	1.5	1.0	0.10	0.38 Al, 0.38 Ti
HK-40 (c)	Bal.	19.8	26.4	-	0.5[b]	0.6	0.8	0.38	
Ferritic Steel									
2¼ Cr-1 Mo	Bal.	-	2.25	-	1.0	0.5	0.5	0.15[b]	
9 Cr-1 Mo	Bal.	-	9.0	-	1.0	0.5	0.6	0.15[b]	
Type 446 SS	Bal.	-	25.0	-	-	1.5[b]	1.0[b]	0.20[b]	
C12 (c)	Bal.	-	8.2	-	1.1	0.35	0.35	0.16	
HC (c)	Bal.	3.1	26.9	-	-	1.0	0.7	0.12	
CA-40 (c)	Bal.	0.4	12.9	-	-	0.4	0.7	0.31	

[a](c) = cast alloy.

[b]Maximum.

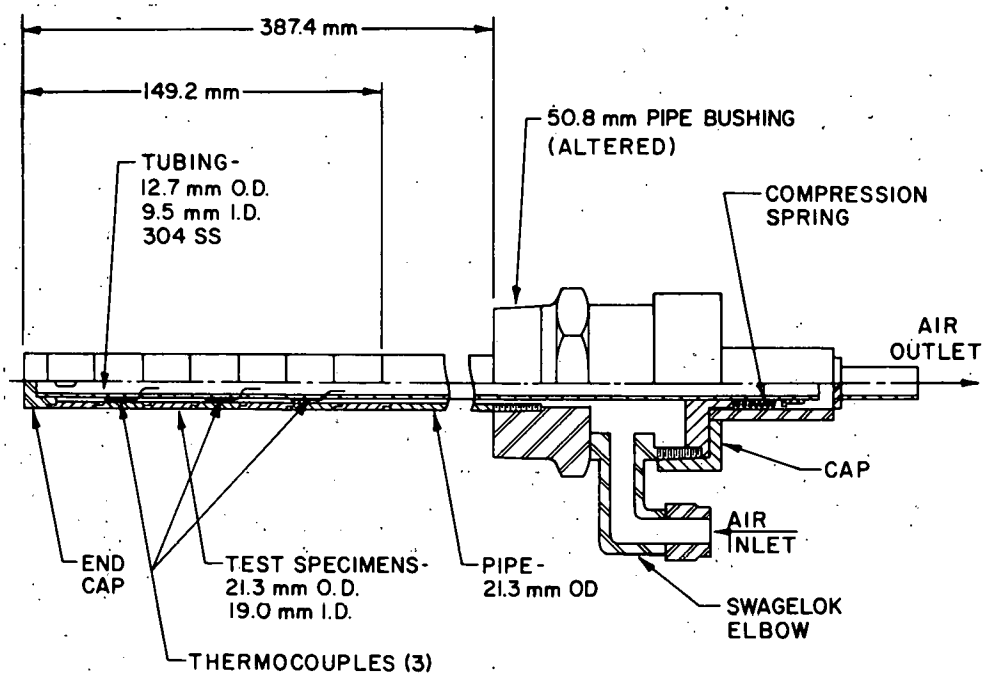

Fig. 33. Schematic of Air-Cooled Corrosion Probe.

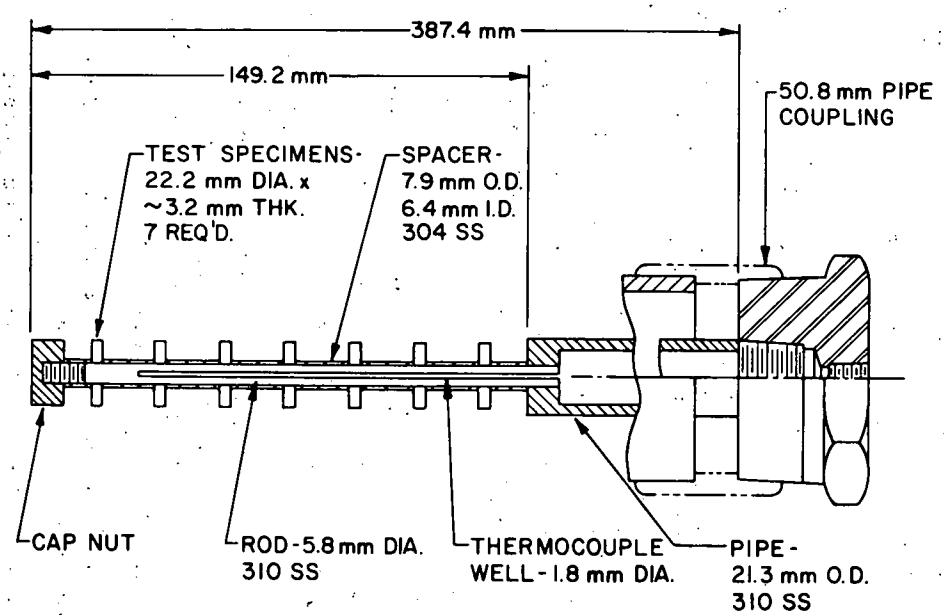

Fig. 34. Schematic of Uncooled Corrosion Coupon Holder.

Table 12. Materials, Locations, and Temperatures of Corrosion Specimens for Run CT-1. No sulfation-enhancement agent added.

Corrosion Probe Designation[a]	Specimen Material[b]	Probe Location	Mean Temperature,[c] °C
		Bed Section	
C-1	Inconel 601, Inconel 671, Hastelloy-X, Type 310 SS Haynes 188, RA 333, Type 347 SS	102 mm above gas distributor plate	848
AC-2	Type 321 SS, Inconel 601, Type 310 SS, Incoloy 800, Inconel 617, RA 333, Type 309 SS	305 mm above gas distributor plate	598, 675, 724
AC-1	Type 304 SS, Type 446 SS, 2¼ Cr-1 Mo Steel, Incoloy 800, 9 Cr-1 Mo Steel, Type 316 SS, Type 309 SS	508 mm above gas distributor plate	429, 699, 727
C-2	Inconel 625, Inconel 718, Incoloy 800, Type 310 SS, Inconel 617, Type 304 SS, Type 316 SS	610 mm above gas distributor plate	844
		Freeboard Section	
C-4	Type 304 SS, Incoloy 800, Alloy 713C, Type 310 SS, IN 738, Haynes 188, Type 347 SS	394 mm above top of bed	673
AC-3[d]	Type 321 SS, Inconel 601, Type 310 SS, Incoloy 800, Inconel 617, RA 333, Type 309 SS	1003 mm above top of bed	466, 471, 585
C-3	Inconel 601, Hastelloy-X, Inconel 617, Type 310 SS, Inconel 671, Haynes 188, RA 333	1308 mm above top of bed	566

[a] AC = air-cooled probe; C = uncooled coupon holder.

[b] Materials listed according to stacking sequence on the probe: first specimen near the pipe bushing, last specimen near the end cap.

[c] The temperatures listed for air-cooled probes were measured in specimens of Type 321 SS, Type 304 SS, Incoloy 800, and Type 309 SS.

[d] No coolant air was required for this probe.

Table 13. Materials, Locations, and Temperatures of Corrosion Specimens for Run CT-2. ∿0.3 mol % $CaCl_2$ added.

Corrosion Probe Designation[a]	Specimen Material[b]	Probe Location	Mean Temperature[c] °C
		Bed Section	
C-2	Inconel 625, Inconel 718, Incoloy 800, Type 310 SS, Inconel 617, Type 304 SS, Type 316 SS	102 mm above gas distributor plate	819
AC-2	Inconel 601, Type 321 SS, Type 310 SS, Incoloy 800, Inconel 601, RA 333, Type 309 SS	305 mm above gas distributor plate	590, 646, 681
AC-1	Type 446 SS, Type 304 SS, 2¼ Cr-1 Mo Steel, Incoloy 800, 9 Cr-1 Mo Steel, Type 316 SS Type 309 SS	508 mm above gas distributor plate	528, 545, 599
C-1	Inconel 601, Inconel 671, Hastelloy-X, Type 310 SS, Haynes 188, RA 333, Type 347 SS	610 mm above gas distributor plate	844
		Freeboard Section	
C-4	Alloy HK-40, Alloy HC, Alloy CA-40, Alloy C-12, Alloy 713C, IN 738, Incoloy 800	394 mm above top of bed	693
AC-3[d]	Inconel 601, Type 321 SS, Type 310 SS, Incoloy 800, Inconel 617, RA 333, Type 309 SS	1003 mm above top of bed	604, 609, 614
C-3	Haynes 188, Hastelloy-X, Inconel 601, Inconel 617, Inconel 671, RA 333, Type 310 SS	1308 mm above top of bed	587

[a] AC = air-cooled probe; C = uncooled coupon holder.

[b] Materials listed according to stacking sequence on the probe: first specimen near the pipe bushing, last specimen near the end cap.

[c] The temperatures listed for air-cooled probes were measured in specimens of Type 321 SS, Type 304 SS, Incoloy 800, and Type 309 SS.

[d] No coolant air was required for this probe.

Table 14. Materials, Locations, and Temperatures of Corrosion Specimens for Run CT-3. ∿0.5 mol % NaCl added.

Corrosion Probe Designation[a]	Specimen Material[b]	Probe Location	Mean Temperature,[c] °C
		Bed Section	
C-2	Inconel 625, Inconel 718, Incoloy 800, Type 310 SS, Inconel 617, Type 304 SS, Type 316 SS	102 mm above gas distributor plate	852
AC-1	Type 446 SS, Type 304 SS, 2¼ Cr-1 Mo Steel, Incoloy 800, 9 Cr-1 Mo Steel, Type 316 SS, Type 321 SS	305 mm above gas distributor plate	588, 631, 613
AC-2	Inconel 601, Type 321 SS, Type 310 SS, Type 304 SS, Inconel 617, RA 333, Type 309 SS	508 mm above gas distributor plate	552, 596, 597
C-1	Inconel 601, Inconel 671, Hastelloy-X, Type 310 SS, Haynes 188, RA 333, Type 347 SS	610 mm above gas distributor plate	851
		Freeboard Section	
C-4	Alloy HK-40, Alloy HC, Alloy CA-40, Alloy C-12, Alloy 713C, IN 738, Incoloy 800	394 mm above top of bed	701
AC-3[d]	Inconel 601, Type 321 SS, Type 310 SS, Incoloy 800, Inconel 617, RA 333, Type 309 SS	1003 mm above top of bed	621, 640, 645
C-3	Haynes 188, Hastelloy-X, Inconel 601, Inconel 617, Inconel 671, RA 333, Type 310 SS	1308 mm above top of bed	605

[a] AC = air-cooled probe; C = uncooled coupon holder.

[b] Materials listed according to stacking sequence on the probe: first specimen near the pipe bushing, last specimen near the end cap.

[c] The temperatures listed for air-cooled probes were measured in specimens of Type 321 SS, Type 304 SS, Incoloy 800, and Type 309 SS.

[d] No coolant air was required for this probe.

Table 15. Materials, Locations, and Temperatures of Corrosion Specimens for Run CT-4. ∿1.9 mol % Na_2CO_3 added.

Corrosion Probe Designation[a]	Specimen Material[b]	Probe Location	Mean Temperature,[c] °C
		Bed Section	
C-2	Inconel 625, Inconel 718, Incoloy 800, Type 310 SS, Inconel 617, Type 304 SS, Type 316 SS	102 mm above gas distributor plate	854
AC-2	Inconel 601, Type 321 SS, Type 310 SS, Incoloy 800, Inconel 617, RA 333, Type 309 SS	305 mm above gas distributor plate	626, 648, 673
AC-1	Type 446 SS, Type 304 SS, 2¼ Cr-1 Mo Steel, Incoloy 800, 9 Cr-1 Mo Steel, Type 316 SS, Type 309 SS	508 mm above gas distributor plate	538, 587, 611
C-1	Inconel 601, Inconel 671, Hastelloy-X, Type 310 SS, Haynes 188, RA 333, Type 347 SS	610 mm above gas distributor plate	855
		Freeboard Section	
C-4	Alloy HK-40, Alloy HC, Alloy CA-40, Alloy C-12, Alloy 713C, IN 738, Incoloy 800	394 mm above top of bed	647
AC-3[d]	Inconel 601, Type 321 SS, 9 Cr-1 Mo Steel, Incoloy 800, 2¼ Cr-1 Mo Steel, Type 310 SS, Type 309 SS	1003 mm above top of bed	548, 574, 579
C-3	Haynes 188, Hastelloy-X, Inconel 601, Inconel 617, Inconel 671, RA 333, Type 310 SS	1308 mm above top of bed	535

[a] AC = air-cooled probe; C = uncooled coupon holder.

[b] Materials listed according to stacking sequence on the probe: first specimen towards pipe bushing, last specimen near the end cap.

[c] The temperatures listed for air-cooled probes were measured in specimens of Type 321 SS, Type 304 SS, Incoloy 800, and Type 309 SS.

[d] No coolant air was required for this probe.

The Ca/S mole ratios required to maintain ∿700 ppm SO_2 in the dry off-gas during each of the four 100-h corrosion test runs are given in Table 8. Based on the Ca/S mole ratios listed in this table, it appears that low-concentration additions of either $CaCl_2$ (Run CT-2) or NaCl (Run CT-3) gave insignificant sulfation enhancement of Grove limestone sorbent. As discussed above, the disparity between these results and those of previously reported laboratory-scale experiments is attributed to differences in the manner in which the two types of experimental data were generated.

Chemical analyses of riffled samples of the various solids streams added to, or removed from, the combustion system during the four 100-h corrosion test runs were completed. Based on these analyses and the analyses of the dry off-gas for SO_2, CO_2, CO, and CH_4, calculations were made of carbon, sulfur, and calcium material balances, as well as combustion efficiencies, for the four runs. Results of the calculations are summarized in Table 16.

Table 16. Carbon, Sulfur, and Calcium Material Balances and Combustion Efficiencies for 100-h Corrosion Test Runs

Experimental Conditions

Temperature: 850°C
Pressure: 101.3 kPa (1 atm)
Gas Velocity: 1 m/s
Fluidized-Bed Height: 813 mm
Excess O_2: 3% dry off-gas

Sulfur Retention: ∿85% (∿700 ppm SO_2 in dry off-gas)
Coal: Sewickley, 5.46% S, -12 +100 mesh
Sorbent: Grove limestone (ANL-9501), 95.3% $CaCO_3$, -10 +30 mesh

Run No.	Ca/S Mole Ratio	Percent Accounted for			Combustion Efficiency,[d] %
		Carbon[a]	Sulfur[b]	Calcium[c]	
CT-1	3.4	89	88	101	88
CT-2[e]	3.5	102	101	98	87
CT-3[f]	3.6	99	111	109	88
CT-4[g]	2.0	93	107	106	91[h]

[a] Analytical accuracy, ±5% relative for solid samples.

[b] For >5% sulfur, analytical accuracy, ±5% relative for solid samples. For <5% sulfur, analytical accuracy, +10% relative for solid samples.

[c] Analytical accuracy, ±2% relative.

[d] Defined as the percent of total combustible carbon fed that was completely burned to CO_2.

[e] Run conducted with ∿0.3 mol % $CaCl_2$ added to Grove limestone sorbent.

[f] Run conducted with ∿0.5 mol % NaCl added to Grove limestone sorbent.

[g] Run conducted with ∿1.9 mol % Na_2CO_3 added to Grove limestone sorbent.

[h] Questionable value since the CO_2 analyzer is suspected of being inaccurate during this run.

The material balances ranged from 89 to 102% for carbon, from 88 to 111% for sulfur, and from 98 to 109% for calcium. Since the possibilities for inaccuracies in weighing, sampling, analysis of the various solids streams, and analysis of the dry off-gas are numerous, material balances of 100 ± 10% are considered acceptable. Of the twelve values shown in Table 16, nine (or 75%) of the values are within this range and the remaining three values are only 1 to 2% outside of this range. Combustion efficiency, expressed as the percentage of total combustible carbon fed to the combustor that was burned to CO_2, varied slightly (87 to 88%) in the first three runs. The higher combustion efficiency of 91% in the fourth run is questionable since the accuracy of the CO_2 analyzer during this run was suspect.

2. Evaluation of Corrosion Behavior

(O. K. Chopra*)

a. Introduction

The experimental conditions and the materials, location, and temperature of the specimens for the corrosion tests are given in Section B.1 above. The corrosion specimens were examined metallographically to evaluate the corrosion behavior in terms of an average thickness of the surface scale and average depth of internal corrosive penetration in the specimens. The surface scale and depth of internal corrosion were measured at several locations on the specimens to obtain an average value. The distribution and nature of the corrosion products were evaluated by electron microprobe analyses.

b. Results

The top and bottom views of the air-cooled probes and uncooled coupon holders from the four corrosion tests are shown in Figs. 35-42. The air-cooled tubular specimens and the flat coupons which had been placed inside the fluidized bed had thin oxide scales and 20- to 80-μm-thick surface deposits from the bed material. Some of the surface scale spalled during cooling. The corrosion specimens that had been placed in the freeboard section of the combustor had a fine powdery deposit on the bottom surfaces and a loose particulate deposit on the top surfaces.

Uncooled Corrosion Coupons. The corrosion behavior of uncooled corrosion coupons was evaluated by measuring the thickness of the surface scale and the depth of internal corrosive penetration at the side surfaces and the top and bottom edges of the specimens (the side surfaces were parallel to and the top and bottom edges perpendicular to the flow of fluidizing gas and bed material). Average values for the thickness of the surface scale and internal corrosive penetration are given in Tables 17-20. The average temperature of the specimens in these tests was ∿850°C.

The corrosion specimens had 2- to 3-μm-thick oxide scale on the surface. The internal corrosive penetration primarily consisted of internal oxidation along the grain boundaries and patches of sulfides ahead of the oxidation front.

---

*Materials Science Division, Argonne National Laboratory.

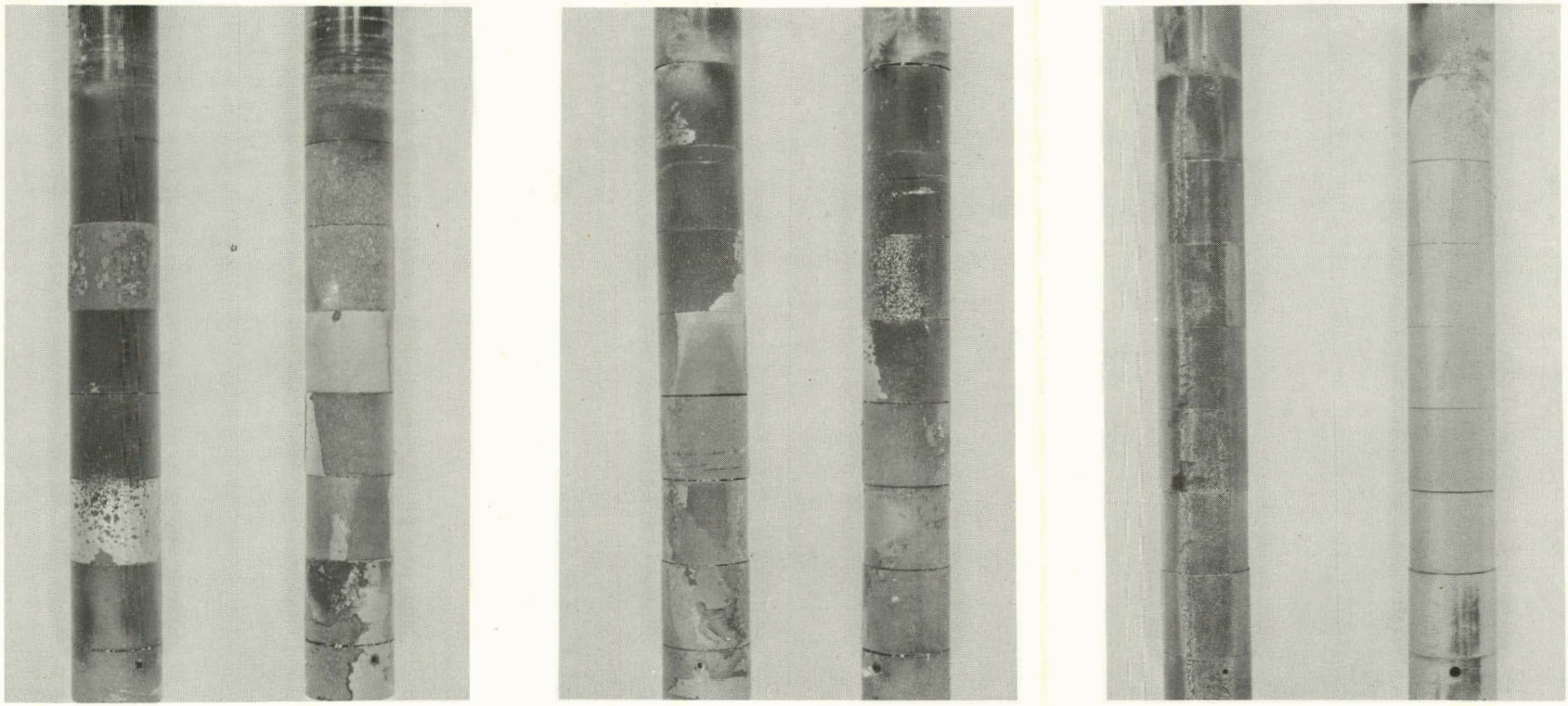

Fig. 35. Top and Bottom Views of Air-cooled Probes from Corrosion Test Run CT-1. No sulfation-enhancement agent added. Specimens stacked from top to bottom in the sequence in Table 12. ANL Neg. No. 306-79-53.

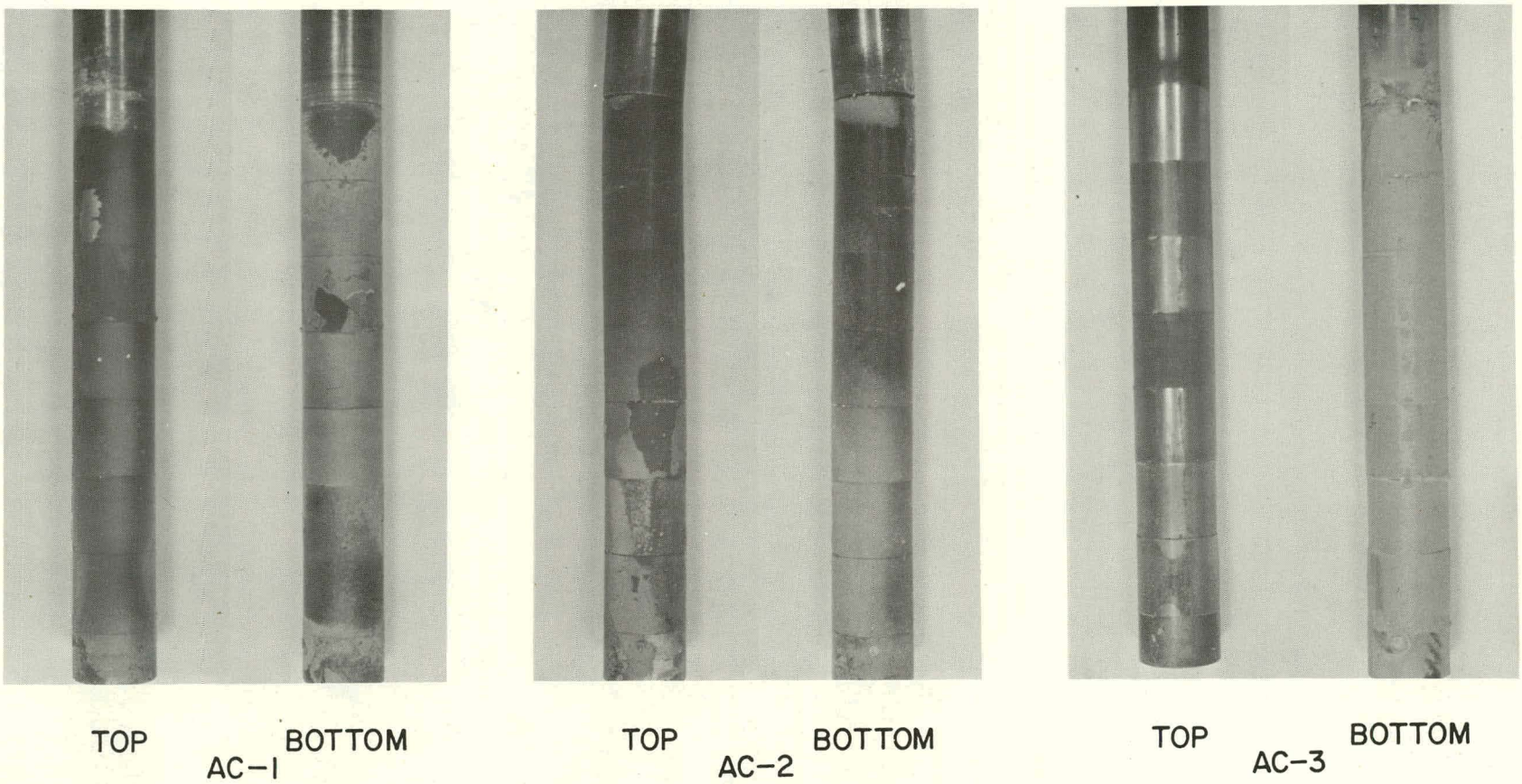

Fig. 36. Top and Bottom Views of Air-cooled Probes from Corrosion Test Run CT-2. ∿0.3 mol % $CaCl_2$ added. Specimens stacked from top to bottom in the sequence in Table 13. ANL Neg. No. 306-79-54.

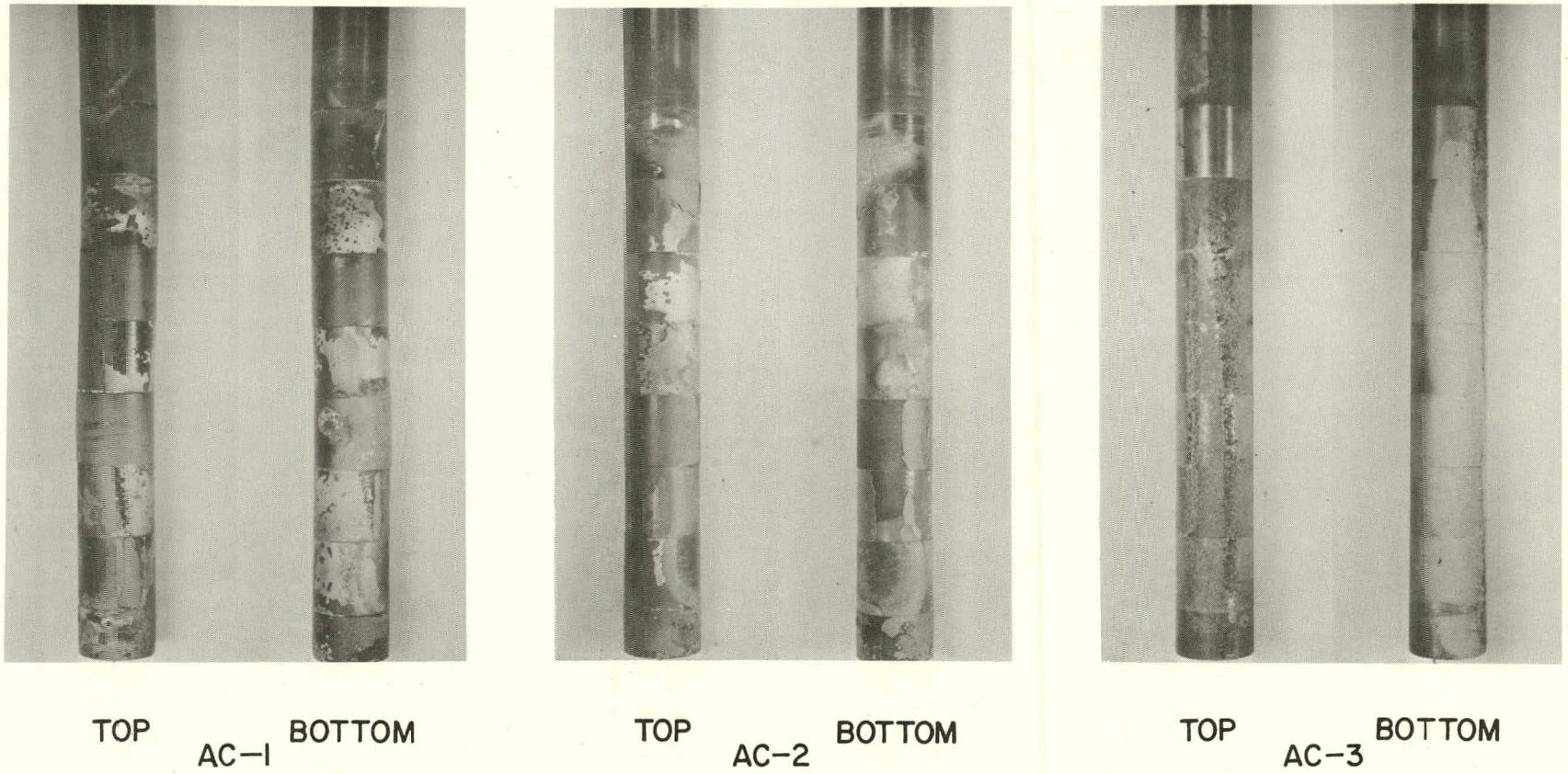

Fig. 37. Top and Bottom Views of Air-cooled Probes from Corrosion Test Run CT-3. ∿0.5 mol % NaCl added. Specimens stacked from top to bottom in the sequence in Table 14. ANL Neg. No. 306-79-52.

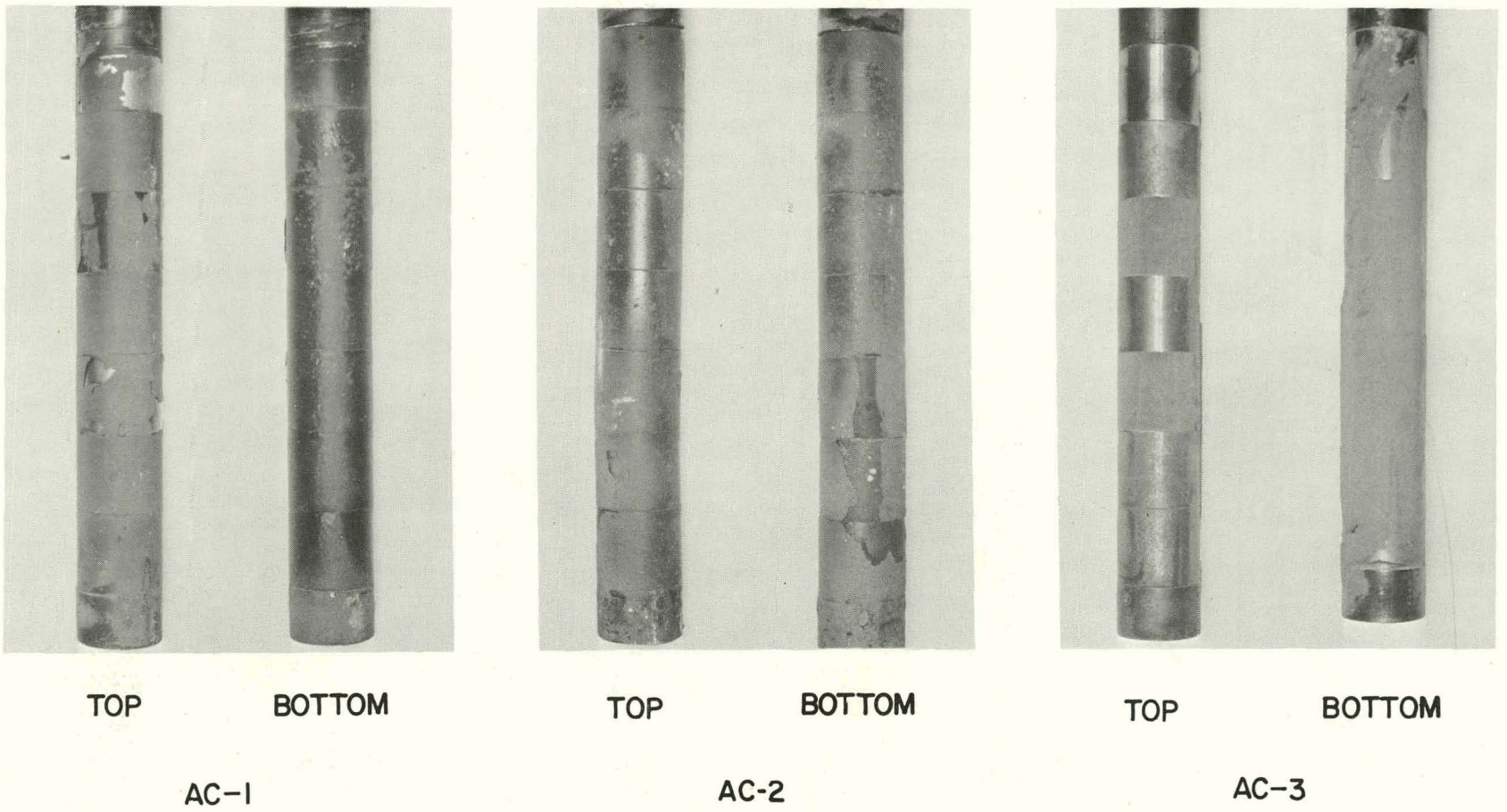

Fig. 38. Top and Bottom Views of Air-cooled Probes from Corrosion Test Run CT-4. 1.9 mol % Na_2CO_3 added. Specimens stacked from top to bottom in the sequence in Table 15. ANL Neg. No. 306-79-386.

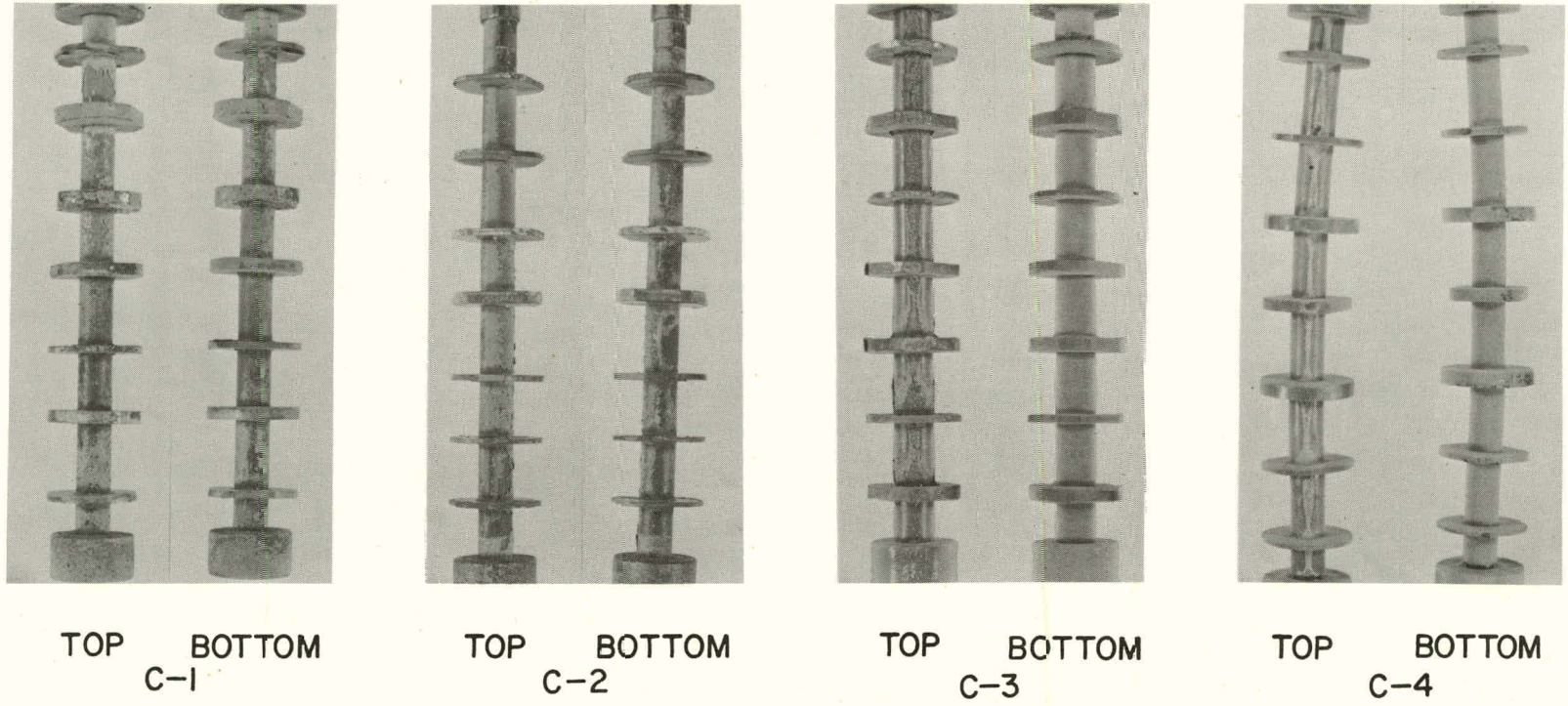

Fig. 39. Top and Bottom Views of Uncooled Coupon Holders from Corrosion Test Run CT-1. No sulfation-enhancement agent added. Specimens stacked from top to bottom in the sequence in Table 12. ANL Neg. No. 306-79-49.

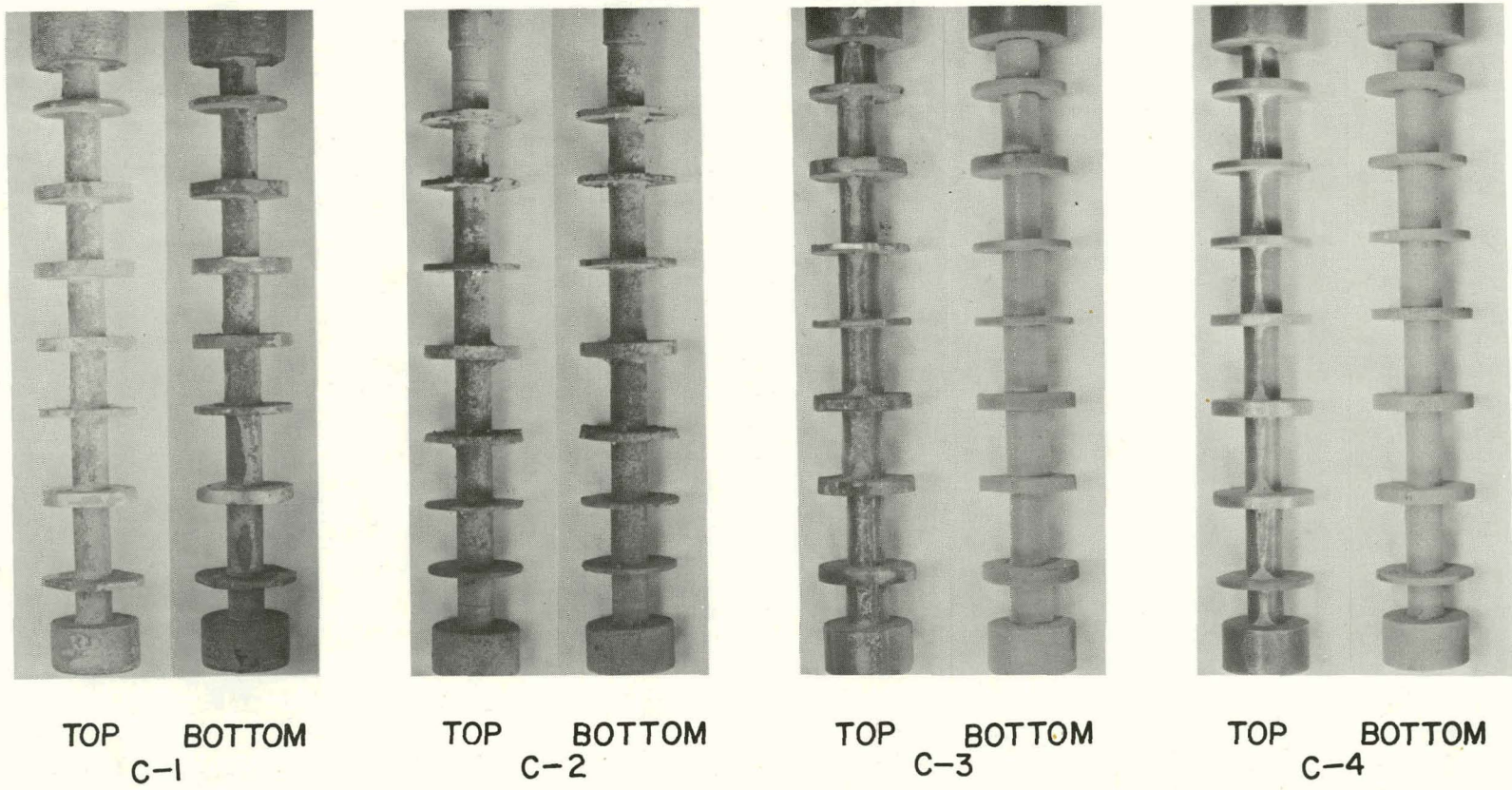

Fig. 40. Top and Bottom Views of Uncooled Coupon Holders from Corrosion Test Run CT-2. ~0.3 mol % $CaCl_2$ added. Specimens stacked from top to bottom in the sequence in Table 13. ANL Neg. No. 306-79-51.

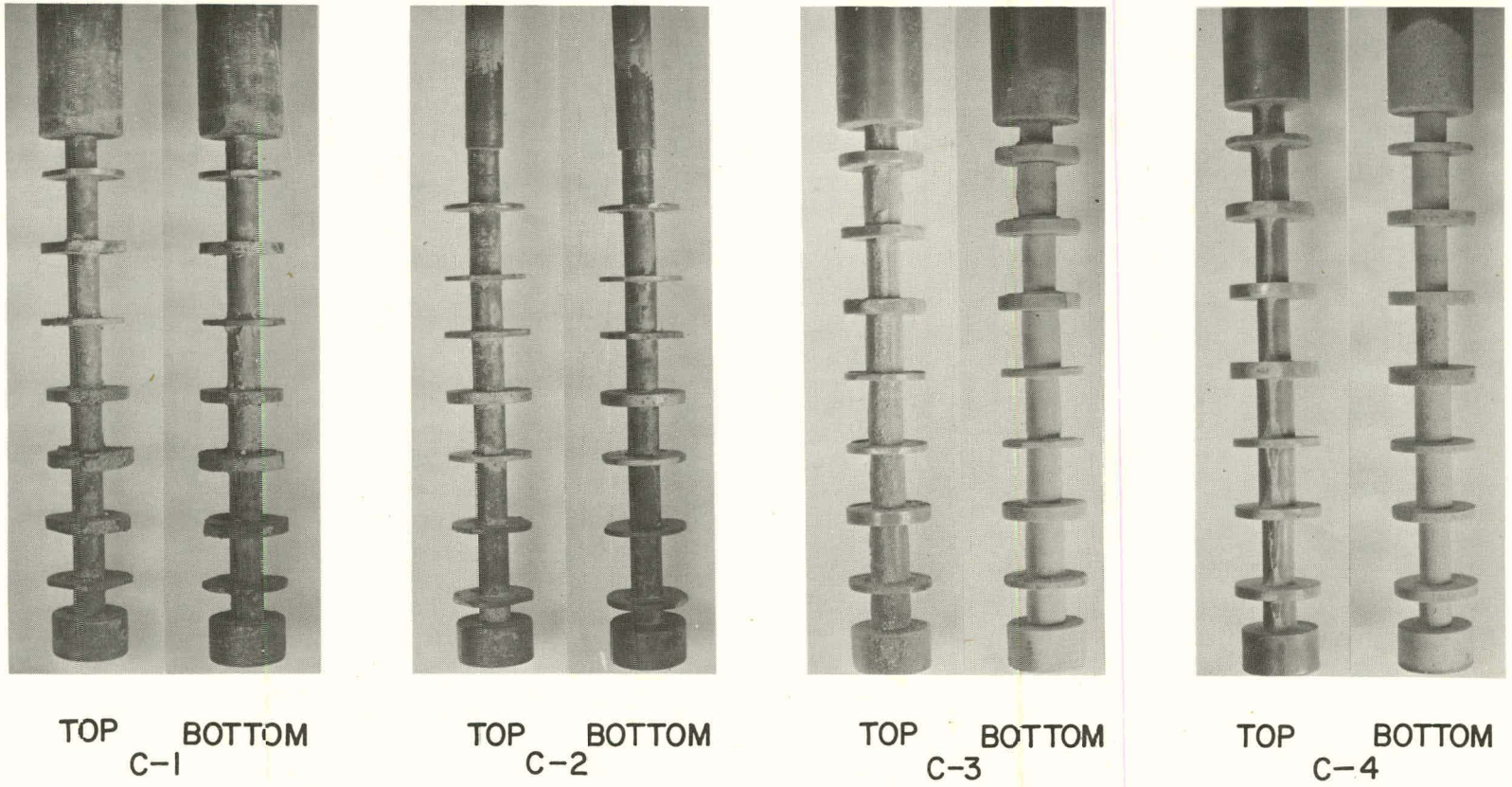

Fig. 41. Top and Bottom Views of Uncooled Coupon Holders from Corrosion Test Run CT-3. ∿0.5 mol % NaCl added. Specimens stacked from top to bottom in the sequence in Table 14. ANL Neg. No. 306-79-50.

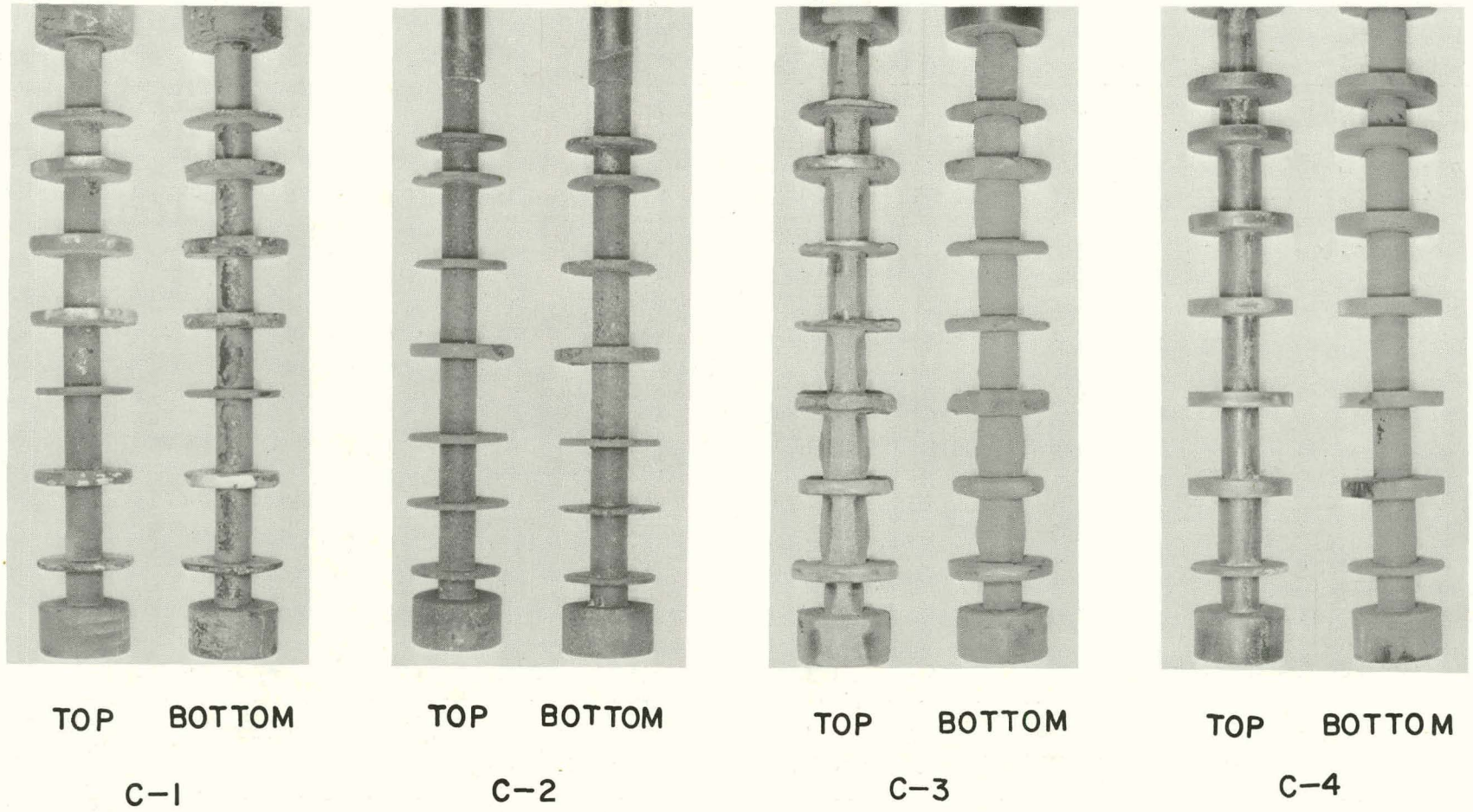

Fig. 42. Top and Bottom Views of Uncooled Coupon Holders from Corrosion Test Run CT-4. ∿1.9 mol % Na_2CO_3 added. Specimens stacked from top to bottom in the sequence in Table 15. ANL Neg. No. 306-79-385.

Table 17. Average Values of the Thickness of Surface Scale and Internal Corrosive Penetration Measured in Uncooled Corrosion Coupons for Run CT-1. No sulfation-enhancement agent added. Average temperature of the specimens was ∿845°C.

Specimen Holder	Material	Surface-scale Thickness, μm			Corrosive Penetration, μm			Remarks
		Top	Bottom	Side	Top	Bottom	Side	
C-1	Inconel 601	1.7	2.0	2.0	5.3	5.3	4.1	Some grain-boundary attack, ∿50 μm deep
	Inconel 671	3.1	3.4	2.5	6.4	8.5	6.6	Preferential corrosive attack of one phase ∿15 μm deep
	Hastelloy-X	a	1.2	1.2	5.1	4.2	3.5	
	Type 310 SS	1.5	1.4	2.6	17.1	11.5	21.2	Internal corrosion--mainly sulfides
	Haynes 188	2.0	a	1.9	9.3	8.5	9.2	
	RA 333	1.5	a	2.4	12.7	10.7	15.2	
	Type 347 SS	1.0	a	1.9	6.0	6.4	7.3	
C-2	Inconel 625	1.4	1.7	1.4	7.8	9.3	7.4	
	Inconel 718	a	3.1	2.0	5.4	5.1	5.9	
	Incoloy 800	1.7	a	2.7	11.0	21.2	8.8	
	Type 310 SS	a	a	1.6	9.1	12.9	12.7	Internal corrosion--mainly sulfides
	Inconel 617	3.2	a	3.3	16.5	16.1	9.3	Some grain-boundary attack, ∿40 μm deep
	Type 304 SS	3.8	1.7	3.1	20.3	11.4	11.9	
	Type 316 SS	2.7	2.9	2.7	9.1	25.0	8.5	

[a]Surface scale spalled.

Table 18. Average Values of the Thickness of Surface Scale and Internal Corrosive Penetration Measured in Uncooled Corrosion Coupons for Run CT-2. ∿0.3 mol % $CaCl_2$ added. Average temperature of the specimens was ∿845°C.

Specimen Holder	Material	Surface-scale Thickness, μm			Corrosive Penetration, μm			Remarks
		Top	Bottom	Side	Top	Bottom	Side	
C-1	Inconel 601	a	2.0	2.0	7.4	6.7	3.0	Some grain-coundary attack, ∿33 μm deep
	Inconel 671	a	5.6	6.7	63.0	77.5	11.5	
	Hastelloy-X	a	a	2.0	20.7	10.7	7.3	
	Type 310 SS	1.3	a	2.0	7.6	11.0	9.8	Internal corrosion--mainly sulfides
	Haynes 188	a	a	1.3	11.3	13.3	8.6	
	RA 333	2.3	a	1.7	8.5	13.5	7.6	
	Type 347 SS	a	3.0	3.4	5.3	9.7	10.2	
C-2	Inconel 625	1.3	1.3	2.1	9.8	9.1	8.8	
	Inconel 718	2.0	1.7	1.5	5.9	5.9	5.1	
	Incoloy 800	3.7	1.2	1.2	5.3	7.8	7.6	
	Type 310 SS	3.4	3.0	2.3	27.1	15.4	14.6	Internal corrosion--mainly sulfides
	Inconel 617	3.3	5.3	3.3	18.7	19.5	14.4	Some grain-boundary attack, ∿25 μm deep
	Type 304 SS	2.2	3.0	2.1	13.5	11.1	10.1	
	Type 316 SS	3.4	2.5	2.5	12.3	8.0	12.7	

[a]Surface scale spalled.

Table 19. Average Values of the Thickness of Surface Scale and Internal Corrosive Penetration Measured in Uncooled Corrosion Coupons for Run CT-3. ∿0.5 mol % NaCl acced. Average temperature of the specimens was ∿850°C.

Specimen Holder	Material	Surface-scale Thickness, μm			Corrosive Penetration, μm			Remarks
		Top	Bottom	Side	Top	Bottom	Side	
C-1	Inconel 601	a	a	3.8	32.2	40.2	38.1	
	Inconel 671	a	7.6	6.8	51.9	97.4	80.4	
	Hastelloy-X	1.9	1.7	1.7	14.8	10.6	15.6	
	Type 310 SS	2.0	2.0	2.7	15.2	10.2	15.2	Internal corrosion--mainly sulfides
	Haynes 188	1.7	a	1.2	11.8	8.5	12.3	
	RA 333	a	a	2.9	22.0	37.2	37.7	Corrosion attack in some regions, ∿80 μm deep
	Type 347 SS	a	a	2.5	11.0	10.1	9.3	
C-2	Inconel 625	2.5	a	2.4	17.8	16.9	9.8	
	Inconel 718	2.5	2.4	2.0	7.1	8.5	5.8	
	Incoloy 800	a	a	3.4	22.9	19.5	24.6	
	Type 310 SS	a	a	2.9	33.9	31.3	23.7	Internal corrosion--mainly sulfides
	Inconel 617	2.6	a	2.4	27.5	32.8	34.8	
	Type 304 SS	2.2	a	2.4	10.8	9.3	11.8	
	Type 316 SS	a	a	3.1	8.1	9.8	18.6	

[a]Surface scale spalled.

Table 20. Average Values of the Thickness of Surface Scale and Internal Corrosive Penetration Measured in Uncooled Corrosion Coupons for Run CT-4. ∿1.9 mol % Na_2CO_3 added. Average temperature of the specimens was ∿855°C.

Specimen Holder	Material	Surface-scale Thickness, μm			Corrosive Penetration, μm			Remarks
		Top	Bottom	Side	Top	Bottom	Side	
C-1	Inconel 601	2.7	2.1	3.0	6.8	12.3	16.6	Some grain-boundary attack, ∿50 μm deep
	Inconel 671	7.6	4.7	3.1	50.8	46.6	a	Corrosion behavior not uniform
	Hastelloy-X	3.0	3.0	2.9	b	10.2	12.9	
	Type 310 SS	3.4	3.4	3.2	13.5	17.8	12.8	Internal corrosion--mainly sulfides
	Haynes 188	2.1	1.8	2.1	8.0	9.8	9.5	Some grain-boundary attack, ∿24 μm deep
	RA 333	2.0	b	2.4	9.8	11.8	10.2	
	Type 347 SS	2.7	2.7	2.4	10.2	9.8	9.3	Internal corrosion--mainly sulfides
C-2	Inconel 625	3.8	3.1	4.1	21.1	22.9	23.7	
	Inconel 718	2.2	2.2	2.7	11.0	10.2	14.6	
	Incoloy 800	3.4	3.6	3.6	21.2	25.0	19.5	
	Type 310 SS	3.4	3.2	3.4	18.2	18.2	19.1	
	Inconel 617	3.2	3.6	3.6	25.4	21.2	26.5	
	Type 304 SS	2.9	2.4	3.0	18.6	16.2	22.0	
	Type 316 SS	3.4	3.4	3.4	16.1	22.2	23.3	

[a]Extensive corrosion on one side of the specimen and very little internal corrosive penetration on the other.

[b]Surface scale spalled.

Shown in Figs. 43 and 44, respectively, are the average thicknesses of surface scale and internal corrosive penetration, measured on the side surfaces of the specimens that were located inside the fluidized bed at a distance 102 and 610 mm above the fluidizing-gas distributor plate. In the absence of salt, total corrosion (*i.e.*, the combined value of the thickness of surface scale and internal corrosive penetration) for the different materials varied from 7 to 15 μm. The results for the corrosion tests in which salt was present showed that for all materials, the addition of 0.3 mol % $CaCl_2$ to the limestone sorbent had no significant effect on corrosion behavior. In general, the addition of 0.5 mol % NaCl or 1.9 mol % Na_2CO_3 increased the total corrosion for most of the materials. A significant increase in internal corrosive penetration occurred in the high-nickel alloys, namely, Inconels 601, 617, and 671; RA 333; and Incoloy 800. Micrographs of the cross sections of Inconels 617 and 671 specimens for corrosion tests in which salt was present are shown in Fig. 45.

Comparison of the corrosion behavior of Type 310 stainless steel in Figs. 43 and 44 for the four corrosion tests shows that the total corrosion of this material was greater at the location 102 mm above the gas distributor plate than at the 610-mm position. For Haynes Alloy 188 and Types 310 and 347 stainless steel, total corrosion in the presence and absence of salt was essentially the same. Micrographs of Type 310 stainless steel specimens which had been located inside the fluidized bed 102 and 610 mm above the gas distributor plate are shown in Figs. 46 and 47, respectively.

Metallographic examination of corrosion coupons which had been placed in the freeboard section of the combustor 394 and 1300 mm above the top of the bed (*i.e.*, coupon holders C-4 and C-3, respectively, Table 15), revealed no measurable corrosion; only the cast alloy C-12 was oxidized. The average temperatures of the specimens on coupon holder C-4 for runs CT-1, -2, -3, and -4 were 673, 693, 701, and 647°C, respectively. The average temperatures of the specimens placed on coupon holder C-3 were 100 to 110°C lower. Scanning-electron micrographs of the surface region of alloy C-12 for corrosion tests with salt addition are shown in Fig. 48. The thicknesses of the surface oxides for tests CT-2 and -3 were between 100 and 140 μm, whereas in CT-4, the extent of oxidation was less because the temperature was ∿50°C lower.

Air-cooled Specimens. The corrosion behavior of the air-cooled tubular specimens was not uniform, and the nature of the deposits on the specimen surface varied. For example, corrosion was greater under the deposits containing a significant amount of ash than in the regions where the deposits consisted mainly of limestone material. In a fluidized-bed environment, the nature of the deposits on the surface of the tubes can differ depending on the position of the surface with respect to the flow of the fluidizing gas and bed material. Consequently, the orientation of the specimen surface inside the combustor was marked on each specimen, and the thickness of the surface scale and the depth of corrosive penetration were measured at intervals of ∿20° around the circumference of a specimen. The average values for (1) temperature and (2) corrosion of specimens exposed inside the fluidized bed in the four corrosion tests are given in Tables 21 to 24. For the air-cooled corrosion probes, the temperature of three of the seven specimens was monitored during the test. The average temperature of the remaining

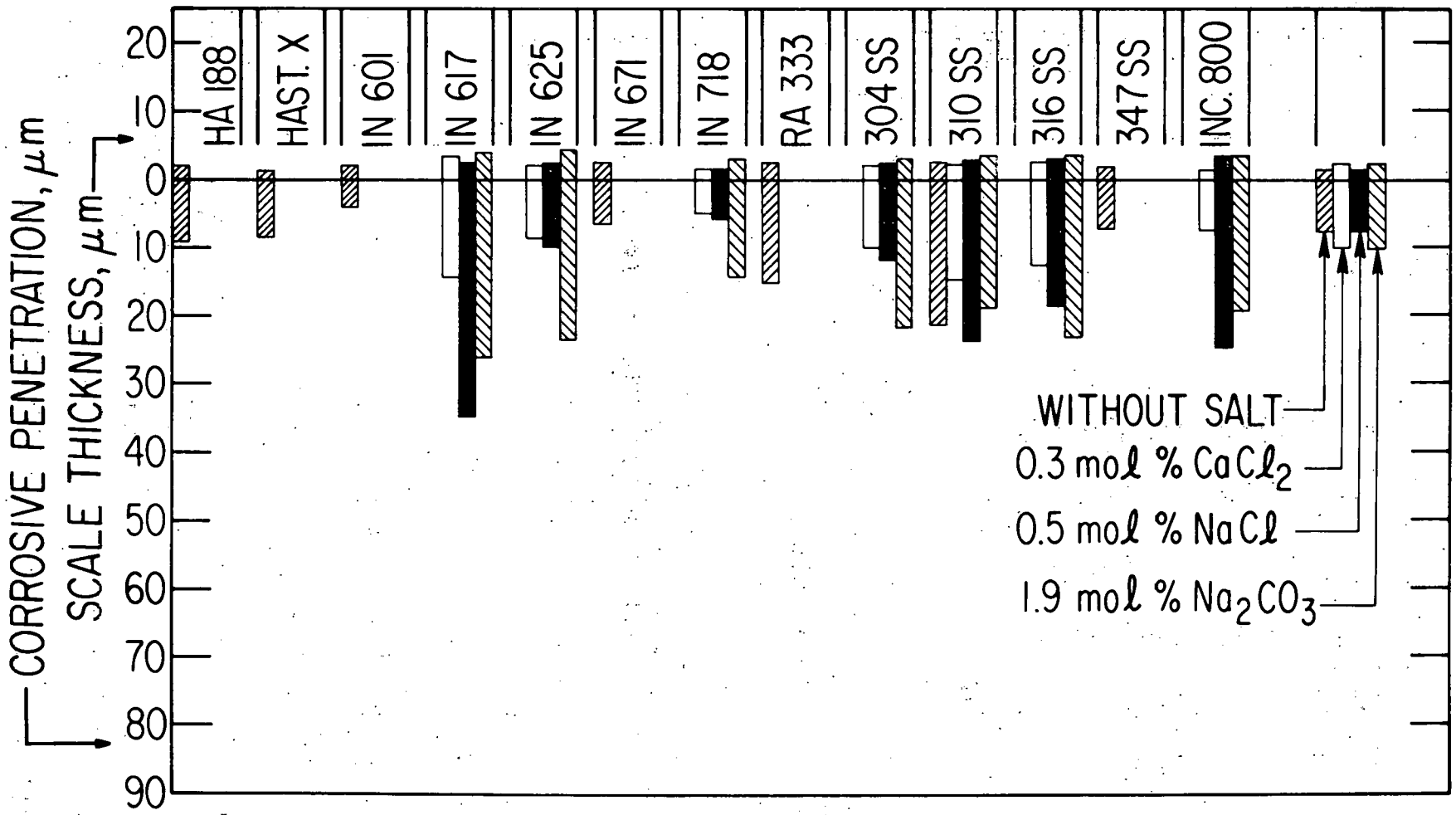

Fig. 43. Average Thickness of Surface Scale and Internal Corrosive Penetration for Corrosion Coupons Exposed at 845°C Inside the Fluidized Bed for 100 h at a Location 102 mm Above the Gas Distributor Plate. ANL Neg. No. 306-79-380.

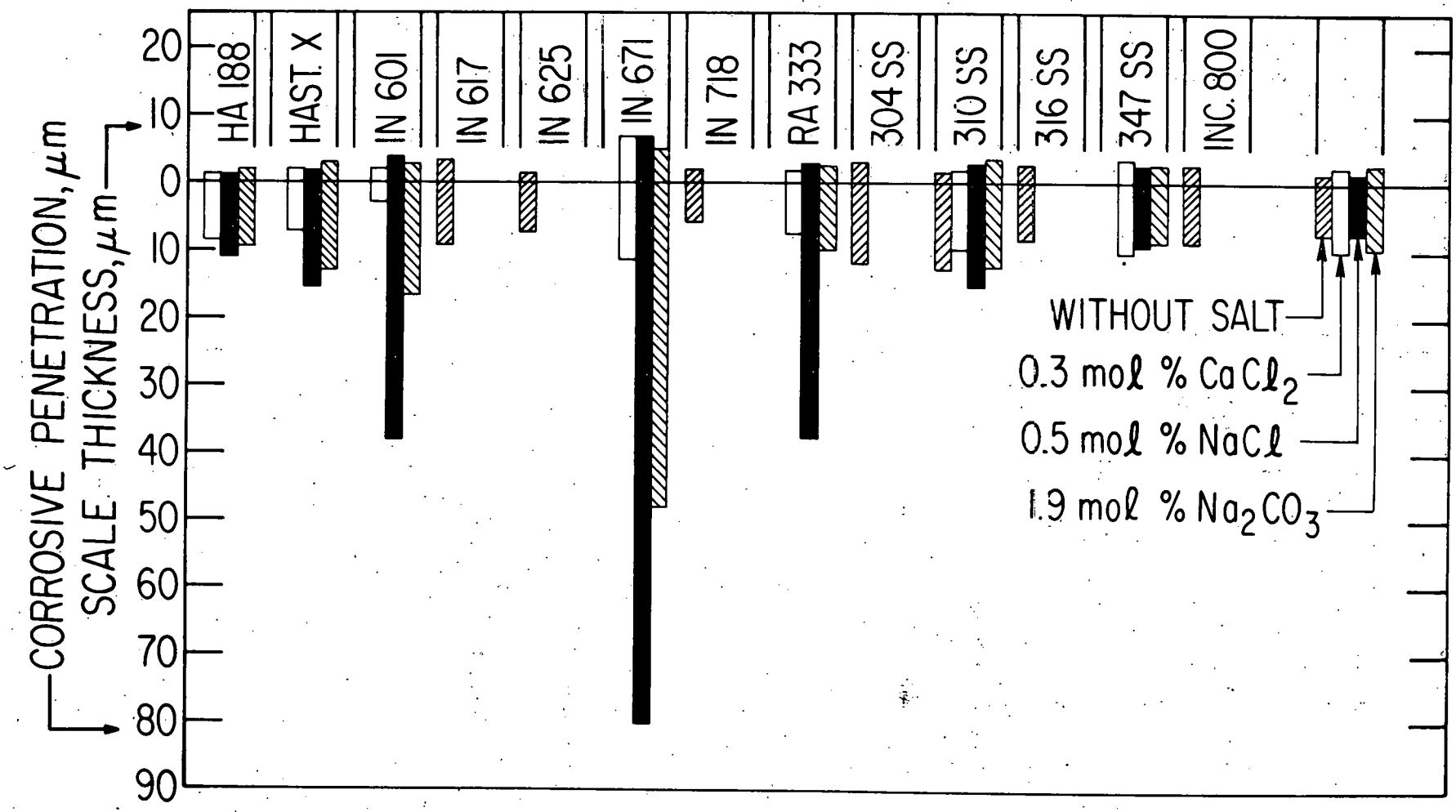

Fig. 44. Average Thickness of Surface Scale and Internal Corrosive Penetration for Corrosion Coupons Exposed at 845°C Inside the Fluidized Bed for 100 h at a Location 610 mm Above the Gas Distributor Plate. ANL Neg. No. 306-79-379.

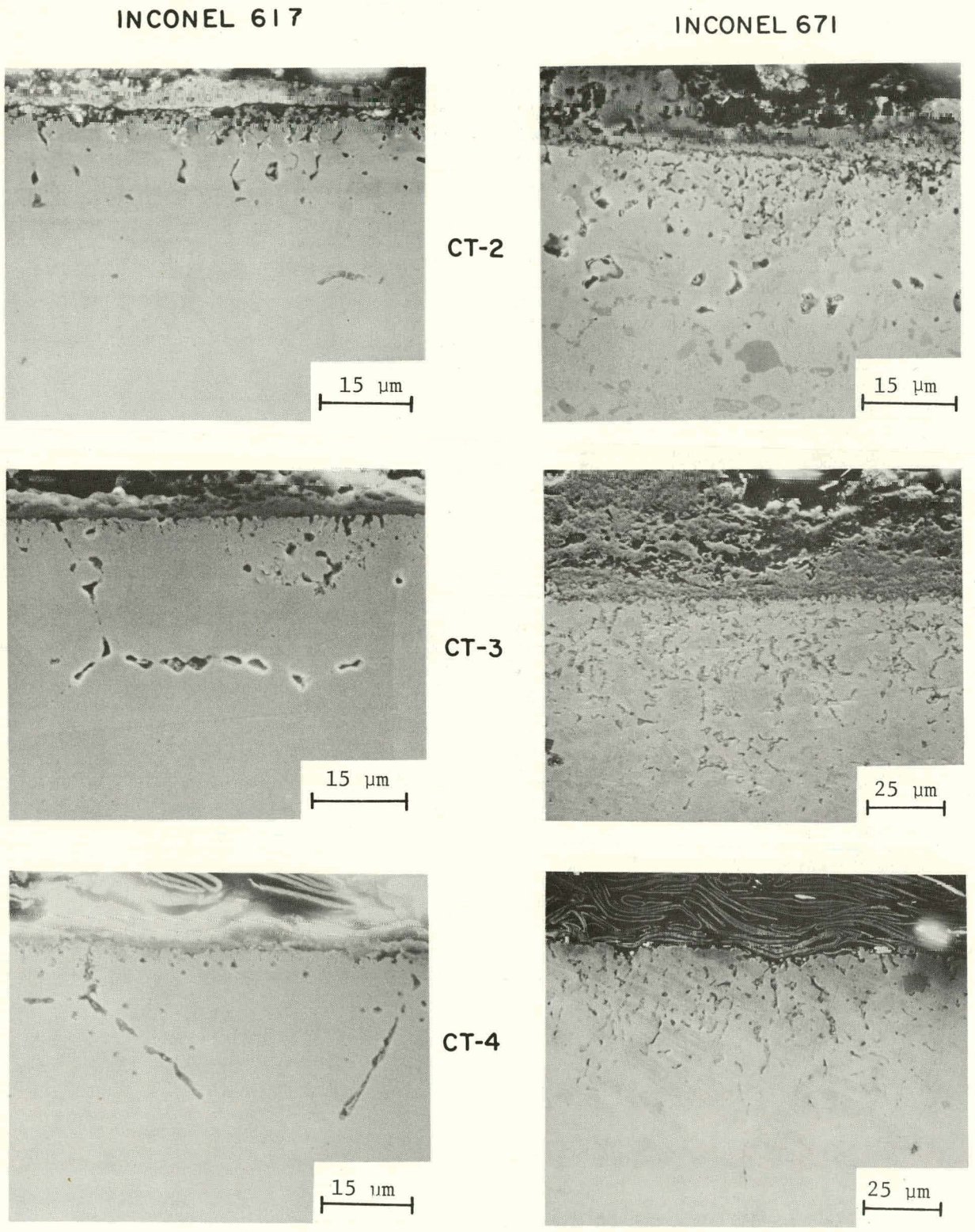

Fig. 45. SEM Micrographs of Inconels 617 and 671 After a 100-h Exposure Inside the Fluidized Bed. CT-2, 0.3 mol % $CaCl_2$; CT-3, 0.5 mol % NaCl; and CT-4, 1.9 mol % Na_2CO_3. ANL Neg. No. 306-79-382.

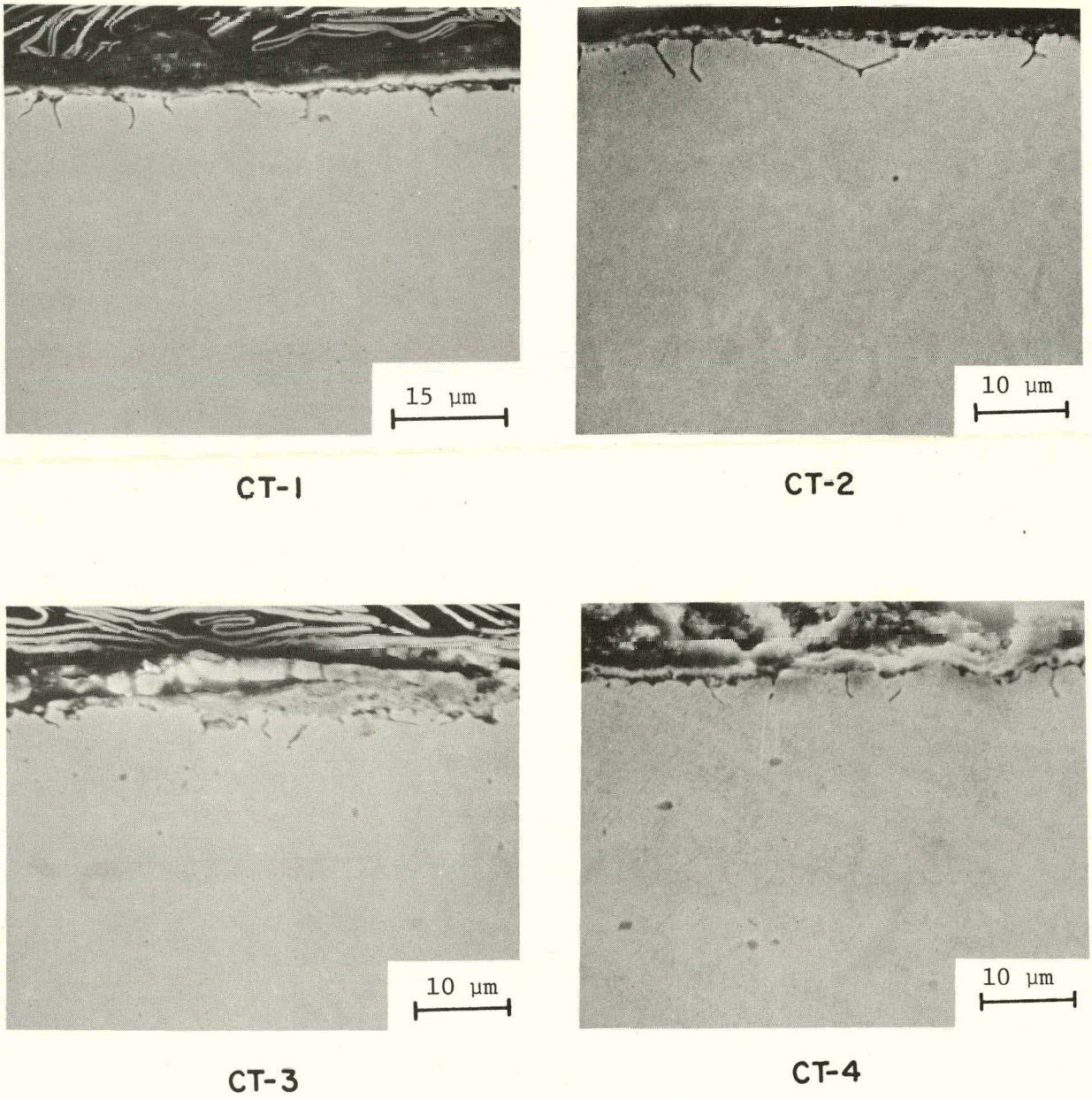

Fig. 46. SEM Micrographs of Type 310 Stainless Steel After a 100-h Exposure Inside the Fluidized Bed 102 mm Above the Gas Distributor Plate. CT-1, without salt; CT-2, 0.3 mol % $CaCl_2$; CT-3, 0.5 mol % NaCl; and CT-4, 1.9 mol % Na_2CO_3. ANL Neg. No. 306-79-383.

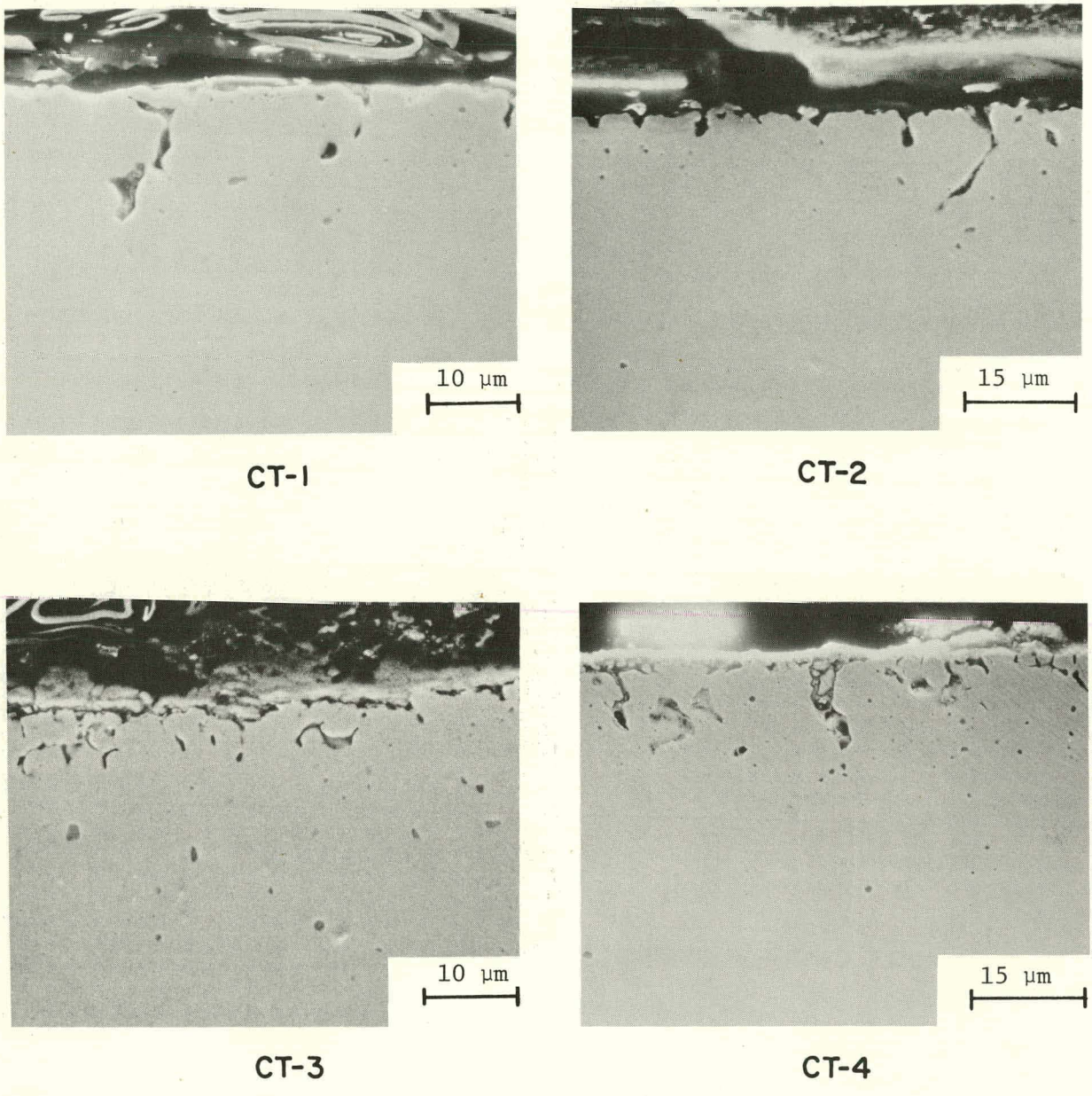

Fig. 47. SEM Micrographs of Type 310 Stainless Steel After a 100-h Exposure Inside the Fluidized Bed 610 mm Above the Gas Distributor Plate. CT-1, without salt; CT-2, 0.3 mol % $CaCl_2$; CT-3, 0.5 mol % NaCl; and CT-4, 1.9 mol % Na_2CO_3. ANL Neg. No. 306-79-381.

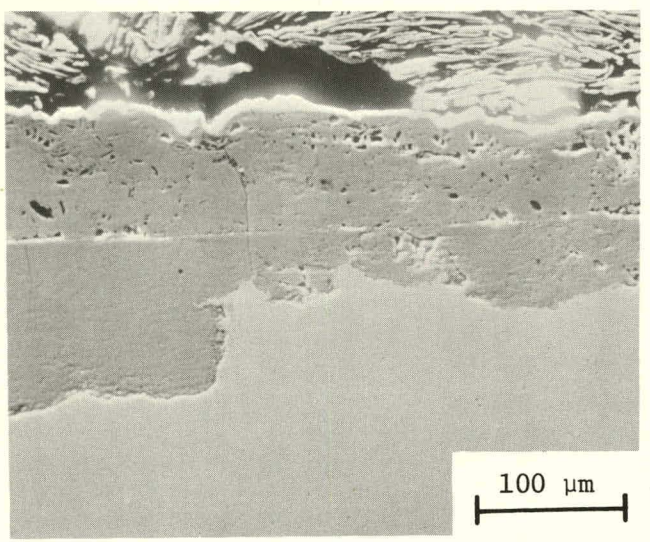

CT-2

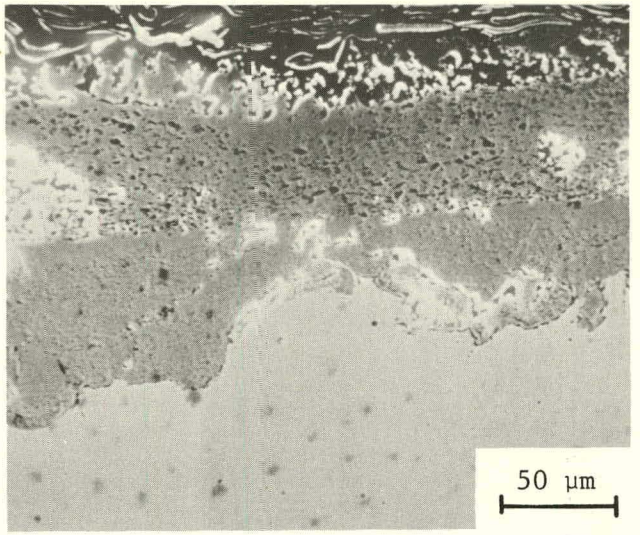

CT-3

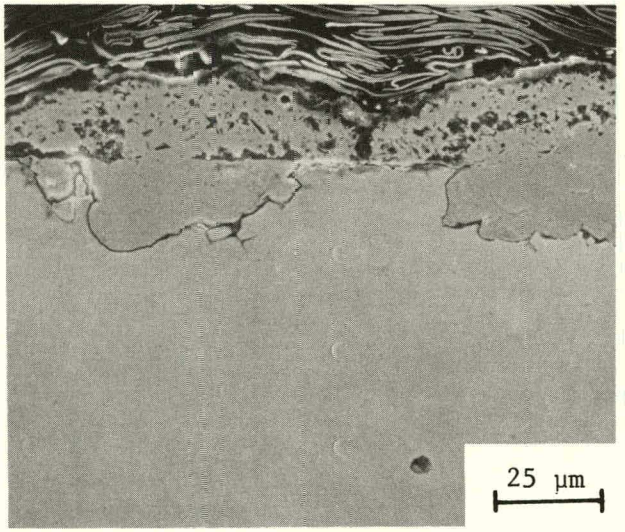

CT-4

Fig. 48. SEM Micrographs of Alloy C-12 After a 100-h Exposure in the Freeboard Section of the Combustor. CT-2, 0.3 mol % $CaCl_2$; CT-3, 0.5 mol % NaCl; and CT-4, 1.9 mol % Na_2CO_3. ANL Neg. No. 308-79-384

Table 21. Average Values of the Thickness of Surface Scale and Internal Corrosive Penetration Measured in Air-cooled Corrosion Specimens for Run CT-1

Corrosion Probe Designation[a]	Material	Average Temp., °C	Surface-scale Thickness, μm	Corrosive Penetration, μm	Total Corrosive Attack, μm	Remarks
AC-2	Inconel 601	603	2.6	4.7	7.3	Maximum corrosive attack, ∿15 μm
AC-2	Inconel 617	697	2.5	2.6	5.1	
AC-2	RA 333	712	2.4	4.5	6.9	
AC-1	Type 304 SS	627	2.4	1.0	3.4	
AC-1	Type 309 SS	727	2.3	2.7	5.0	
AC-2	Type 309 SS	727	5.6	5.9	11.5	Interaction between surface scale and deposits
AC-2	Type 310 SS	652	4.9	6.9	11.8	Interaction between surface scale and deposits
AC-1	Type 316 SS	712	2.4	4.1	6.5	
AC-2	Type 321 SS	627	2.9	2.1	5.0	
AC-1	Incoloy 800	677	3.2	3.6	6.8	Interaction between surface scale and deposits
AC-2	Incoloy 800	677	2.5	3.9	6.4	Interaction between surface scale and deposits
AC-1	Type 446 SS	603	2.1	2.2	4.3	
AC-1	9 Cr-1 Mo Steel	697	-	-	18.3	Maximum corrosion, ∿35 μm
AC-1	Fe-2¼ Cr-1 Mo Steel	652	-	-	171.9	Maximum corrosion, ∿320 μm

[a]The air-cooled corrosion probes AC-1 and AC-2 were located inside the fluidized bed at distances 508 and 305 mm, respectively, above the fluidizing-gas distributor plate.

Table 22. Average Values of the Thickness of Surface Scale and Internal Corrosive Penetration Measured in Air-cooled Corrosion Specimens for Run CT-2

Corrosion Probe Designation[a]	Material	Average Temp., °C	Surface-scale Thickness, μm	Corrosive Penetration, μm	Total Corrosive Attack, μm	Remarks
AC-2	Inconel 601	567	1.7	1.8	3.5	
AC-2	Inconel 601	663	2.2	2.6	4.8	
AC-2	RA 333	677	3.0	6.2	9.2	Internal corrosion mainly sulfides
AC-1	Type 304 SS	527	1.2	1.6	2.8	
AC-1	Type 309 SS	597	2.0	3.5	5.5	
AC-2	Type 309 SS	685	2.0	4.1	6.1	
AC-2	Type 310 SS	623	2.3	5.0	7.3	
AC-1	Type 316 SS	583	1.2	2.1	3.3	
AC-2	Type 321 SS	597	2.1	2.0	4.1	
AC-1	Incoloy 800	560	2.3	3.5	5.8	
AC-2	Incoloy 800	646	1.7	3.7	5.4	
AC-1	Type 446 SS	501	2.1	2.8	4.9	
AC-1	9 Cr-1 Mo Steel	575	-	-	12.9	Maximum corrosion, ∿25 μm
AC-1	Fe-2¼ Cr-1 Mo Steel	544	-	-	142.3	Maximum corrosion, ∿160 μm

[a]The air-cooled corrosion probes AC-1 and AC-2 were located inside the fluidized bed at distances 508 and 305 mm, respectively, above the fluidizing-gas distributor plate.

Table 23. Average Values of the Thickness of Surface Scale and Internal Corrosive Penetration Measured in Air-cooled Corrosion Specimens for Run CT-3

Corrosion Probe Designation[a]	Material	Average Temp., °C	Surface-scale Thickness, μm	Corrosive Penetration, μm	Total Corrosive Attack, μm	Remarks
AC-2	Inconel 601	529	1.9	1.7	3.6	Corrosion in some regions, ∿10 μm
AC-2	Inconel 617	600	2.7	3.8	6.5	
AC-2	RA 333	605	2.0	1.7	3.7	Corrosion in some regions, ∿10 μm
AC-1	Type 304 SS	588	2.4	1.7	4.1	
AC-2	Type 304 SS	589	1.6	1.2	3.8	
AC-2	Type 309 SS	605	1.7	1.9	3.6	
AC-2	Type 310 SS	570	2.5	1.0	3.5	
AC-1	Type 316 SS	630	1.8	2.3	4.1	
AC-1	Type 321 SS	634	2.2	3.5	5.7	
AC-2	Type 321 SS	550	3.1	3.2	6.3	Intergranular attack
AC-1	Incoloy 800	612	2.4	4.0	6.4	
AC-1	Type 446 SS	577	3.0	3.2	6.2	Intergranular attack
AC-1	9 Cr-1 Mo Steel	622	-	-	16.5	Maximum corrosion, ∿40 μm
AC-1	Fe-2¼ Cr-1 Mo Steel	600	-	-	101.0	Maximum corrosion, ∿140 μm

[a]The air-cooled corrosion probes AC-1 and AC-2 were located inside the fluidized bed at locations 305 and 508 mm, respectively, above the fluidizing-gas distributor plate.

Table 24. Average Values of the Thickness of Surface Scale and Internal Corrosive Penetration Measured in Air-cooled Corrosion Specimens for Run CT-4

Corrosion Probe Designation[a]	Material	Average Temp., °C	Surface-scale Thickness, μm	Corrosive Penetration, μm	Total Corrosive Attack, μm	Remarks
AC-2	Inconel 601	617	2.1	1.4	3.5	
AC-2	Inconel 617	660	1.3	1.4	2.7	
AC-2	RA 333	667	2.1	3.2	5.3	
AC-1	Type 304 SS	550	2.2	1.7	3.9	
AC-1	Type 309 SS	605	2.7	3.8	6.5	
AC-2	Type 309 SS	675	4.2	5.3	9.5	Interaction between surface scale and deposits
AC-2	Type 310 SS	640	2.1	2.6	4.7	
AC-1	Type 316 SS	605	2.2	2.1	4.3	
AC-2	Type 321 SS	628	2.3	1.9	4.2	
AC-1	Incoloy 800	589	2.6	3.0	5.6	
AC-2	Incoloy 800	650	2.5	3.1	5.6	Interaction between surface scale and deposits
AC-1	Type 446 SS	529	2.4	1.0	3.4	
AC-1	9 Cr-1 Mo Steel	600	-	-	13.2	Maximum corrosion, ∿25 μm
AC-1	Fe-2¼ Cr-1 Mo Steel	570	-	-	113.5	Maximum corrosion, ∿180 μm

[a]The air-cooled corrosion probes AC-1 and AC-2 were located inside the fluidized bed at locations 508 and 305 mm, respectively, above the fluidizing-gas distributor plate.

corrosion specimens was obtained from the temperature profile along the length of the probe. The average temperature of the various corrosion specimens varied from 527°C to 727°C.

The results show that at these temperatures, the addition of salt (*i.e.*, NaCl, $CaCl_2$, or Na_2CO_3) had no significant effect on the corrosion behavior of any of the materials. In general, corrosion specimens of the various iron- and nickel-base alloys containing >15% chromium had a 2- to 3-μm-thick surface scale and 2- to 5-μm internal corrosive attack. The total corrosion in the specimens for test CT-1 with no salt added was somewhat greater than that for the other corrosion tests because the average temperature of the specimens during this test was ∿50°C higher. Micrographs of cross sections of Type 310 stainless steel, Incoloy 800, Inconel 601, and RA 333 specimens from the four corrosion tests are shown in Figs. 49 and 50.

The corrosion behavior of Fe-2¼ Cr-1 Mo steel specimens from the four corrosion tests is shown in Fig. 51 and that of Fe-9 Cr-1 Mo in Fig. 52. For these specimens, the thickness of the surface scale and the depth of internal corrosive penetration were not measured separately because the depth of internal corrosion was relatively small compared to the thickness of the scale. For the various experimental conditions in the four runs, the average values of the total corrosion at temperatures near 627°C for Fe-2¼ Cr-1 Mo and Fe-9 Cr-1 Mo specimens were ∿135 and 15 μm, respectively. The corrosion scales for these steels were quite porous, indicating interaction with the deposits from the bed material. Similar behavior was observed in several high-chromium alloys, *e.g.*, Type 309 stainless steel and Incoloy 800.

The distribution and nature of the corrosion products in the surface scales were investigated by electron microprobe analyses. The X-ray images for Fe, O, Cr, Ca, S, Si, and K in the scales observed on Fe-2¼ Cr-1 Mo and Fe-9 Cr-1 Mo specimens are shown in Figs. 53 and 54, respectively. The results indicate that the scales consist of two distinct layers: an inner layer of a mixed oxide of iron and chromium and an outer layer containing various elements (*e.g.*, Fe, O, Ca, S, Si, and K) from the bed material. The presence of these elements indicates that the outer layer of the scale forms by the interaction of the deposits with the scale, whereas the inner layer forms by corrosion of the specimen material. For the Fe-9 Cr-1 Mo steel, the extent of interaction between the deposits and the scale is less than that for Fe-2¼ Cr-1 Mo steel. This difference is probably due to the higher concentration of chromium in the surface scales.

The corrosion behavior of the specimens installed on air-cooled type corrosion probes which were exposed in the freeboard region of the combustor is being evaluated. The results will provide a better understanding of the mechanism of the reaction of the deposits with the scale. Longer duration (500 to 1000 h) corrosion tests are being conducted to further evaluate the effect of salts on the performance of various structural materials in the fluidized-bed combustion environment.

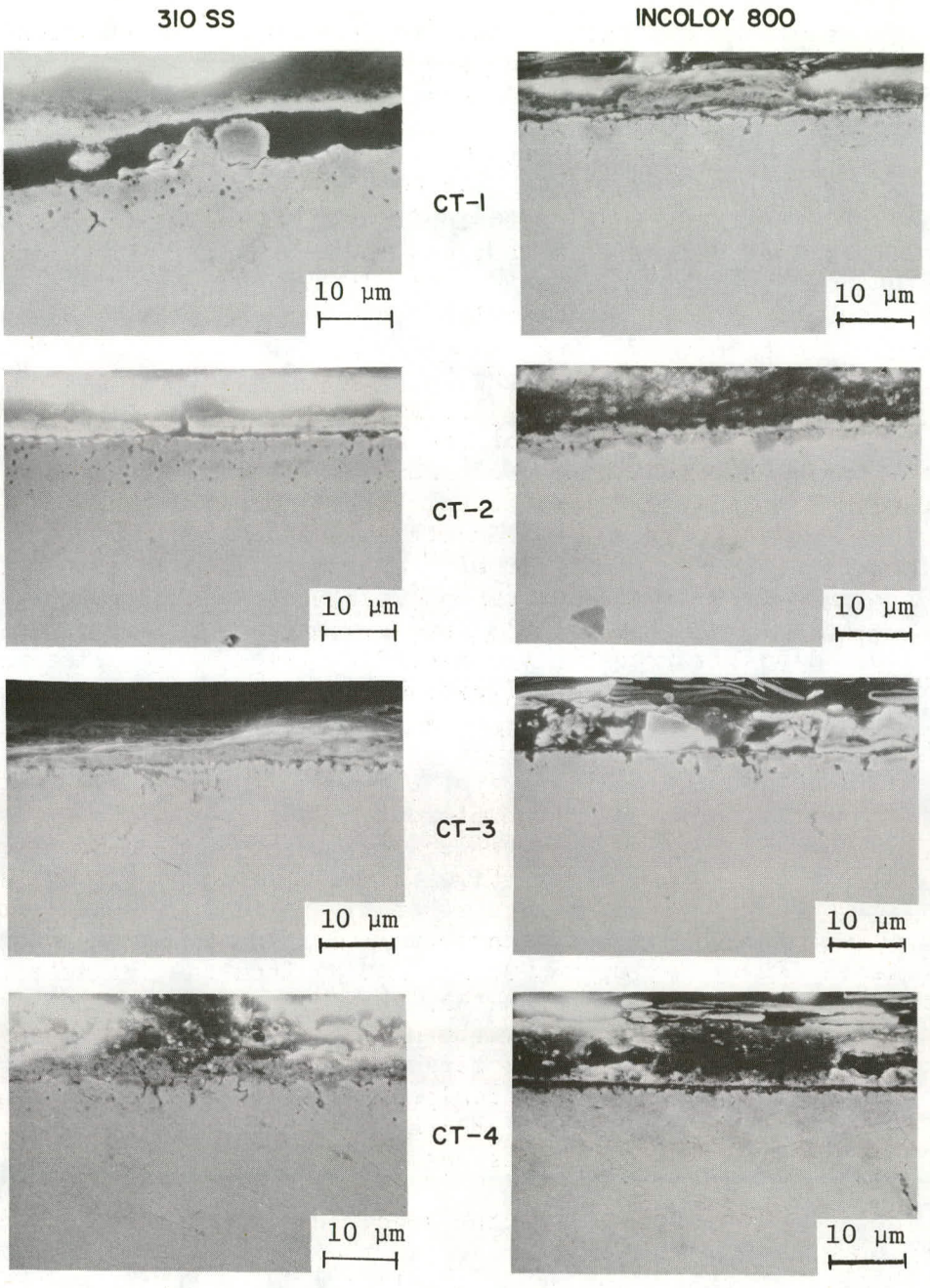

Fig. 49. SEM Micrographs of Type 310 Stainless Steel and Incoloy 800 After a 100-h Exposure Inside the Fluidized Bed. CT-1, without salt; CT-2, 0.3 mol % $CaCl_2$; CT-3, 0.5 mol % NaCl; and CT-4, 1.9 mol % Na_2CO_3. ANL Neg. No. 306-79-681.

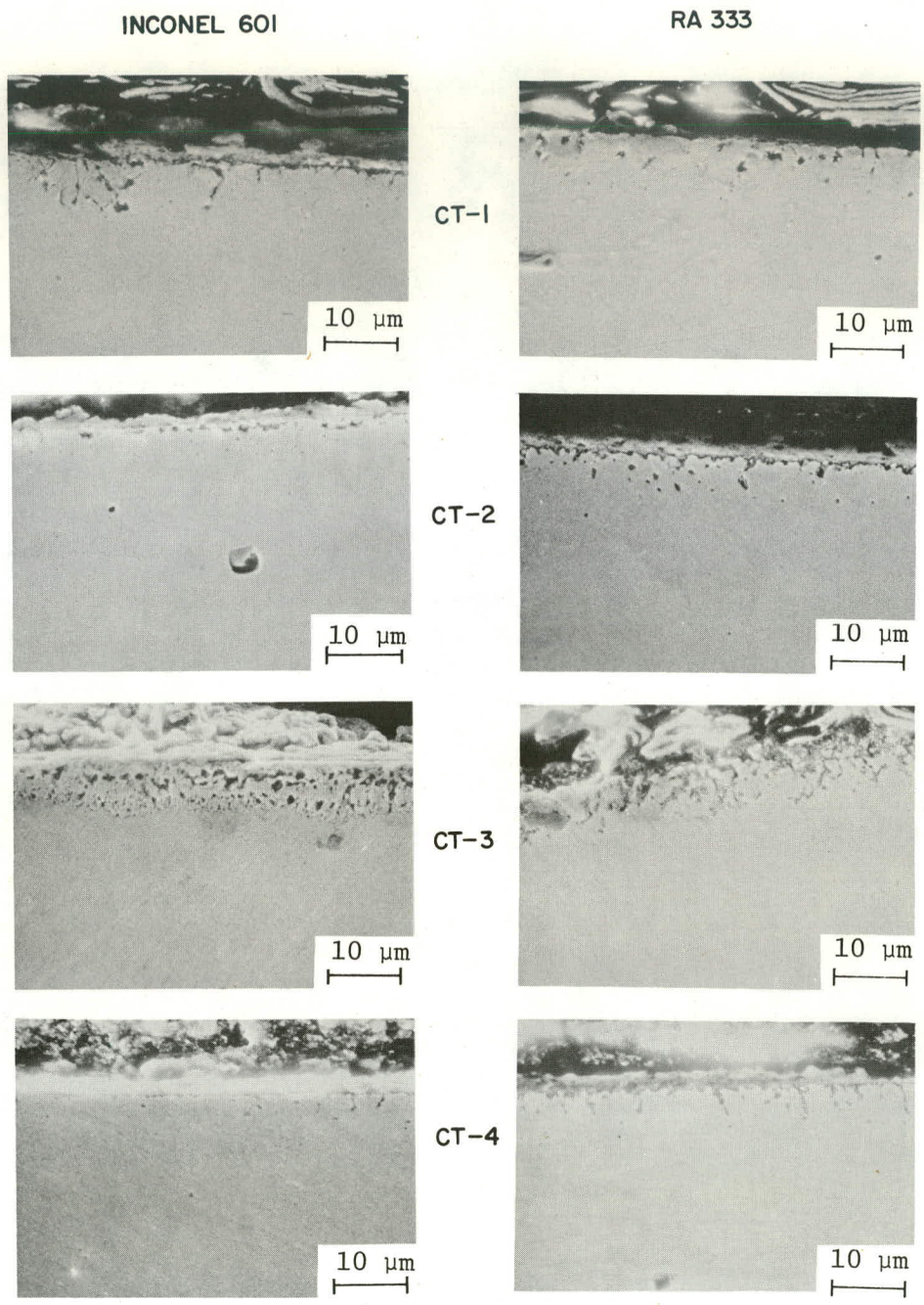

Fig. 50. SEM Micrographs of Inconel 601 and RA 333 After a 100-h Exposure Inside the Fluidized Bed. CT-1, without salt; CT-2, 0.3 mol % $CaCl_2$; CT-3, 0.5 mol % NaCl; and CT-4, 1.9 mol % Na_2CO_3. ANL Neg. No. 309-79-682.

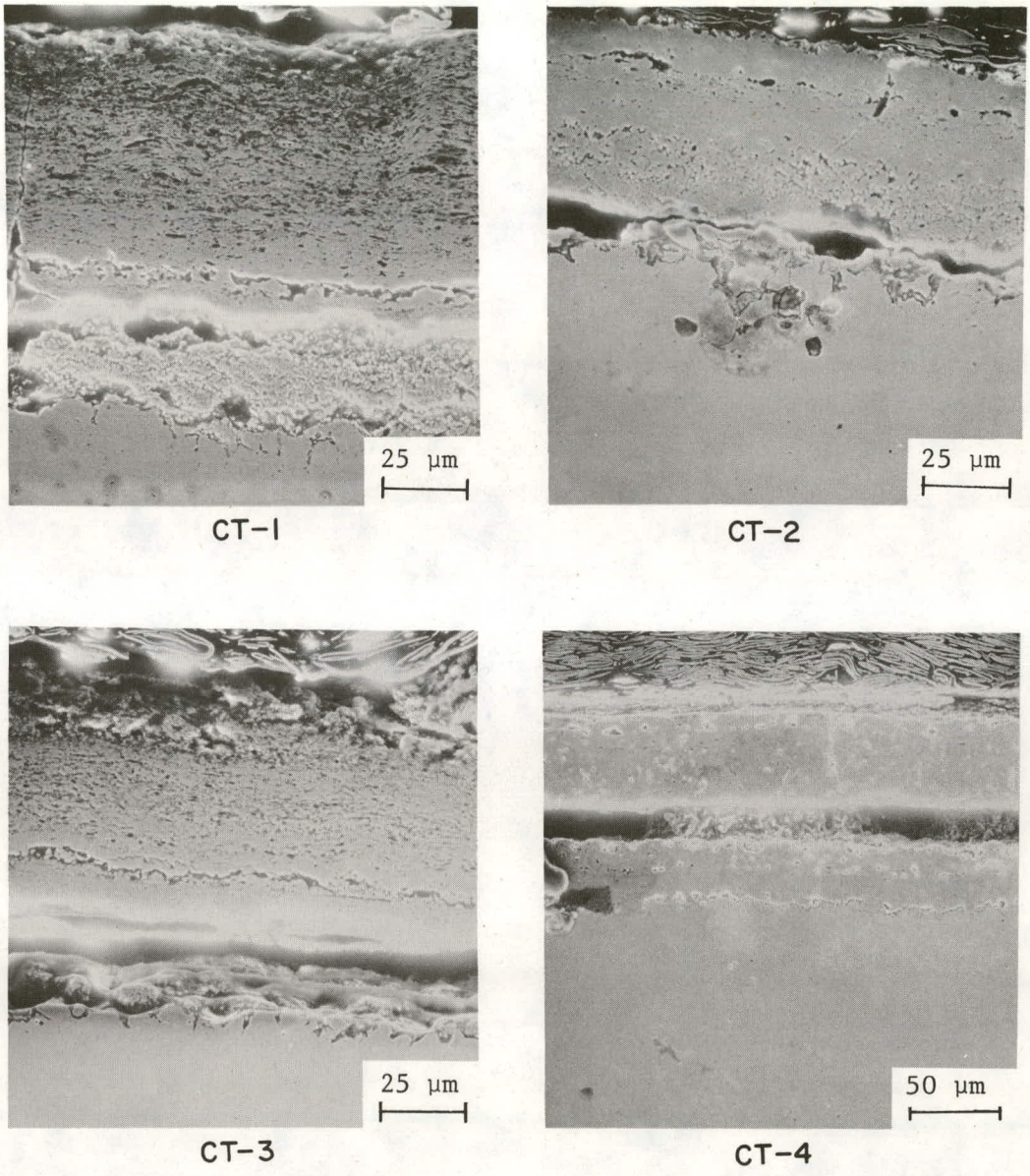

Fig. 51. SEM Micrographs of Fe-2¼ Cr-1 Mo Steel After a 100-h Exposure Inside the Fluidized Bed. CT-1, without salt; CT-2, 0.3 mol % $CaCl_2$; CT-3, 0.5 mol % NaCl; and CT-4, 1.9 mol % Na_2CO_3. ANL Neg. No. 306-79-683.

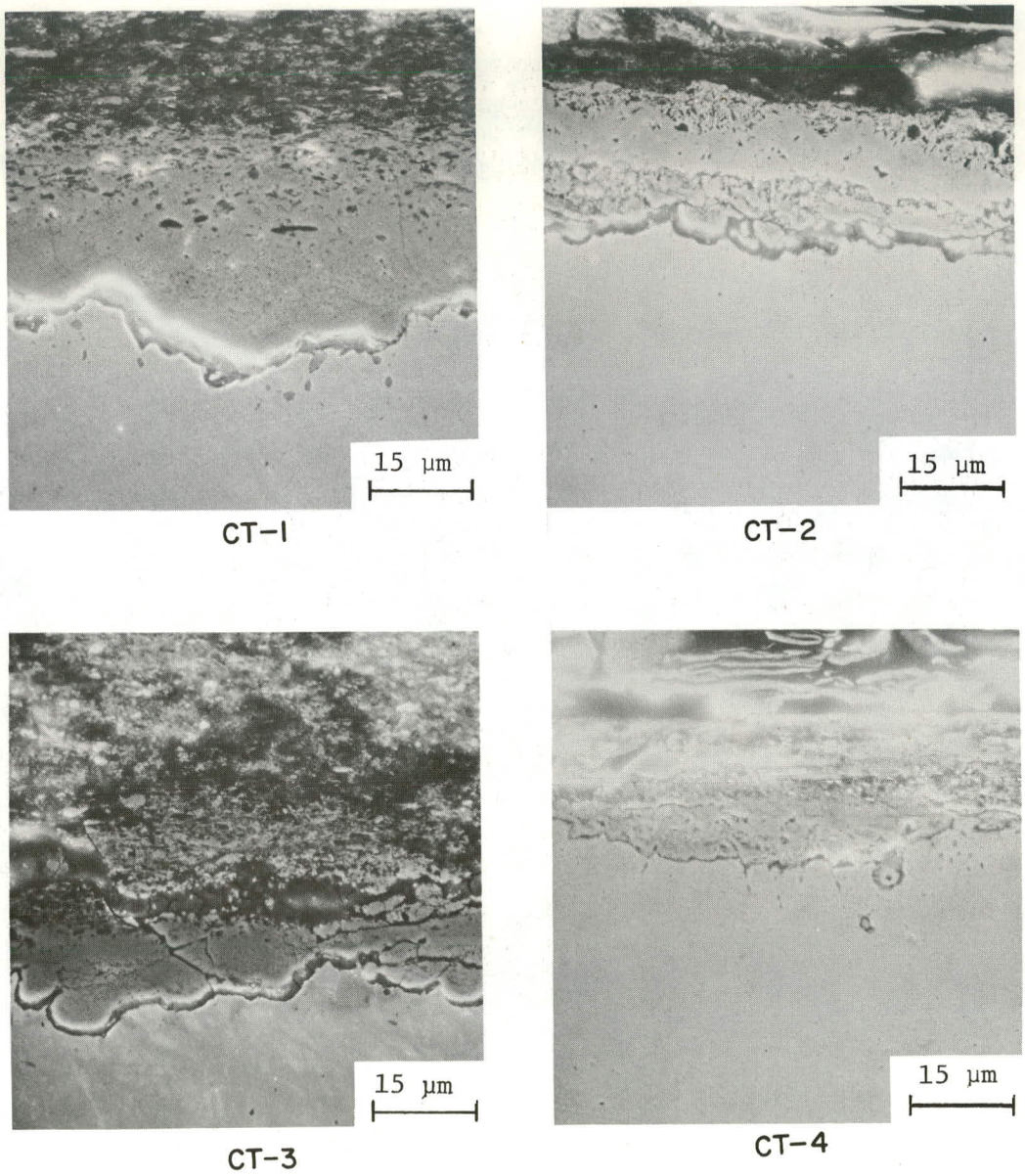

Fig. 52. SEM Micrographs of Fe-9 Cr-1 Mo Steel After a 100-h Exposure Inside the Fluidized Bed. CT-1, without salt; CT-2, 0.3 mol % $CaCl_2$; CT-3, 0.5 mol % NaCl; and CT-4, 1.9 mol % Na_2CO_3. ANL Neg. No. 306-79-684.

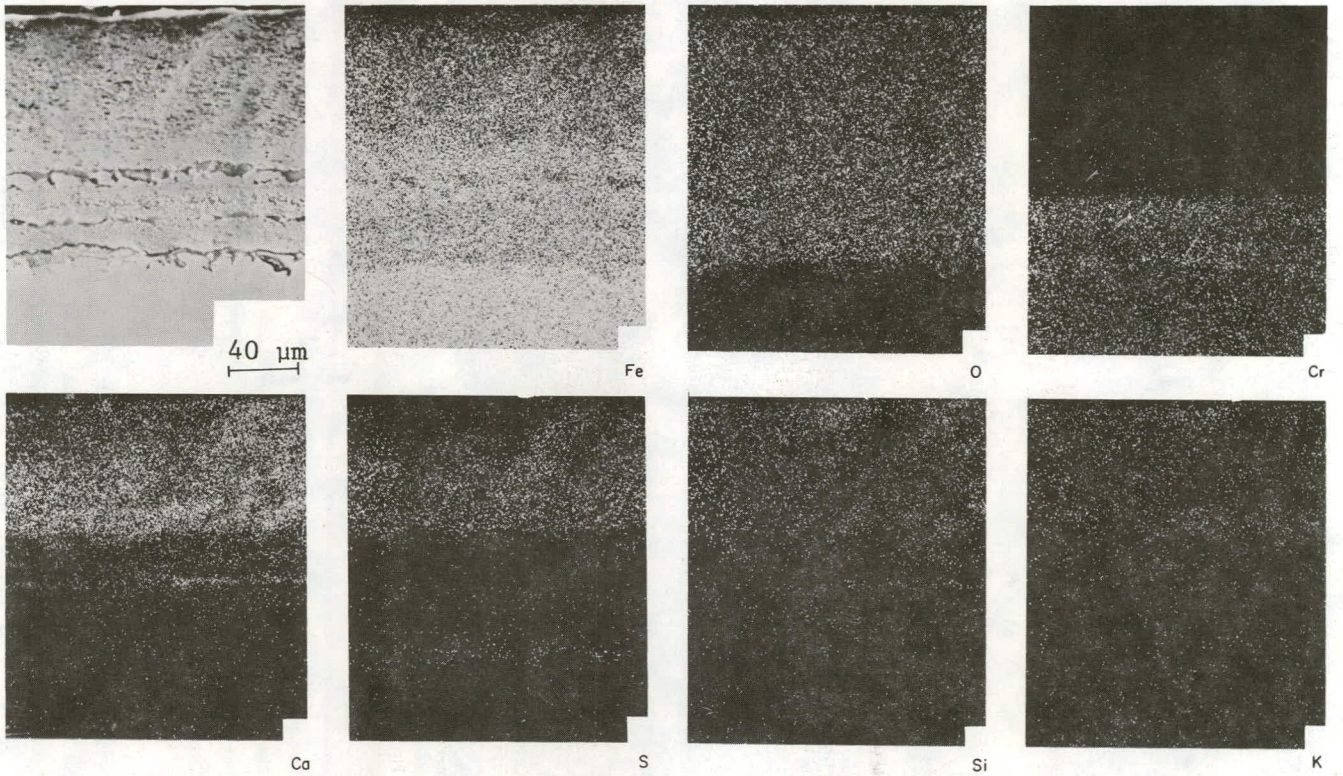

Fig. 53a. SEM Micrograph and X-ray Images for Fe, O, Cr, Ca. S, Si, and K from an Fe-2 1/4 Cr-1 Mo Steel Specimen Exposed for 100 h at 650°C Inside the Fluidized Bed. ANL Neg. No. 306-79-686.

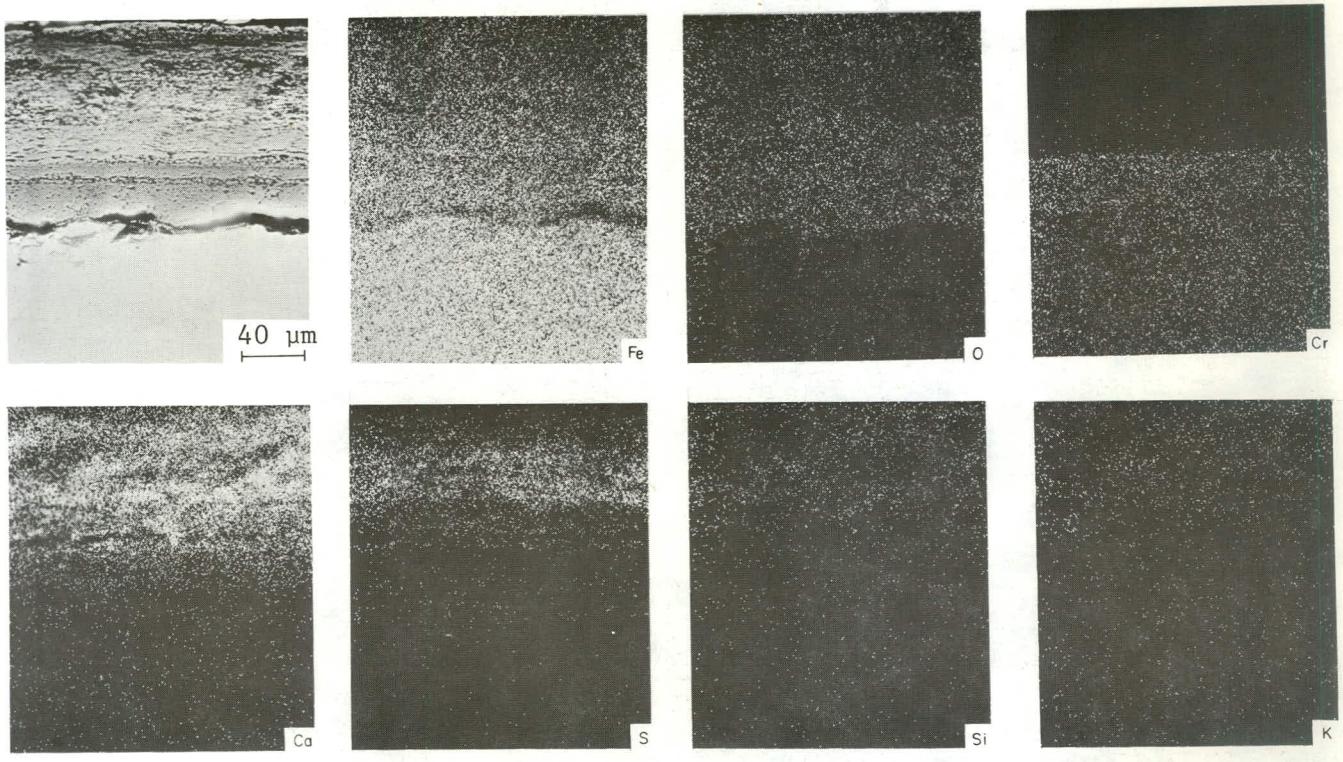

Fig. 53b. SEM Micrograph and X-ray Images for Fe, O, Cr, Ca, S, Si, and K from an Fe-2¼ Cr-1 Mo Steel Specimen Exposed for 100 h at 600°C Inside the Fluidized Bed Containing 0.5 mol % NaCl. ANL Neg. No. 306-79-685.

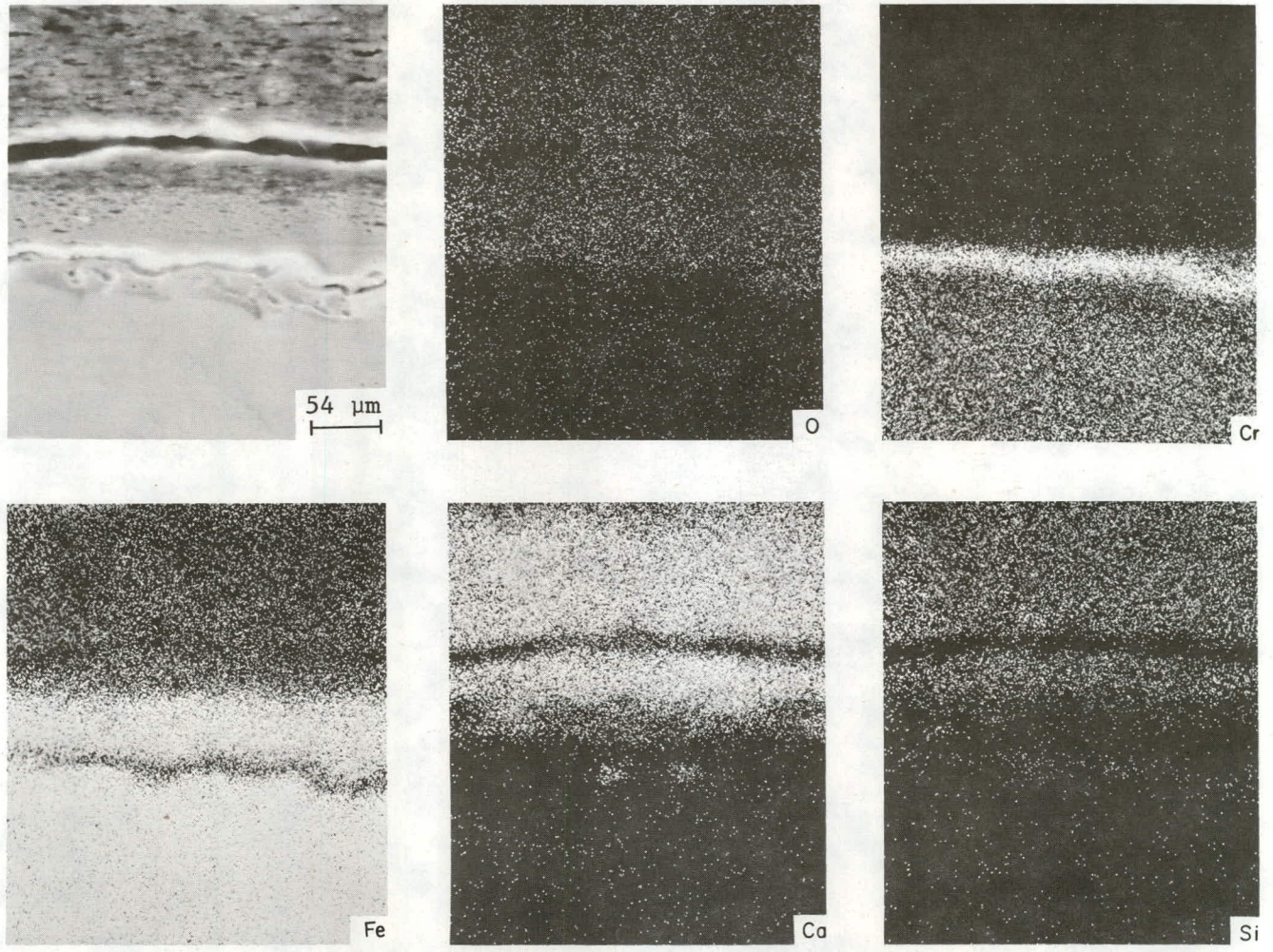

Fig. 54a. SEM Micrograph and X-ray Images for O, Cr, Fe, Ca, and Si from an Fe-9 Cr-1 Mo Steel Specimen Exposed for 100 h at 700°C Inside the Fluidized Bed. ANL Neg. No. 306-79-687.

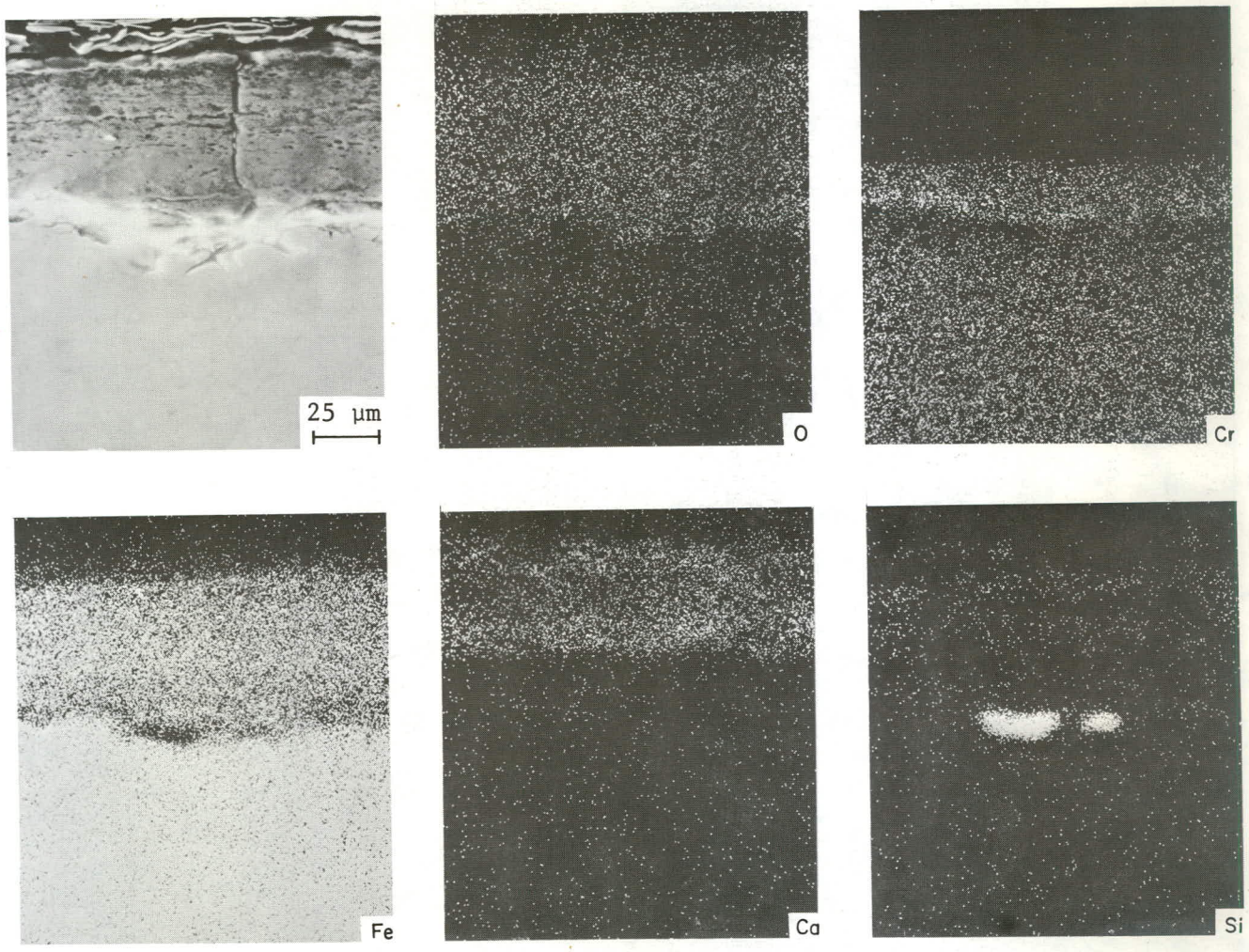

Fig. 54b. SEM Micrograph and X-ray Images for O, Cr, Fe, Ca, and Si from an Fe-9 Cr-1 Mo Steel Specimen Exposed for 100 h at 625°C Inside the Fluidized Bed Containing 0.5 mol % NaCl. ANL Neg. No. 306-79-688.

c. Conclusions

Results from the 100-h tests indicate that at ~850°C, the addition of 0.3 mol % $CaCl_2$ to the fluidized bed had no significant effect on the corrosion behavior of the various materials. The addition of 0.5 mol % NaCl or 1.9 mol % Na_2CO_3 increased the corrosion rates of most of the materials. In general, austenitic stainless steels and Haynes Alloy 188 exhibit better resistance to accelerated corrosion in the presence of salts than do the high-nickel alloys. Except for Fe-9 Cr-1 Mo Steel (alloy C-12) which was oxidized, materials located in the freeboard section of the combustor at temperatures between 525 and 705°C showed no detectable corrosion (*i.e.*, <2 μm).

The results for the air-cooled specimens exposed in the fluidized bed at temperatures between 525 and 730°C show that salt addition has no effect on the corrosion behavior of any of the materials. At these temperatures, the low alloy Fe-2¼ Cr-1 Mo steel shows considerable oxidation regardless of the presence or absence of salt, and the surface scale interacts with the deposits from the bed material.

REFERENCES

1. J. A. Shearer, I. Johnson, and C. B. Turner, *The Effect of Sodium Chloride on the Reaction of SO_2/O_2 Mixtures with Limestones and Dolomites*, Argonne National Laboratory Report ANL/CEN/FE-78-8 (June 1978).

2. Pope, Evans, and Robbins, Inc., *Optimization of Limestone Utilization and Sulfur Capture in a Single Combustion Zone Fluidized-Bed Boiler*, Final Report to the Office of Coal Research (March 20, 1974).

3. D. A. Wenz, I. Johnson, and R. D. Wolson, J. Chem. Eng. Data *14*(2), 250-252 (1969).

4. J. A. Shearer, I. Johnson, and C. B. Turner, *The Effects of $CaCl_2$ Additive on the Reaction of SO_2/O_2 Mixtures with Carbonate Rocks*, Argonne National Laboratory Report ANL/CEN/FE-79-7 (July 1979).

5. R. H. Borqwardt and R. D. Harvey, J. Environ. Sci. Technol. *6*(4), 350-360 (1971).

6. A. A. Jonke, *et al.*, *Reduction of Atmospheric Pollution by the Application of Fluidized-Bed Combustion, Annual Report, July 1970-June 1971*, Argonne National Laboratory Report ANL/ES-CEN-1004.

Distribution for ANL/CEN/FE-79-15

Internal:

R. Bane
W. L. Buck
L. Burris
F. Cafasso
E. Carls
O. K. Chopra
E. J. Croke
L. Cuba
P. T. Cunningham
W. A. Ellingson
D. C. Fee
J. Fischer
J. D. Gabor
J. E. Harmon
J. E. Helt
R. F. Henry
H. Huang
B. R. Hubble
K. Jensen
I. Johnson (20)
A. A. Jonke (6)
A. B. Krisciunas
S. H. D. Lee
J. F. Lenc
W. E. Massey
A. F. Melton
S. A. Miller
D. S. Moulton
K. M. Myles
E. G. Pewitt
W. Podolski
J. Royal
N. Sather
A. A. Siczek
S. Siegel
J. Shearer
J. W. Simmons
G. W. Smith
E. B. Smyk
W. M. Swift
F. G. Teats
C. E. Till
C. B. Turner
S. Vogler
D. S. Webster
W. I. Wilson
J. E. Young
ANL Contract File
ANL Libraries (5)
TIS Files (6)

External:

DOE-TIC, for distribution per UC-90e (458)
Manager, Chicago Operations and Regional Office, DOE
Chief, Office of Patent Counsel, DOE-CORO
V. H. Hummel, DOE-CORO
M. Jackson, DOE-CORO
President, Argonne Universities Association
Chemical Engineering Division Review Committee:
- C. B. Alcock, U. Toronto
- R. C. Axtmann, Princeton U.
- J. T. Banchero, U. Notre Dame
- T. Cole, Ford Motor Co.
- P. W. Gilles, U. Kansas
- R. I. Newman, Warren, N. J.
- H. Perry, Resources for the Future, Washington
- G. M. Rosenblatt, Pennsylvania State U.
- W. L. Worrell, U. Pennsylvania

D. H. Archer, Westinghouse Research Labs., Pittsburgh
E. C. Bailey, John Dolio and Associates, Chicago
O. L. Bennett, West Virginia U.
R. Bertrand, Exxon Research and Engineering, Linden, N. J. (5)
R. R. Boericke, General Electric Co., Schenectady
M. Boyle, Valley Forge Labs., Devon, Pa.
J. A. Brooks, Amoco Oil Co., Naperville, Ill.
R. D. Brooks, General Electric Co., Schenectady
C. Busch, Spectron Development Laboratory, Inc., Costa Mesa, Calif.
J. Chen, Lehigh U.
D. Cherrington, Exxon Research and Engineering Co., Florham Park, N. J.
J. Clark, Tennessee Valley Authority, Chattanooga
N. Coates, The MITRE Corp., McLean, Va.
R. C. Corey, Office of Fossil Energy, USDOE
R. Covell, Combustion Engineering, Inc.

G. Curran, Conoco Coal Development Co., Library, Pa.
D. DeCoursin, Fluidyne Engineering Co., Minneapolis
J. Dodge, Tetra Tech, Inc., Arlington, Va.
M. Dudukovic, Washington U.
S. Ehrlich, Electric Power Research Inst.
M. Evans, Aerotherm Division of ACUREX Corp., Mountain View, Calif.
M. H. Farmer, Exxon Research and Engineering Co., Linden, N. J.
C. Fisher, U. Tennessee
T. Fitzgerald, Oregon State U.
J. F. Flagg, Universal Oil Products Co., Des Plaines, Ill.
H. B. Forbes, Stone & Webster Engineering Corp., Boston
F. Frable, Bethlehem Mines Corp.
G. Frazier, U. Tennessee
S. Freedman, Office of Fossil Energy, USDOE
R. L. Gamble, Foster Wheeler Energy Corp., Livingston, N. J.
D. E. Garrett, Garrett Energy Research and Engineering, Inc., Ojai, Calif.
L. Gasner, U. Maryland
J. Geffken, Office of Fossil Energy, USDOE (5)
C. Georgakis, Massachusetts Inst. Technology
R. Glenn, Combustion Processes, Inc., New York City
J. S. Gordon, TRW, Inc., McLean, Va.
O. J. Hahn, U. Kentucky
J. Halow, Morgantown Energy Technology Center
W. Hansen, Babcock & Wilcox Co., Barberton, O.
M. J. Hargrove, Combustion Engineering, Inc.
R. D. Harvey, Illinois State Geological Survey, Urbana
R. Helfenstein, Illinois State Geological Survey, Urbana
R. G. Hickman, Lawrence Libermore Lab.
F. Hsing, Pratt & Whitney, East Hartford
D. Huber, Burns and Roe, Inc., Paramus, N. J.
F. D. Hutchinson, Gibbs and Hill, New York City
D. L. Keairns, Westinghouse Research Labs., Pittsburgh
D. Kirchgessner, U. S. Environmental Protection Agency, Research Triangle Park (16)
C. B. Leffert, Wayne State U.
A. M. Leon, Door-Oliver, Inc., Stamford, Conn.
R. M. Lundberg, Commonwealth Edison Co., Chicago
J. J. Markowsky, American Electric Power Service Corp., New York City
M. J. Mayfield, Tennessee Valley Authority, Chattanooga
W. McCurdy, Office of Fossil Energy, USDOE
J. Mesko, Pope, Evans and Robbins, New York City (2)
A. Metcalfe, Solar Turbine International, San Diego
T. A. Milne, Solar Energy Research Inst.
S. Moskowitz, Curtiss-Wright Corp., Wood Ridge, N. J.
W. Norcross, Combustion Engineering, Inc.
F. F. Nunes, Woodridge, Ill.
T. A. Pearce, Dow Chemical, Freeport, Tex.
W. A. Peters, Massachusetts Inst. of Technology
C. Petty, Michigan State U.
M. I. Rednicki, Aerojet Energy Conversion, Sacramento
R. Reed, Pope, Evans and Robbins, Inc., Alexandria, Va.
A. F. Sarofim, Massachusetts Inst. Technology
S. Saxena, U. Illinois, Chicago
J. Shang, Morgantown Energy Technology Center

A. Sherman, Combustion Power Co., Menlo Park
C. Space, Reynolds, Smith & Hills, Jacksonville, Fla.
W. K. Stair, U. Tennessee
F. Staub, General Electric Corp., Schenectady
M. Steinberg, Brookhaven National Lab.
D. Stewart, Gilbert Associates, Reading, Pa.
L. Strickland, Morgantown Energy Technology Center
W. Strieder, U. Notre Dame
S. E. Tung, Massachusetts Inst. Technology
V. Underkoffler, Gilbert Associates, Inc., Reading, Pa.
W. E. Wallace, Jr., Morgantown Energy Technology Center
F. A. Walton, Combustion Power Co., Menlo Park
A. E. Weller, Battelle Columbus Labs.
G. Weth, Office of Fossil Energy, USDOE
T. D. Wheelock, Iowa State U.
J. S. Wilson, Morgantown Energy Technology Center
K. Yeager, Electric Power Research Inst.
D. Zallen, U. New Mexico, Albuquerque
R. E. Zoellner, Stearns-Roger, Denver
J. F. Davidson, U. Cambridge, England
J. Highley, U. K. National Coal Board, Gloucestershire, England
H. R. Hoy, BCURA Ltd., Leatherhead, England
G. Moss, Esso Research Centre, Abington, England
H. Schreckenberg, Bergbau-Forschung GmbH, Essen, Germany
B. A. Wiechula, Imperial Oil Enterprises, Sarnia, Canada